Department of Oral and Maxillofacial Diseases
University of Helsinki
Helsinki, Finland

Doctoral School in Health Sciences,
Doctoral Program in Clinical Research

Towards more reliable *in vitro* drug testing for head and neck squamous cell carcinoma via a human tumor–derived matrix

Katja Tuomainen
University of Helsinki,
Finland

ACADEMIC DISSERTATION

To be presented, with the permission of the Faculty of Medicine of
the University of Helsinki, for public examination in Lecture Hall 2, Biomedicum 1,
Haartmaninkatu 8
on December 17th, 2021, at 12 noon.

Helsinki 2021

Supervised by:

Tuula Salo, DDS, PhD, Professor
Department of Oral and Maxillofacial Diseases
University of Helsinki,
Helsinki, Finland

Outi Monni, MSc, PhD, Docent
Applied Tumor Genomics Research Program and
Department of Oncology,
University of Helsinki,
Helsinki, Finland

Antti Mäkitie, MD, PhD, Professor
Department of Otorhinolaryngology,
Head and Neck Surgery, University of Helsinki and Helsinki University Hospital
Helsinki, Finland

Reviewed by:

Sara Zanivan, MSc, PhD, Professor
Institute of Cancer Sciences
University of Glasgow
Glasgow, United Kingdom

Klaus Elenius, MD, PhD, Professor
Institute of Biomedicine
University of Turku
Turku, Finland

Official opponent:

Jukka Westermarck, MD, PhD, Professor
Institute of Biomedicine
University of Turku
Turku, Finland

Cover adapted from “Types of Head and Neck Cancers” by BioRender.com.
ISBN 978-951-51-7719-3 (print)
ISBN 978-951-51-7720-9 (PDF)
ISSN 2342-3161 (print)
ISSN 2342-317X (online)
http://ethesis.helsinki.fi
Unigrafia Helsinki 2021

Nothing in life is to be feared, it is only to be understood.
-Marie Curie

CONTENTS

LIST OF ORIGINAL PUBLICATIONS

This thesis is based on the following publications, which are referred to in the text by their Roman numerals:

I **Tuomainen K**, Al-Samadi A, Potdar S, Turunen L, Turunen M, Karhemo P-R, Bergman P, Risteli M, Åström P, Tiikkaja R, Grenman R, Wennerberg K, Monni O, and Salo T. Human Tumor–Derived Matrix Improves the Predictability of Head and Neck Cancer Drug Testing. *Cancers (Basel)* 2019;12(1):92

II **Tuomainen K**, Hyytiäinen A, Al-Samadi A, Ianevski P, Ianevski A, Potdar S, Turunen L, Saarela J, Kuznetsov S, Wahbi W, Risteli M, Mäkitie A, Monni O, and Salo T. High-throughput compound screening identifies navitoclax combined with irradiation as a candidate therapy for HPV-negative head and neck squamous cell carcinoma *Sci Rep* 2021;11(1):14755

III Al-Samadi A*, Poor B*, **Tuomainen K**, Liu V, Hyytiäinen A, Sulymanova I, Mesimäki K, Wilkman T, Mäkitie A, Saavalainen P, Salo T. *In vitro* humanized 3D microfluidic chip for testing personalized immunotherapeutics for head and neck cancer patients. *Exp. Cell Res.* 2019;383(2):111508

*Equal contributions

ABBREVIATIONS

5-FU	5-fluorouracil
AKT	serine/threonine protein kinase B
AUC	area under curve
Bcl-2	B-cell lymphoma-2
Bcl-xL	B-cell lymphoma-extra large
BzCl	benzethonium chloride
CAF	cancer-associated fibroblast
CCRT	concurrent chemoradiotherapy
CDKN2A	cyclin dependent kinase inhibitor 2A
CR	complete response
CRT	chemoradiotherapy
CT	chemotherapy or computed tomography
CTG	CellTiter-Glo
CTLA-4	cytotoxic T-lymphocyte-associated protein 4
dCRT	definitive chemoradiotherapy
DFS	disease-free survival
DISC	death-inducing signaling complex
DMEM	Dulbecco's Modified Eagle Medium
DMSO	dimethyl sulfoxide
DRST	drug sensitivity and resistance testing
DSB	double-strand DNA break
DSS	drug sensitive score
EC_{50}	half maximal effective concentration
ECM	extracellular matrix
EDTA	ethylenediaminetetraacetic acid
EGFR	epidermal growth factor receptor
EMT	epithelial–mesenchymal transition
FBS	fetal bovine serum
FDA	Food and Drug Administration
Gy	Gray
HDAC	histone deacetylase
HER	human epidermal growth factor receptor
HIF1α	hypoxia-inducible factor 1-alpha
HNC	head and neck cancer
HNSCC	head and neck squamous cell carcinoma
HPV	human papilloma virus
HTS	high-throughput screening
IAP	inhibitor of apoptosis
IC_{50}	half maximal inhibitory concentration
IDO1	indoleamine 2,3-dioxygenase 1
IMRT	intensity modulated radiation therapy

KMT2D	histone-lysine N-methyltransferase 2D
LA-HNSCC	locally advanced head and neck squamous cell carcinoma
mAb	monoclonal antibody
MAPK	mitogen-activated protein kinase
MDSC	myeloid-derived suppressor cell
MEK	mitogen-activated protein kinase kinase
MOMP	mitochondrial outer membrane permeabilization
MRI	magnetic resonance imaging
mTOR	mammalian target of rapamycin
mTORC1	mTOR complex 1
NOTCH1	neurogenic locus notch homolog protein 1
NSCLC	non-small cell lung cancer
NSD1	nuclear receptor binding SET domain-containing protein 1
ORR	objective response rate
OS	overall survival
PARP1/2	poly [ADP-ribose] polymerase 1 and 2
PBMC	peripheral blood mononuclear cell
PBS	phosphate-buffered saline
PD	progressive disease
PD-1	programmed death-1
PD-L1	programmed death-ligand 1
PDMS	polydimethylsiloxane
PDO	patient-derived organoids
PET	positron emission tomography
PFS	progression-free survival
PI3K	phosphoinositide 3-kinase
PIP2	phosphatidylinositol-4, 5-bisphosphate
PIP3	phosphatidylinositol-3, 4, 5-triphosphate
PLK1	polo like kinase 1
PMNC	peripheral blood mononuclear cell
PR	patial response
R/M	recurrent and metastatic
RECIST	response evaluation criteria in solid tumors
ROS	reactive oxygen species
RT	radiotherapy
SCC	squamous cell carcinoma
SD	stable disease
SDS-PAGE	sodium dodecyl sulfate polyacrylamide gel electrophoresis
sDSS	selective DSS
SMAC	second mitochondrial-derived activator of caspase
TAM	tumor-associated macrophage
TCGA	Cancer Genome Atlas
TGF-α	transforming growth factor-α
TME	tumor microenvironment
TPF	T=docetaxel, P= cisplatin, and F=fluorouracil combination

ABSTRACT

Head and neck squamous cell carcinoma (HNSCC) is the 8th most common cancer worldwide. Despite improved therapy, the 5-year overall survival rate remains unchanged, being approximately 50%. Treatment approaches for HNSCC consist of surgery and radiotherapy, either alone or in combination and can include adjuvant chemo-, immuno-, or targeted therapy. Chemotherapeutic agents are nonselective and associate with severe adverse effects. The only approved targeted therapies for HNSCC are the epidermal growth factor receptor (EGFR) inhibitor, cetuximab, and the immunotherapeutic PD-1 inhibitors, nivolumab and pembrolizumab. The combination of cetuximab and irradiation is shown to improve patient survival. However, response rates to cetuximab remain low. Immunotherapy is emerging as a promising approach in the management of HNSCC. However, only a minor proportion of patients benefit from immunotherapy. Therefore, new molecular targeted therapies are urgently needed in addition to existing treatment approaches.

Current *in vitro* anticancer compound testing features a low predictive value, since only 10% of compounds showing efficacy in preclinical tests are approved in the following clinical trials. Traditionally, *in vitro* cancer cell studies are used to predict the efficacy of new anticancer compounds. However, these studies are often conducted on a plastic surface or using animal–derived extracellular matrices, which overlook important aspects of the interaction between cancer cells and the human tumor microenvironment (TME). To overcome this problem, we have developed a human leiomyoma–derived matrix Myogel.

The aim of this PhD project was to develop a reliable *in vitro* method for HNSCC anticancer drug testing by providing a human TME for cancer cells. The first approach was to investigate whether the use of a Myogel matrix could improve the reliability of drug screening compared to conventional plastic or the typically applied mouse sarcoma–derived matrix, Matrigel. We screened 19 anticancer compounds, targeting EGFR, MEK, or PI3K/mTOR on 12 HNSCC cell lines. We applied a high-throughput drug screening assay under five different culturing conditions; cells on a plastic surface and on top of or embedded in Myogel or Matrigel. The efficacy of the anticancer compounds was compared to the response rates of HNSCC monotherapy clinical trials. We found that cells cultured in Myogel were less sensitive to the EGFR and MEK inhibitors than Matrigel or plastic cultured cells. However, PI3K/mTOR inhibitors exhibited similar sensitivity under all culturing conditions. Additionally, Myogel cultured cells reflected better the response rates of EGFR inhibitor clinical trials compared to the other cultures. Therefore, we concluded that Myogel improves the predictability of *in vitro* anticancer drug testing compared to the plastic and animal–derived matrix.

Since more effective and selective combination therapies are urgently needed, we performed a high-throughput drug screen to identify synergistic compound–radiation combinations using a compound library (n=396) and ionizing radiation. The assay was run using five HNSCC cell lines cultured on Myogel. In the initial screen, several compounds with strong synergistic and antagonistic effects were identified and further investigated in a dose–response matrix assay. The Bcl-2/Bcl-xL inhibitor navitoclax, which emerged as the most promising radiosensitizer, exhibited a synergy with irradiation regardless of the p53 mutation status in an extended screen using 13 HNSCC cell lines. Additionally, an apoptosis assay performed for two HNSCC cell lines revealed that the navitoclax–irradiation combination halted the cell cycle and increased the irradiation-induced apoptosis. Overall, we demonstrated that the navitoclax–irradiation combination resulted in strong synergistic antitumor effects in HNSCC cell lines, and thereby it might possess therapeutic potential for HNSCC patients.

The third approach was to develop the treatment plan towards personalized medicine utilizing Myogel. Currently, no predictive method for a patient's immunotherapy response exists. We manufactured a fully human *in vitro* microfluidic chip assay to test immunotherapeutic agents for personalized medicine purposes for HNSCC patients. First, the assay was run using the oral tongue cancer cell line (HSC-3) embedded in a Myogel–fibrin mixture and immune cells, peripheral blood mononuclear cells (PBMCs) isolated from healthy blood samples. After successful testing, the chip was applied for freshly isolated cancer cells, patient serum and immune cells. Immune checkpoint inhibitors, IDO1 inhibitor (NLG-919) and a PD-L1 antibody were applied to chips and the immune cell migration and cancer cell proliferation were measured over three days. We found that the immune cell migration was associated with cancer cell density. The IDO1 inhibitor increased the immune cell migration towards cancer cells in HSC-3 and two patient samples. We successfully applied the first humanized *in vitro* microfluidic chip assay to test immunotherapy against HNSCC patient samples. In the future, this assay could possibly be utilized to predict an individual patient's immunotherapy response against HNSCC.

TIIVISTELMÄ

Pään ja kaulan alueen levyepiteelikarsinooma on maailmanlaajuisesti kahdeksanneksi yleisin syöpätyyppi. Kehittyneistä hoidoista huolimatta, viiden vuoden eloonjäämisennuste on edelleen vain 50 %. Hoitomuotoja ovat kirurgia ja sädehoito joko yksittäin tai yhdessä ja tarvittaessa yhdistettynä solunsalpaaja-, immunoterapia- tai täsmälääkehoitoon. Solunsalpaajat eivät kuitenkaan ole selektiivisiä ja aiheuttavat usein vakavia sivuvaikutuksia. Ainoat hyväksytyt täsmälääkkeet pään ja kaulan alueen syöville ovat epidermaalisen kasvutekijän reseptorin (EGFR) estäjä, setuksimabi sekä immunoterapeuttiset PD-1-estäjät, nivolumabi ja pembrolitsumabi. Setuksimabin ja sädehoidon yhdistelmän on osoitettu parantavan potilaiden ennustetta, mutta vaste on osoittautunut alhaiseksi. Immunoterapia on lupaava hoitomuoto pään ja kaulan alueen syöpiin, mutta vain pieni osuus potilaista hyötyy hoidosta, eikä immunoterapiavasteelle ole ennustavaa menetelmää. Tämän takia uusia täsmälääkkeitä sekä potilasvasteen ennustavia menetelmiä tarvitaan kiireellisesti.

Edustavampia *in vitro* -solututkimusmalleja tarvitaan parantamaan syöpälääkkeiden tehon ennustettavuutta, sillä nykyisten prekliinisten syöpälääkekokeiden ennustearvo on alhainen: vain alle 5 % *in vitro* -kokeiden perusteella valituista lääkeaineista läpäisee kliiniset kokeet. Solututkimukset tehdään tavallisesti muovialustalla tai käyttämällä kaupallisia eläinperäisiä väliaineita, kuten hiiren fibrosarkoomasta valmistettua Matrigeeliä. Nämä menetelmät jäljittelevät kuitenkin heikosti ihmisyöpäsolujen kasvuympäristöä. Parantaaksemme *in vitro* -kokeiden ennustettavuutta, olemme kehittäneet ihmisen kohdun myoomasta valmistetun väliaineen, Myogeelin.

Tämän väitöskirjatyön tavoitteena oli kehittää luotettavampia *in vitro* -menetelmiä tarjoamalla syöpäsoluille ominaisempi kasvuympäristö. Ensimmäiseksi tutkimme, voisiko Myogeeli-väliaineen käyttö parantaa lääkeseulonnan luotettavuutta verrattuna tavanomaiseen muovialustaan tai Matrigeliin. Tutkimuksessa testattiin 19 täsmälääkkeen (EGFR:n, MEK:n ja PI3K / mTOR:n estäjien) tehoa kahdellatoista pään ja kaulan alueen syöpäsolulinjalla viidessä eri kasvuympäristössä. Solut kasvatettiin muovin päällä, Myogeelillä ja Matrigeelillä päällystetyillä levyillä ja geelien sisällä, jonka jälkeen syöpäsolujen lääkevasteita vertailtiin sekä toisiinsa että julkaistujen kliinisten kokeiden tuloksiin. Myogeelin päällä ja sisällä kasvatetut syöpäsolut reagoivat huomattavasti heikommin EGFR:n ja MEK:n estäjiin kuin muovin päällä tai Matrigeelissä kasvatetut solut. Lisäksi Myogeelissä tehdyt kokeet vastasivat muita koeolosuhteita huomattavasti paremmin kliinisiä EGFR:n estäjillä tehtyjä lääkekokeita. PI3K/mTOR:n estäjiin solut reagoivat samalla tavalla kasvuympäristöstä riippumatta.

Tutkimustuloksien perusteella ihmiskasvainperäinen matriksi voisi parantaa *in vitro* -syöpälääketestausten kliinistä ennustettavuutta.

Koska tehokkaampia ja selektiivisempiä yhdistelmähoitoja tarvitaan, toisena väitöskirjatyön tavoitteena oli etsiä suuritehoisella seulonnalla uusia säde- ja lääkehoitoyhdistelmiä. Tutkimuksessa käytettiin lääkekirjastoa (n = 396) ja sädehoitoa Myogeelissä viljellyille pään ja kaulan alueen syöpäsoluille. Seulonnalla löydettiin useita potentiaalisia lääke- ja sädehoitoyhdistelmiä, joita tutkittiin tarkemmin käyttäen useita sädeannoksia. Lisätutkimukset osoittivat lupaavimman lääkekandidaatin, Bcl-2/Bcl-xL estäjän, navitoklaksin ja sädehoidon yhdistelmällä olevan synerginen vaikutus kolmessatoista testatussa solulinjassa. Lisäksi kahdelle pään ja kaulan alueen syöpäsolulinjalle tehty apoptoosimääritys osoitti navitoklaksin ja sädehoidon yhdistelmän pysäyttävän syöpäsolujen jakautumisen ja voimistavan säteilyn aiheuttamaa apoptoosia. Tutkimuksen perusteella navitoklaksi-sädehoitoyhdistelmällä saattaisi olla terapeuttista potentiaalia pään ja kaulan alueen syövän hoidossa.

Väitöskirjatyön kolmantena aiheena oli kehittää malli yksilöidyn immunoterapiavasteen testaukseen käyttäen Myogeeliä. Valmistimme ensimmäisen täysin ihmisperäisen mikrofluidisen sirumäärityksen pään ja kaulan alueen syöpäpotilaiden immunoterapiavasteen määrittämiseksi. Ensiksi testasimme sirun käyttäen kielisyöpäsolulinjaa (HSC-3) ja terveiden luovuttajien verinäytteistä eristettyjä immuunisoluja. Syöpäsolut kasvatettiin sirun sisällä Myogeeli-fibriini-matriksissa. Immuunijärjestelmän tarkastuspiste-estäjiä, IDO1-estäjää (NLG-919) ja PD-L1-vasta-ainetta lisättiin siruille, minkä jälkeen immuunisolujen siirtymistä syöpäsoluja kohden sekä syöpäsolujen jakautumista mitattiin kolmen päivän ajan. Tämän jälkeen teimme immunoterapeuttisen sirumäärityksen myös potilaista eristetyille syöpäsoluille ja veren immuunisoluille. Tutkimustuloksemme osoittivat syöpäsolujen määrän vaikuttavan immuunisolujen liikkumiseen. IDO1-estäjä lisäsi immuunisolujen liikkumista syöpäsoluja kohden kahdella potilasnäytteellä sekä HSC-3-soluilla. Tutkimuksessa käytimme onnistuneesti täysin ihmisperäistä mikrofluidista sirumääritystä yksilöllisen immunoterapiavasteen testaukseen pään ja kaulan alueen syöpäpotilaille. Määritystä voitaisiin mahdollisesti tulevaisuudessa käyttää apuna potilaan immunoterapiavasteen ennustamisessa.

1 INTRODUCTION

Head and neck squamous cell carcinoma (HNSCC) is a common malignancy worldwide and despite improved treatments, the survival rate has remained basically unchanged [1]. Treatment approaches available for HNSCC are surgery and radiotherapy either as a single modality or combined treatment and in selected cases with adjuvant chemo-, immuno-, or targeted therapy. However, chemotherapeutic agents are non-selective, may damage normal tissues and associate with severe adverse effects. The combination of radio- and chemotherapy or the EGFR inhibitor cetuximab have been shown to improve patient survival. However, the cetuximab response rates have remained low [2]. Therefore, new molecular targeted therapies are urgently needed for integration into existing treatment regimens.

In vitro preclinical models have formed the basis for research since the first human cancer line was established [3]. In typical anticancer compound testing, cancer cells are cultured on a two-dimensional (2D) plastic surface and later in animal models prior to clinical investigations. In recent decades, methods and tools have been improved by shifting from 2D to 3D cell culture, which better mimics a solid tumor tissue's physiological environment and growth pattern [3]. However, these 3D studies are often conducted using animal–derived extracellular matrices, which overlook important aspects of interactions between cancer cells and the human tumor microenvironment (TME). To overcome this problem, we have developed a human tumor leiomyoma–derived matrix, Myogel, which better reflects the human TME [4,5]. Myogel contains human TME components such as laminin, collagen, cytokines and growth factors [4]. All these factors have been shown to affect critically on carcinoma cell behavior, such as proliferation and invasion [6,7].

Immunotherapy and personalized medicine therapeutics are emerging as promising approaches in the management of HNSCC. The FDA has approved two immunotherapy drugs for HNSCC patients targeting the programmed death-1 (PD-1) receptor; pembrolizumab and nivolumab [8,9]. As with other HNSCC treatment options, no predictive method for ascertaining a patient's immunotherapy response exists. This leads to a significant problem in terms of subjecting patients to unnecessary side effects and ineffective treatments, especially when the percentage of the responsive patients remains low. Although, personalized drug testing has been recently undergoing active investigation, the results have not yet been translated into clinical practice, although several assays have been suggested.

2 REVIEW OF THE LITERATURE

2.1 HEAD AND NECK SQUAMOUS CELL CARCINOMA

Head and neck cancer (HNC) forms the eighth most common cancer type worldwide, which comprises malignancies appearing in the lip, oral and nasal cavity, pharynx, larynx, paranasal sinuses, and salivary glands (Fig. 1)[1,10]. Despite localization, cancers of the brain, eyes, esophagus, and thyroid are not included in HNC, but are classified as independent cancer types [10]. Cancers of the skin, muscles and bones of the head and neck area are also excluded from this classification [10]. Over 90% of head and neck cancers are squamous cell carcinomas (HNSCC) originating from the mucosal epithelium [11]. The remaining 10% are mainly salivary gland carcinomas, melanomas and soft tissue tumors [12]. Primary sites of metastasis for HNSCC are cervical lymph nodes of the neck, which is strongly associated with poor patient outcome [11]. The tumor, node and metastasis (TNM) staging system allows clinicians to categorize HNCs for the assessment of disease status, prognosis and treatment plan (Table 1) [13].

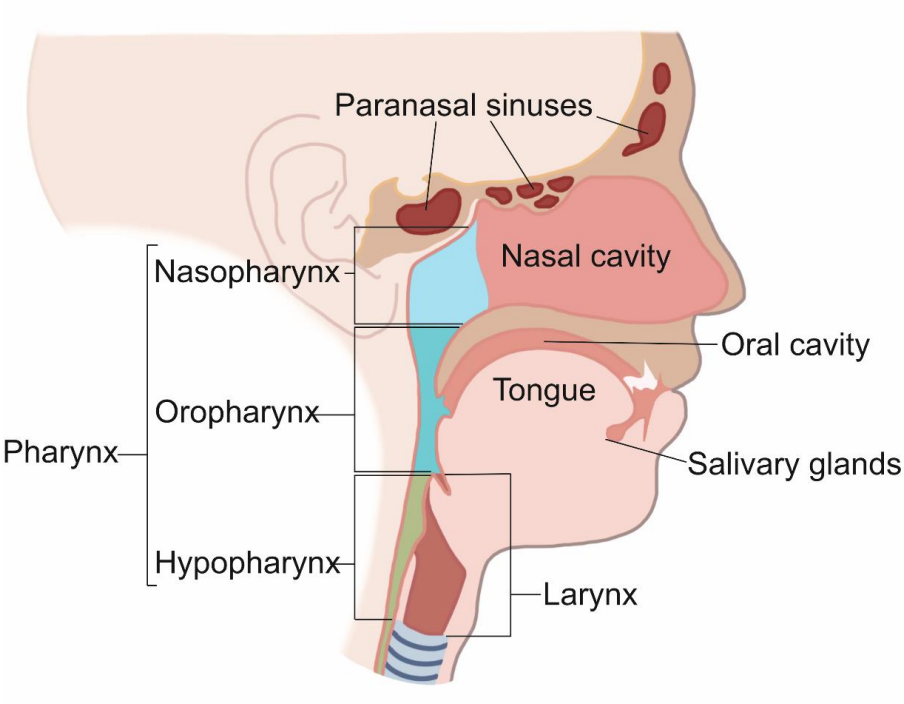

Figure 1. Head and neck cancers include cancers of the lips, oral and nasal cavity, pharynx, larynx, paranasal sinuses, and salivary glands. Figure by Erika Naakka

Table 1. TNM classification of HNCs in the oral cavity. The system is based on three categories: T—the characteristics of the tumor at the primary site; N—the degree of regional lymph node involvement; and M—the absence or presence of distant metastases [13] .

TX	Primary tumor cannot be assessed
T0	No evidence of primary tumor
Tis	Carcinoma *in situ*
T1	Tumor greatest dimension is ≤ 2 cm and depth of invasion ≤ 5 mm
T2	Tumor greatest dimension is ≤ 2 cm and depth of invasion is > 5 mm OR Tumor greatest dimension is > 2 cm but ≤ 4 cm and depth of invasion ≤ 10 mm
T3	Tumor greatest dimension is > 2 cm but ≤ 4 cm and depth of invasion > 10 mm OR Tumor greatest dimension is > 4 cm and depth of invasion ≤ 10 mm
T4a	(Lip) Tumor invades through cortical bone, inferior alveolar nerve, floor of the mouth, or skin (Oral cavity) Tumor size > 4 cm and depth of invasion > 10 mm or Tumor invades through cortical bone or skin, or involves the maxillary sinus
T4b	(Lip and oral cavity) Tumor invades masticator space, pterygoid place or skull base, or encases internal carotid artery
Nx	Regional lymph nodes cannot be assessed
N0	No regional lymph node metastases
N1	Metastasis in single ipsilateral lymph node, greatest dimension ≤ 3 cm without extra-nodal extension
N2a	Metastasis in single ipsilateral lymph node, greatest dimension > 3 cm but ≤ 6 cm without extranodal extension
N2b	Metastases in multiple ipsilateral lymph nodes, greatest dimension ≤ 6 cm, without extra-nodal extension
N2c	Metastases in bilateral or contralateral lymph nodes, greatest dimension ≤ 6 cm, without extranodal extension
N3a	Metastasis in lymph node greatest dimension > 6 cm, without extranodal extension
N3b	Metastasis in single or multiple lymph nodes with clinical extranodal extension
M0	No distant metastasis
M1	Distant metastasis

2.1.1 RISK FACTORS

The main risk factors for HNSCC especially in the oral cavity, larynx, hypopharynx and oropharynx area, are smoking and heavy consumption of alcohol [14,15]. The combination of tobacco and alcohol are reported to cause at least 75% of all HNSCC cases [16]. Infections of human papillomaviruses (HPV), especially the HPV type 16, increases the risk for oropharyngeal cancers in the base of tongue and tonsil area [17,18]. Globally, approximately 30% of oropharyngeal cancers are associated with HPV infection [19]. In

Finland, 58.5% of evaluable oropharyngeal cancers were HPV p16 positive [20]. Moreover, incidence of the HPV-related oropharyngeal cancers is increasing, while incidences of oropharyngeal cancers arising from other causes are decreasing in the United States [17].

Other risk factors for HNSCC include use of paan (betel quid), consumption of highly salted and preserved food, poor oral hygiene, Epstein-Barr virus infection, radiation and occupational exposure to wood dust, asbestos, or synthetic fibers [21-26]. According to a large cohort study, consumption for processed meat associates with HNSCC [27]. However, based on meta-analysis data, high consumption of fruits and vegetables may have a protective role in oral cancer [28].

The risk of HNSCC may also be increased by certain types of common oral mucosal diseases, such as leukoplakia, proliferative verrucous leukoplakia, erythroplakia and lichen planus [29,30]. Based on a systematic review, an average of 3.5% (0.13–34.0%) of leukoplakia patients develop cancer [31]. Proliferative verrucous leukoplakia develops into cancer in 60% of cases, and patients commonly have several consecutive cancers in the gingival area, cheek and tongue [32]. Oral lichen planus also increases the risk for HNSCC, as 1% of people with oral red lichen develop oral cancer [30].

2.1.2 INCIDENCE AND MORTALITY

HNSCCs cover approximately 5% of all cancer incidences, and annually over 650 000 new cases are diagnosed worldwide [33]. HNSCCs cause over 330 000 deaths annually and a five-year overall survival rate is, on average, 50% [33,34]. The survival rate and prognosis in HNSCC vary depending on tumor localization, gender, primary tumor size and lymph node involvement and hypoxia [35]. The incidence of new HNSCC cases has constantly increased over the past two decades [33]. HNSCC is more common in males than females. Particularly high differences between genders are found in larynx, hypopharynx, and oropharyngeal cancers. For example, according to the International Agency for Research Cancer statistics maintained by WHO, 87% of all estimated larynx cancer patients were males in the year 2020 (Both genders: 184 615, males: 160 265, females: 24 350) [36]. However, oral cancer rates in young females have been rising for several decades for an unknown reason [37]. The incidence of HNSCC increases with age and the majority of patients are in the range of 50 to 70 years [10].

2.1.3 GENETIC CHANGES IN HNSCC

Based on the cancer genome atlas (TCGA) data of over 520 human HNSCC tumors, the most frequent mutations in HPV-negative HNSCC are in tumor suppression genes, *TP53* (72%), *FAT1* (23%) and cyclin dependent kinase inhibitor 2A (*CDKN2A*; 22%; Table 2) [38]. Additionally, copy number alterations of *CDKN2A* (32%) are frequent in HNSCC due to loss of chromosome arm 9p21 (Table 2) [39]. *CDKN2A* encodes the $p16^{INK4A}$ protein, which disrupts cell cycle controlling cyclin D–CDK4/6 complexes [39]. The combination of loss of CDKN2A and amplification of cyclin D1 (CCND1) drives cells through the G1/S cell cycle checkpoint and contributes to unscheduled DNA replication [39].

Table 2. Frequent and significant genetic changes in HPV-negative HNSCC.

Cellular process	Gene	Protein	Gene type	Mutation (%)	CNA (%)
Cell cycle	*TP53*	p53	Tumor suppressor	72	1.4
	CDKN2A	$p16^{INK4A}$	Tumor suppressor	22	32
	CCND1	G1–S-specific cyclin D1	Oncogene	0.6	25
WNT signaling	*FAT1*	Protocadherin FAT1	Tumor suppressor	23	8
	NOTCH1	NOTCH1	Tumor suppressor	18	4
Survival	*PIK3CA*	Catalytic p110α subunit of class 1 PI3Ks	Oncogene	18	21
	PTEN	PTEN	Tumor suppressor	3	4
Epigenetic regulation	*KMT2D*	Histone lysine N-methyltransferase KMT2D	Tumor suppressor	16	0.4
	NSD1	Histone lysine N-methyltransferase NSD1	Tumor suppressor	12	0.8
Growth signals	*EGFR*	EGFR	Oncogene	4	11

Data from REFs 38 and 39. Mutation data was taken from The Cancer Genome Atlas (n=504). CNA = copy number alteration.

Other frequently mutated tumor suppression genes are neurogenic locus notch homolog protein 1 (*NOTCH1*; 18%), histone-lysine N-methyltransferase 2D (*KMT2D*; 16%) and nuclear receptor binding SET domain-containing protein 1 (*NSD1*; 12%) [38]. *NOTCH1* and *FAT1* are part of the Wnt signaling pathway, which plays an important role in cell fate, cell orientation and stem cell behavior. *NSD1* and KMT2D are involved in epigenetic regulation by both encoding histone lysine N-methyltransferases [38]. The PI3K/Akt/mTOR

pathway is the most frequently altered oncogenic pathway in HNSCC [40]. Components of this pathway that are commonly altered in HNSCC include frequent mutation and gene amplification in *PIK3CA* and loss of function of the phosphatase and tensin homologue (PTEN) [41]. EGFR is reported to be overexpressed in HNSCCs, but only a few EGFR activating mutations are found in HNSCC [126]. Based on mutation data taken from TCGA, EGFR mutations occur in 4% and copy number alterations in 8% of HNSCC tumors [38]. Mutations in RAS genes are infrequent in HNSCC, however HRAS mutations are the most common (~4%) [38].

HPV-positive tumors are reported to exhibit infrequent genetic changes in *TP53* and *CDKN2A* [38,39]. However, in HPV-induced carcinogenesis, two oncoproteins are encoded, E6 and E7. E6 eliminates the functions of p53, while E7 destroys the cell cycle regulator retinoblastoma-associated protein (RB1) leading to $p16^{INK4A}$ expression [42].

2.1.4 TREATMENTS IN HNSCC

Treatments for individual HNSCC depend on several factors, such as tumor location, tumor stage and patient age [10]. The treatment approach for oral cavity cancers includes surgery followed by radiotherapy, chemo-, immuno- or targeted therapy or chemoradiotherapy [42]. Pharyngeal cancers and advanced laryngeal are treated primarily with chemoradiotherapy [42]. Treatment for HPV-positive oropharyngeal cancer patients differs typically from HPV-negative patients as studies have shown that HPV-positive oropharyngeal tumors respond better to oncological treatment modalities and have more favorable prognosis [10,43].

Surgery in HNSCC

Surgery is the standard treatment for selected HNSCCs and the type of approach often depends on tumor stage (TNM), anatomical location, and desire to achieve organ preservation [44]. Various approaches to surgically reconstruct the oncological tissue defects are performed. Neck dissection (removal of lymph nodes of the neck) is typically performed when nodal extension is suspected or evident [44].

Radiotherapy in HNSCC

In addition to surgery, radiotherapy (RT) has an important role in curative–intent treatment for HNSCC. RT destroys cancer cells and damages the structures of dividing cells with high-energy ionizing radiation. The most established RT technique is intensity-modulated RT (IMRT) [45]. With this technique, the irradiation dose to the surrounding healthy tissue can be

limited, thus reducing the adverse effects associated with RT [10,45]. RT can be applied after surgery, but in some cases, early-stage tumors can be treated with RT alone [46]. RT is often provided as adjuvant therapy after surgery (postoperative RT). In postoperative RT, 4 to 6 weeks are left between surgery and radiotherapy. RT is usually given as a fraction (2 Gy) once a day, five days a week for up to 6 to 7 weeks [46]. The total irradiation dose depends on tolerance of surrounding healthy tissue, tumor volume and location and extent of surgical removal. Additionally, instead of traditional dosing, RT can be administered using hyperfractions or accelerated fractionations [47]. In hyperfractionated treatment, the total dose of irradiation is divided into smaller doses, given typically twice a day, while in accelerated RT, the total dose of irradiation is given over a shorter period of time [47]. HNSCC RT may cause several adverse effects, such as eating and swallowing difficulties, soreness, dry mouth and throat caused by mucositis, changes in smell and taste, inflammation, tiredness, nausea, loss of appetite and weight loss [10].

Chemotherapy in HNSCC

Typically, chemotherapy (CT) is given as adjuvant therapy alongside RT, to destroy the remaining cancer cells after surgical removal of the tumor [46]. However, CT may be given prior to the surgery as neoadjuvant CT to attempt to shrink the cancer size. Induction CT is used in locally advanced HNSCC (LA-HNSCC) to achieve a remission. To this date, the FDA has approved 8 compounds to treat HNSCC, including CT agents, such as cisplatin, carboplatin, docetaxel, paclitaxel and 5-fluorouracil, and targeted agents, EGFR inhibitor, cetuximab and two immunomodulators, nivolumab and pembrolizumab (Table 3) [48]. Platinums, cisplatin and carboplatin are the most common CT agents in HNSCC. Platinums belong to a class of alkylating drugs that act by forming covalent bonds with DNA [49]. Taxanes, such as paclitaxel and docetaxel, act by inhibiting microtubule disassembly, arresting the cell cycle and inducing apoptosis in the G2/M phase [50]. Paclitaxel and second-generation taxane, docetaxel, exhibits antitumor effects on recurrent or metastatic (R/M) HNSCC [51].

Table 3. Approved drugs for HNSCC

Drug	*Brand names*	*Therapy type*	*Drug class*	*Admistration*
cisplatin	Platinol	Concurrent chemotherapy	Platinum-based antineoplastic agent	intravenous
docetaxel	Taxotere, Docecad	Concurrent chemotherapy	Mitotic inhibitor, taxane microtubule stabilizer	intravenous
5-fluorouracil	Adrucil	Concurrent chemotherapy	Antimetabolite	intravenous
cetuximab	Erbitux	Targeted treatment	EGFR inhibitor	intravenous
carboplatin	Paraplatin	Concurrent chemotherapy	Platinum-based antineoplastic agent	intravenous
paclitaxel	Taxol, Abraxane, Paxene	Concurrent chemotherapy	Mitotic inhibitor, taxane microtubule stabilizer	intravenous
nivolumab	Opdivo	Targeted treatment	Immunotherapy, PD-1 inhibitor	intravenous
pembrolizumab	Keytruda	Targeted treatment	Immunotherapy, PD-1 inhibitor	intravenous

Combination chemotherapy

For LA-HNSCC, chemotherapy is often given as drug combinations, which usually are more effective than a single agent. The FDA has approved a TPF (T=docetaxel, P= cisplatin and F=fluorouracil) combination induction therapy for LA-HNSCC [52]. In addition, the cisplatin and fluorouracil (PF) combination is a commonly used regimen [53]. Several clinical trials and meta-analyses have indicated that the addition of docetaxel induction to the PF regimen might improve LA-HNSCC patient outcome with acceptable additional toxicities [54-56].

Chemoradiotherapy in HNSCC

Definitive concurrent chemoradiotherapy (CCRT) is a standard treatment for LA- or unresectable HNSCC [57]. Concomitant CT and RT has proved to be the most effective option, leading to an improvement in overall survival (OS) of approximately 5% for locoregionally advanced HNSCC [58]. CCRT results in the highest laryngectomy-free survival rate, the best locoregional control rate, and low distant metastasis rate compared with RT alone [59]. Platinum-based CCRT has been established as the principal treatment option, although other novel agents are available. However, CCRT is associated with acute and late adverse effects, which can lead to competing morbidities, and decreased overall survival (OS) and long-term disease-free survival (DFS) [57]. Approximately 50% of HNSCC patients receiving CCRT have a risk of

treatment-related toxicity, which aggravates patient outcome [57]. Therefore, the patient selection for CCRT is crucial. Chemotherapy is typically administered once or twice a week together with RT [57].

Targeted therapy in HNSCC

Cetuximab, a chimeric (mouse/human) monoclonal antibody that inhibits EGFR, can be integrated into three treatment regimens: in combination with radiotherapy for LA-HNSCC, as monotherapy for R/M HNSCC after platinum-based treatment failure or as a first-line treatment together with platinum-based chemotherapy or fluorouracil for metastatic HNSCC [2,60,61]. Cetuximab is the first FDA-approved targeted drug for HNSCC [62]. Cetuximab has been actively studied in dozens of clinical trials with various combinations in HNSCC. FDA-approval was based on a randomized phase III trial comparing cetuximab and irradiation to irradiation alone in patients with LA-HNSCC [61]. The cetuximab–irradiation combination significantly improved median OS (49.0 vs 29.3 months) and median progression-free survival (17.1 vs 12.4 months) [61]. However, another randomized phase III trial has reported that cetuximab addition to the irradiation–cisplatin combination did not improve patients' outcome [63]. Moreover, cetuximab monotherapy response rates have been consistently lower than 15% [64]. Cetuximab is administered once a week, starting one week before RT [2]. Currently cetuximab combinations with immune checkpoint inhibitors, such as durvalumab, are evaluated in clinical trials for HNSCC [65]. Other promising EGFR pathway inhibitors are being actively investigated in clinical trials for HNSCC.

Immunotherapy

The FDA has approved two immunotherapeutic agents for HNSCC patients. The first one, pembrolizumab, is a monoclonal antibody directed against the programmed death-1 (PD-1) surface receptor with potential immune checkpoint inhibitory and antitumor effects [8,66]. The second approved PD-1 inhibitor, nivolumab, is a similar monoclonal antibody-based anti-PD-1 drug [9]. These immunomodulators bind to the PD-1 receptor on the surface of activated T cells and block the binding of PD-1 ligands (PD-L1), which leads to activation of a T cell-mediated immune response against tumor cells (Fig. 2) [67]. PD-L1, among other PD-1 ligands, prevents T-cell activation and plays a critical role in tumor evasion of the host immune system [68].

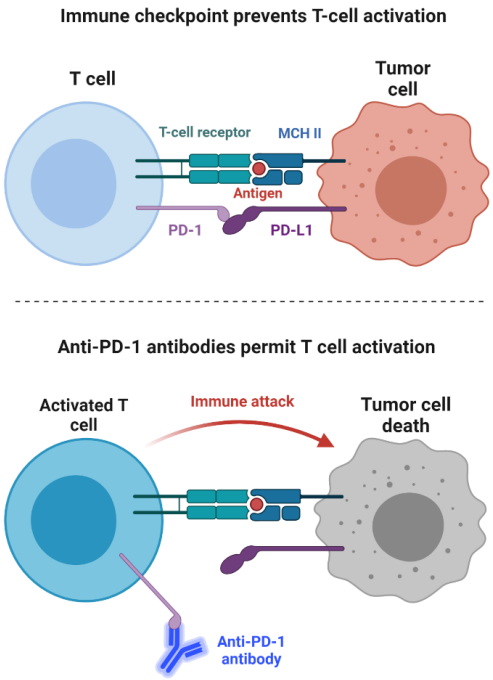

Figure 2 Mechanisms of PD-1 inhibitors. PD-1 inhibitors block the binding of PD-1 and PD-L1 receptors binding allowing the activation of a T cell-mediated immune response against tumor cells. Adapted from "Immune Checkpoint Inhibitor Against Tumor Cell", by Biorender.com (2021). Retrieved from https://app.biorender.com/biorender-templates.

Currently the immunotherapeutic agent can be applied as a second-line treatment after failure of conventional regimens. A recent phase III clinical trial (NCT02252042) reported that treatment with pembrolizumab resulted in a better response (14.6%, 95% CI 10.4 to 19.6) than with the standard regimen (methotrexate, docetaxel, or cetuximab; 10.1%, 95% CI 6.6 to 14.5) for R/M HNSCC [69]. A phase III clinical trial (NCT02105636) for nivolumab reported a 13.3% response rate, which was higher than standard therapy 5.8% [9] In addition, with nivolumab, the overall survival was significantly longer than with a standard therapy (single-agent methotrexate, docetaxel or cetuximab; hazard ratio for death, 0.70; 97.73% CI, 0.51 to 0.96; P = 0.01) [9]. Despite the promising trials, no predictive markers for HNSCC patient response to immunotherapy exist. As a result, patients are unnecessarily exposed to adverse effects and ineffective treatments, particularly drugs with low response rates. A requirement for receiving the PD-1 antibody treatment has been the PD-L1 expression in tumor cells or stroma with a threshold of 1%, but so far, no reliable predictive factors for PD-1 antibodies have been found [8]. Other emerging immunomodulators targeting different molecules, such as PD-L1 and IDO1, are under active investigation.

2.2 DRUG DEVELOPMENT PROCESS

Drug development is a long and multistage process, which typically requires more than 10 years and costs a billion dollars [70]. The drug development process consists of five steps: discovery and development, preclinical research, clinical research, FDA review and FDA post-market drug safety monitoring [71] (Fig. 3). Preclinical oncology includes computer modeling, *in vitro* cell assays and *in vivo* experiments. In *in vitro* studies, the drug candidate is tested in tubes and plates, whereas in *in vivo* studies are conducted in animals, such as in zebrafish and mouse. Preclinical studies determine whether the drug candidate is effective and safe enough to administer to a human in clinical trials. Despite comprehensive investigations, new anticancer agents obtain higher clinical failure rates than in other therapeutic areas [72]. Only 10% of preclinically active anticancer agents are licensed after clinical investigation [73]. The clinical failure rate is much higher in oncology than in other fields, such as 20% for cardiovascular disease.

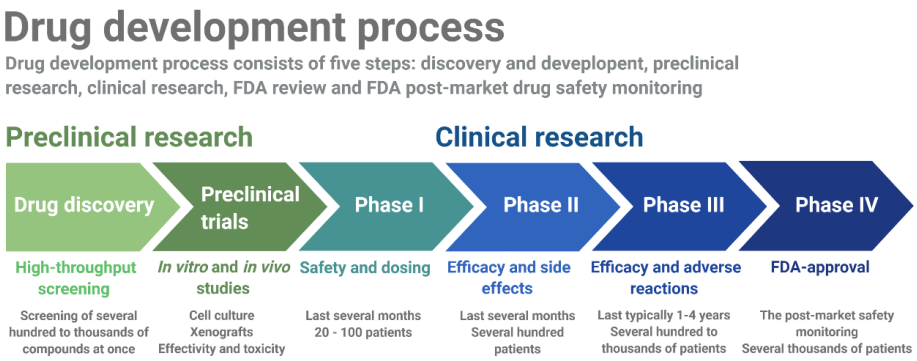

Figure 3. Steps in the drug development process. Created with BioRender.com.

2.2.1 DRUG DISCOVERY AND DEVELOPMENT

Drug discovery is the process where new drug candidates are identified. At this stage, thousands of potential drug candidates are screened at once. Drug libraries contain small molecule compounds including FDA-approved ones, investigational compounds, bioactives, and a diversified sets of chemicals. After an initial screen, only a small portion of the compounds show promising effects and call for a further test [74]. High-throughput screening (HTS) is a method used in drug discovery that utilizes robotics, liquid handling devices, data processing software and sensitive detectors to perform hundreds to millions of tests to identify active compounds in a short period of time [71]. In the development phase, the best dosage and possible toxicity of the drug candidate is investigated further [71].

2.2.2 *IN VITRO* STUDIES

2D and 3D cancer models

In vitro preclinical models have been the basis of research since the first human cancer line was established [3]. In conventional cancer drug testing, cancer cells are cultured on a 2D plastic surface and later in animal models prior to clinical investigations. In recent decades, methods and tools have been improved by shifting from 2D to 3D cell culture, which better mimics a solid tumor tissue's physiological environment and growth pattern [3]. Conventional 2D cell culture lacks appropriate *in vivo* environment-specific intercellular junctions. Additionally, due to the absence of the tumor microenvironment, the cells are unable to form cell-matrix junctions. Cancer cells can be cultured as a monoculture or co-cultured with other cell types, such as stromal fibroblasts, in multicellular spheroids without matrix or with matrix coating (2D) or embedding (3D; Fig. 4a and b) [3]. A number of techniques have been developed to create 3D cell spheroids, such as the hanging drop method [75] and using round bottom ultra-low attachment (ULA) plates (Fig. 4c and d) [76]. Many studies report that 3D spheroid culturing alters cancer cell sensitivity to chemotherapeutics, such as 5-FU, cisplatin, or doxorubicin [3]. Also, the spheroid assay (ULA and hanging drop method) for HNSCC cell lines and patient derived cancer cells have been applied in high-throughput testing using chemotherapy and irradiation [77]. However, spheroids grown in liquid medium still lack essential interaction with extracellular matrix (ECM). The ECM components regulate cell proliferation, differentiation, migration, survival, and adhesion [78]. Moreover, ECM is reported to provide survival and drug resistance signals for cancer cells [79].

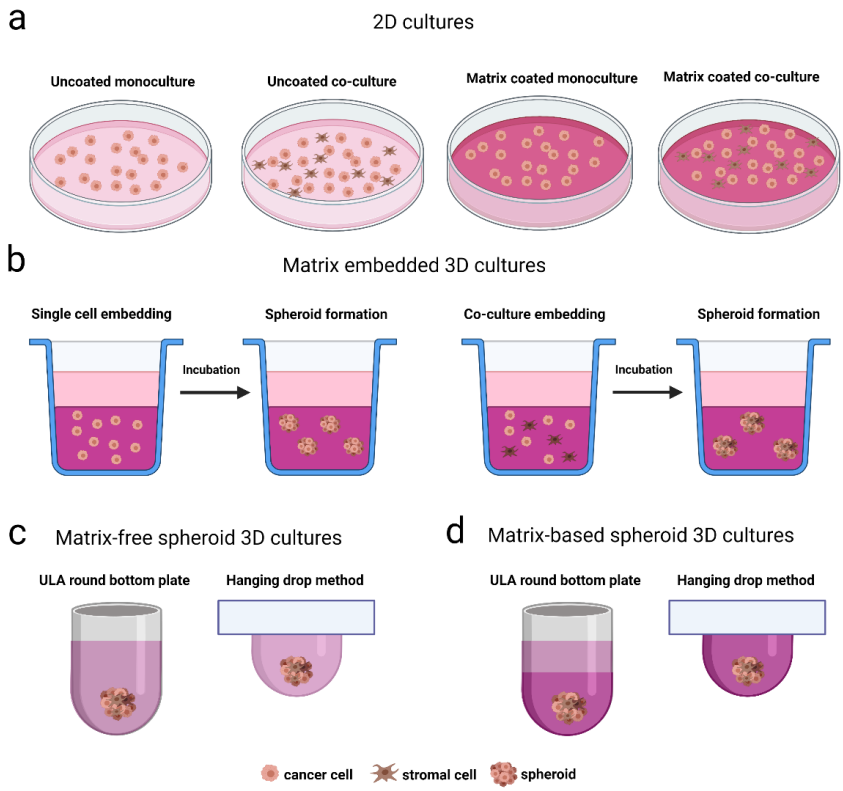

Figure 4. 2D and 3D culture systems. (a) Uncoated or matrix coated mono- and co-cultures. (b) Matrix embedded 3D cell cultures derived from single cells or pre-formed spheroids. (c) Matrix-free and (d) matrix-based spheroid cultures generated using ULA round bottom plates or hanging drop method. Created with BioRender.com.

Matrices for 3D cell cultures

Matrices used in 3D models are available both with a synthetic and a biological origin [80-82]. Synthetic scaffolds are typically applied as hydrogels including polyglycolic acid (PGA), polylactide glycolic acid (PLGA), polypropylene fumarate (PPF), polyethylene glycol (PEG) and polyacrylic acid (PAA) [81,82]. The advantages of synthetic hydrogels are accurate composition and comparability of study results [82]. However, the synthetic hydrogels can never accurately mimic an *in vivo* situation.

Several biological matrices have been developed for 3D cultures, most of which are of animal origin. The downside of biological matrices is the variability between batches. One example of a commercial and widely used biological matrix is Matrigel, which is derived from mouse Engelbrecht-Holm-Swarm (EHS) sarcoma [83]. There are several other equivalent EHS sarcoma-derived

products from different companies available today, such as ECMatrixTM (Millipore), ECM gel (Sigma-Aldric), Cultrex BME (Amsbio) and Geltrex (Gibro Life Technologies). Matrigel contains mainly basement membrane components, such as laminin, type IV collagen and entactin, but also various growth factors, including EGF, transforming growth factor beta (TGF-β) and insulin-like growth factor (IGF-1) [83]. Since collagens are the most abundant proteins in ECM, rodent-derived collagens are typically applied as an ECM mimicking matrix [84]. Collagen Type I derived from rat tail is typically applied in *in vitro* studies. Human-derived matrices such as fibrinogen and fibronectin are also available [85,86]. However, Myogel is the only matrix derived from human tumor [4]. Myogel is prepared by a protocol similar to that of Matrigel. Myogel has been applied successfully in various *in vitro* assays, such as cell adhesion, invasion and migration assays [7]. The protein composition of Myogel and Matrigel overlap by only 34% [4]. Basic ECM components, laminin, collagen IV, heparan sulfate proteoglycans, nidogen and EGF were found in both matrices, whereas Matrigel lacked tenascin-C, collagen XII and XIV, which were present in Myogel [4].

Cancer-on-chip models

Microfluidic chips are cell culture devices produced from optically transparent glass, plastic or flexible polymer, such as polydimethylsiloxane (PDMS) [87]. Chips contain hollow perfused microchannels and chambers populated by living cells to mimic organ-level physiology by recreating tissue-level and organ-level structures and functions *in vitro* [87]. '*Chips*' are named after the computer microchip manufacturing method, which was applied for the first microchip production [87]. Microfluidic chips can be applied to create "tissues chips," using a chamber filled with cells from one tissue type, or more complex "organ chips" where two or more tissue/cell types are used [87]. ECM gels can be applied to fill channels or chambers and viability of the cells and tissues is supported with culture medium [87]. Microfluidic cancer-on-a-chip models have been applied for various cancer types, such as lung [88] and breast [89] cancer. Microfluidic platforms have been created for immunotherapy testing and tracking immune cell behavior toward tumor cells for many tumor types, such as colon cancer and melanoma cells [90,91]. However, immunotherapy *in vitro* testing is challenging, particularly when different cell types, such as cancer cells and immune cells with different adherent properties are co-cultured. Additionally, access to patient samples and clinical information are limiting factors for designing microfluidic chip assays for personalized immunotherapy. In most chip protocols, channels and cancer cells are embedded in animal-derived matrix, Matrigel or collagen, or non-animal derived hydrogels [92], which have limitations in their ability to mimic the human TME.

Patient-derived organoids

Organoid technologies have opened new avenues for the development of more relevant human cancer models, and to build the bridge between *in vitro* cancer research and xenografts [93]. Organoids established from patient tumor samples can be genetically characterized and used for drug testing. Organoids allow a comparison of the genetic background and drug response of the tumor [93]. So far, many organoid cultures have been successfully established from many different tumor types, such as primary colorectal, pancreas, stomach, head and neck, and breast cancer tissues and metastatic colon, prostate and breast cancer biopsies [93-95]. Patient-derived organoids (PDOs) are cultured in a 3D environment and many studies have reported that they recapitulate basic features of the original tumors [95,96]. HNSCC patient-derived organoids are reported to recapitulate EGFR expression levels of the respective tissues [95]. PDOs are typically generated from single cancer cells isolated from tumor samples, which are embedded into ECM matrix, such as Matrigel or collagen to form tumor organoids [95,96]. Tumor stem cells are typically enriched in PDOs using cancer-specific growth factors, which leads to loss of the original tumor heterogeneity and development of a central necrosis over time [93,97]. PDOs have been applied as a potential platform for predicting a patient's drug response in co-clinical trials, disease modeling via gene editing and basic research [95,96,98]. Despite active investigation in personalized drug testing with patient-derived material, the results have not been exploited in clinical practice, although several protocols for drug testing have been suggested.

2.2.3 *IN VIVO* STUDIES

Mice are predominantly used for xenografts, although other model organisms, such as yeasts, African clawed frog (*Xenopus laevis*), nematode (*Caenorhabditis elegans*), fruit fly (*Drosophila melanogaster*) and zebrafish (*Danio rerio*) have been applied for preclinical oncology [99]. Zebrafish larva xenograft is a new promising *in vivo* cancer model, which has been applied for several cancer types, such as gastric, colorectal and head and neck cancer [100-103]. This xenograft possess several advantages, such as a high number of offspring, small size, cost-effectiveness and short assay duration. The zebrafish larva model has been applied to cancer cell proliferation, metastasis, angiogenesis and drug testing assays [103-105].

One common *in vivo* platform in preclinical anti-cancer drug development includes immunodeficient mice, so-called nude mice, in which human cancer cells are grown subcutaneously [106]. In HNSCC xenografts, cancer cells can be also injected orthotopically in the floor of the mouth of athymic nude mice [107]. Nude mice have been used for almost all types of primary solid and

hematological human tumor studies over two decades [106]. Patient-derived xenografts (PDX) obtained by implanting fresh tumor material are now applied in drug discovery and personalized medicine [99]. However, the routine use of PDX has turned out to be challenging due to the low engraftment time, since development of the PDX model for preclinical study typically takes months, which is too long for personalized medicine purposes [108] Another shortfall is the substitution of patient-derived tumor stroma by murine stroma while the tumor grows [108].

Clinical research

While preclinical research is conducted by applying *in vitro* and animal models, clinical research is done in humans [74]. Clinical research consists of four phases (Fig. 3). Phase I typically lasts several months and includes 20 to 100 healthy volunteers or people with disease. The purpose is to investigate safety and dosing. According to the FDA web page, 70% of new drug candidates will enter the next phase (Fig. 3). Phase II investigates efficacy and side effects and requires typically up to several hundred people with the disease. This phase takes several months to two years. Approximately 33% of drugs proceed to the next phase. In phase III, the efficacy and adverse reactions are investigated more extensively. The study length is typically one to four years. Approximately 25–30% of drugs enter the next phase. Phase IV is executed once the drug has been approved by the FDA during the post-market safety monitoring. In this last phase, safety and efficacy of the drug is confirmed in several thousands of patients. Current preclinical drug testing for solid tumors has a low prognostic value since 90% (±5) of current therapeutic approaches fail [73]

Clinical evaluation of anticancer compounds

A typical parameter for evaluating the activity and efficacy of anticancer compounds in solid tumors is Response Evaluation Criteria in Solid Tumors (RECIST) [109]. RECIST defines, based on tumor size, when a patient's tumor responds, stay stable or progresses during treatment. RECIST evaluation is based on computed tomography (CT), magnetic resonance imaging (MRI) or positron emission tomography (PET) scans, and it is divided into four categories: complete response (CR), partial response (PR), stable disease (SD) and progressive disease (PD; Table 4). The objective response rate (ORR) is defined by the FDA as the proportion of patients with tumor size reduction, which sums PR and CR. RECIST criteria have been updated to include metastases (RECIST1.1) [110] and to test immunotherapeutics (iRECIST) [111]. The principles of RECIST 1.1 and iRECIST to determine ORR have remained largely unchanged. However, iRECIST takes into account atypical responses, such as delayed responses that occur after pseudoprogression by measuring also unconfirmed progressive disease (UPD) [111]. Responses

assigned using iRECIST have a prefix of "i" (immune)—e.g., "immune" partial response (iPR) [111]. Other endpoint parameters evaluated in clinical trials are overall survival (OS), disease-free survival (DFS) and progression-free survival (PFS) [109].

Table 4. RECIST evaluation of anticancer compound effects on target lesions.

RECIST tumor response	Definition
Complete response (CR)	Disappearance of all target lesions
Partial response (PR)	At least a 30% decrease in a sum of the longest diameter (LD) of target lesions, taking as reference the baseline sum LD.
Stable disease (SD)	Neither sufficient shrinkage to qualify for PR nor sufficient increase to qualify for PD, taking as reference the smallest sum LD since the treatment started.
Progressive disease (PD)	At least a 20% increase in the sum of the LD of target lesions, taking as reference the smallest sum LD recorded since the treatment started or the appearance of one or more new lesions [72].

2.3 TUMOR MICROENVIRONMENT

Each tissue has its unique mixture of extracellular proteins, cytokines and growth factors secreted by different cell types. Cancer tissue also has a complex and heterogeneous microenvironment that contains cancer cells and stromal cells surrounded by extracellular matrix (ECM) [112] This unique niche around the tumor, comprised of blood vessels, fibroblasts, immune cells, signaling molecules and structural proteins form an entity referred to as the tumor microenvironment (TME; Fig. 5) [113]. Interactions between cancer cells and the TME play a significant role in tumor progression [113]. Tumor cells modify their surroundings by secreting molecules, for instance growth factors, to generate a beneficial environment for tumor progression and metastasis [114]. Therefore, interactions of cancer cells and the TME form an essential field for anticancer research.

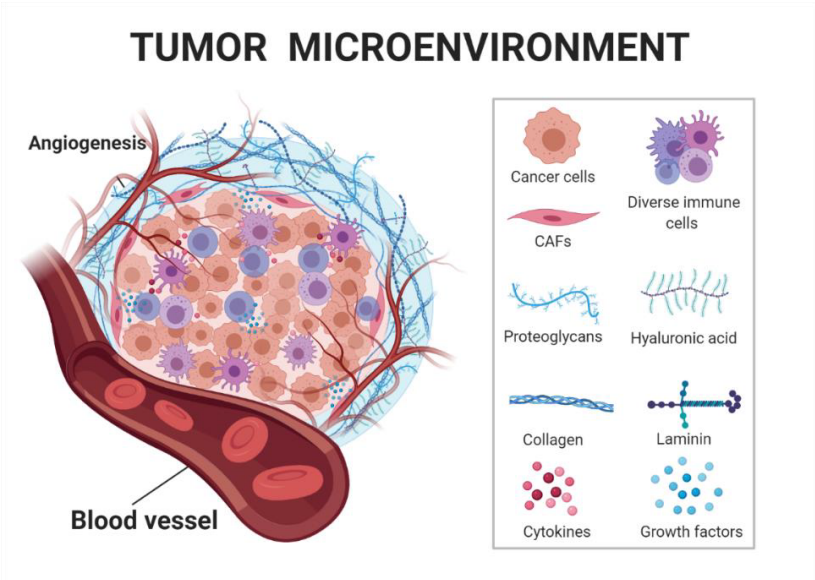

Figure 5. The tumor microenvironment (TME) is a heterogeneous niche consisting not only of tumor cells but also immune cells, cancer-associated fibroblasts (CAFs), endothelial cells and extracellular matrix. Adapted from "Tumor Extracellular Matrix Reduces Therapeutic Efficiency in Solid Tumors," by Biorender.com (2021). Retrieved from https://app.biorender.com/biorender-templates.

2.3.1 EXTRACELLULAR MATRIX

The extracellular matrix (ECM) provides structural support for tissues and organs by forming basement membranes and allowing individual cell movement [112]. ECM is a 3D macromolecular network surrounding the cells containing structural proteins such as collagens, glycosaminoglycans, elastin, fibronectin, and laminin (Fig. 6) [114]. These structural proteins are connected to each other as well as cell adhesion receptors [115]. The cell adhesion receptors transmit signals from the ECM to the cell, thus regulating essential cell functions, including survival, growth, and differentiation. As a dynamic structure, the ECM is constantly re-organized, remodeled and degraded to maintain homeostasis in tissue [114,115].

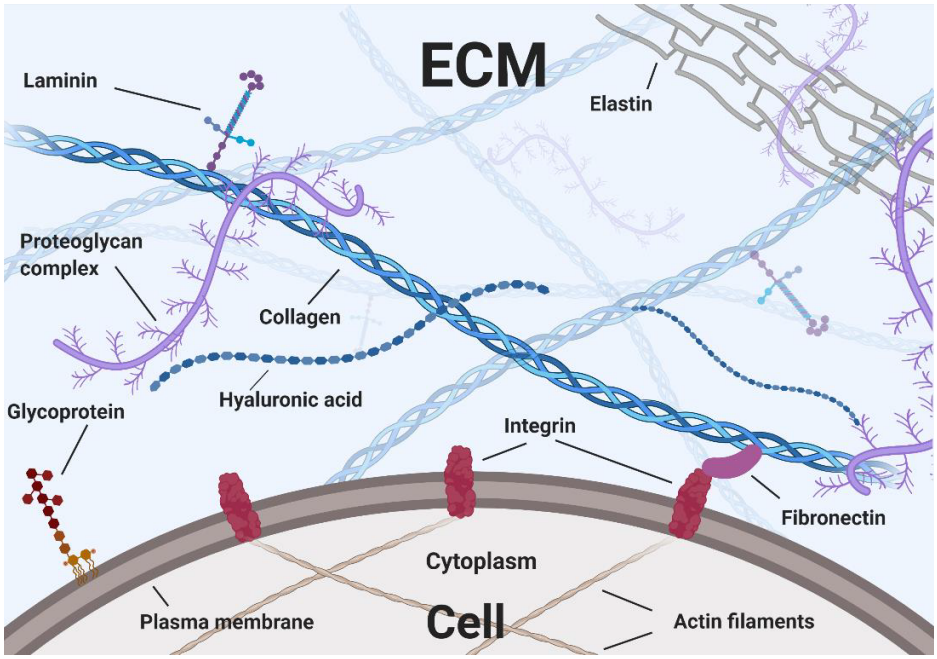

Figure 6. The most abundant proteins in ECM and cell surface adhesion molecules. Adapted from "ECM (Extracellular Matrix)", by Biorender.com (2021). Retrieved from https://app.biorender.com/biorender-templates.

2.3.2 TME CELL TYPES

Fibroblasts

Fibroblasts are involved in all stages of cancer progression, and their structural and functional contributions are well characterized. In physiological conditions, fibroblasts remodel the ECM, regulate epithelial differentiation and inflammation, and are involved in wound healing [116]. Fibroblasts synthesize many proteins, such as type I, III and V collagen and fibronectin [116]. Additionally, fibroblasts secrete ECM-degrading proteases, such as matrix metalloproteinases (MMPs), which play a critical role in homeostasis by balancing the ECM turnover [116]. Cancer-associated fibroblasts (CAFs) are one of the most abundant cell types in the tumor stroma [99,116]. Recent studies associate CAFs to cancer progression and epithelial–mesenchymal transition (EMT) through their ECM remodeling capability and secretion of various soluble factors, such as growth factors and cytokines [116,117]. CAFs also have a role in metabolic and immune reprogramming of the TME, which is reported to have an impact on adaptive resistance to chemotherapy [116,118].

Endothelial cells

Angiogenesis promotes invasion and metastasis and is one of hallmarks of advanced cancers [119]. The majority of HNSCCs (>90%) express angiogenic factors such as vascular endothelial growth factor (VEGF) [119]. Additionally, other angiogenesis promoters, such as interleukin 8 (IL-8) and EGFR are highly expressed in HNSCCs [120]. Various studies have reported angiogenic markers as important prognostic factors, which are associated with cancer progression, increased microvessel density, immune function modulation, and formation of lymph node metastases in head and neck cancer [121].

Immune cells

Immune cells have a critical role in tumor progression. Several studies report that the presence of innate immune cells, such as macrophages type M1 and M2 and natural killer (NK) cells, and adaptive immune cells, T cells and B cells, have major roles in tumor progression [122]. Certain cytokines typically present in TME, such as IL-4, enhance the number of immunosuppressive macrophages [122]. Studies suggest that tumor-associated macrophages (TAMs) promote tumor growth, angiogenesis, tissue remodeling, and antitumor immunity suppression [123]. Another immune cell type, typically present in TME, is the myeloid-derived suppressor cell (MDSC). MDSCs in TME suppress T cells and regulate the innate immune system, and sculpt the TME and pre-metastatic niche [122]. MDSCs promote cancer stem cells properties, and enhance angiogenesis and EMT through IL-6 secretion [122].

Immunoediting is a dynamic process in which the immune system can both protect from and promote cancer development. Immunoediting consists of three phases called elimination, equilibrium, and escape [124]. In the elimination phase, both innate and adaptive immune systems participate to recognize, attack, and destroy abnormal cells, which have escaped the regulatory mechanisms of cell growth [125]. This is the key step for tumor suppression because it promotes immune cell activation and T cell priming, as well as reduction of immunosuppressive signals in the TME and retains the T cells in the tumor tissue [124]. The equilibrium phase occurs if sporadic tumor clones manage to survive the elimination process. In the escape process immunologically sculpted tumors proceed to grow and form immunosuppressive TME [125].

The immunoediting process modulates the tumor microenvironment, also while the patient is receiving immunotherapies [124]. Tumors can be considered as inflamed (hot) or non-inflamed (cold) by the transcriptional signature and number of infiltrated immune cells [124]. Immunologically hot tumors are often rich in infiltrated immune cells, such as CD8+ and CD4+ T cells. Hot tumors typically express PD-L1 [126]. Immunologically cold tumors

are those called “immune-desert”, which lacks T cells in tumor tissue and stroma, or “immune cell excluded,” in which T cells are present in the stroma, but not within the tumor [127]. Patients with these phenotypes tend to have poor immunotherapy responses [127].

Important barriers in the treatment response are innate and acquired resistance [124]. Innate resistance is defined as complete lack of responsiveness of a tumor to therapy. This might be caused by systemic immunosuppression or so-called “immunological ignorance” caused by age or viral infections such as HIV [124].

In acquired resistance, a cancer has initially responded to immunotherapy but relapsed and progressed after a certain period of time [128]. Possible explanations for the relapse are loss of T-cell function or recognition of tumor antigens, or development of mutations which make cancer cells resistant to immunotherapy [128].

2.4 EMERGING TARGETED THERAPIES FOR HNSCC

2.4.1 EGFR SIGNALING IN HNSCC

EGFR is a transmembrane glycoprotein and one of the four members of the ErbB tyrosine kinase receptor family [129]. Ligands, such as growth factors, EGF and TGF-α bind to EGFR and this binding leads to autophosphorylation of EGFR and subsequent activation of signal transduction pathways, which regulate proliferation, differentiation, and cell survival [129]. EGFR is reported to be overexpressed on 80–90% of HNSCCs. However only a few EGFR activating mutations are found in HNSCC [130]. EGFR point mutations occur in 1%–7% of the cases depending on ethnicity [131,132]. EGFR gene amplification varies between studies, from 10 to 30% [38,130]. Additionally, studies report inconsistent data on the prognostic value of EGFR expression levels, since 60% of studies report EGFR associating with a poor prognosis, whereas 40% of studies report a lack of association [130]. EGFR activation promotes downstream signaling pathways, such as the MAPK/ERK and the PI3K/AKT/mTOR signaling pathways (Fig. 7) [130]. In HNSCC, mutations in these pathways are frequent. In the PI3K/AKT/mTOR pathway, somatic mutations in PIK3CA are found in 10–20% and an inactivating mutation of tumor suppressor PTEN is found in 10% of HNSCCs [130].

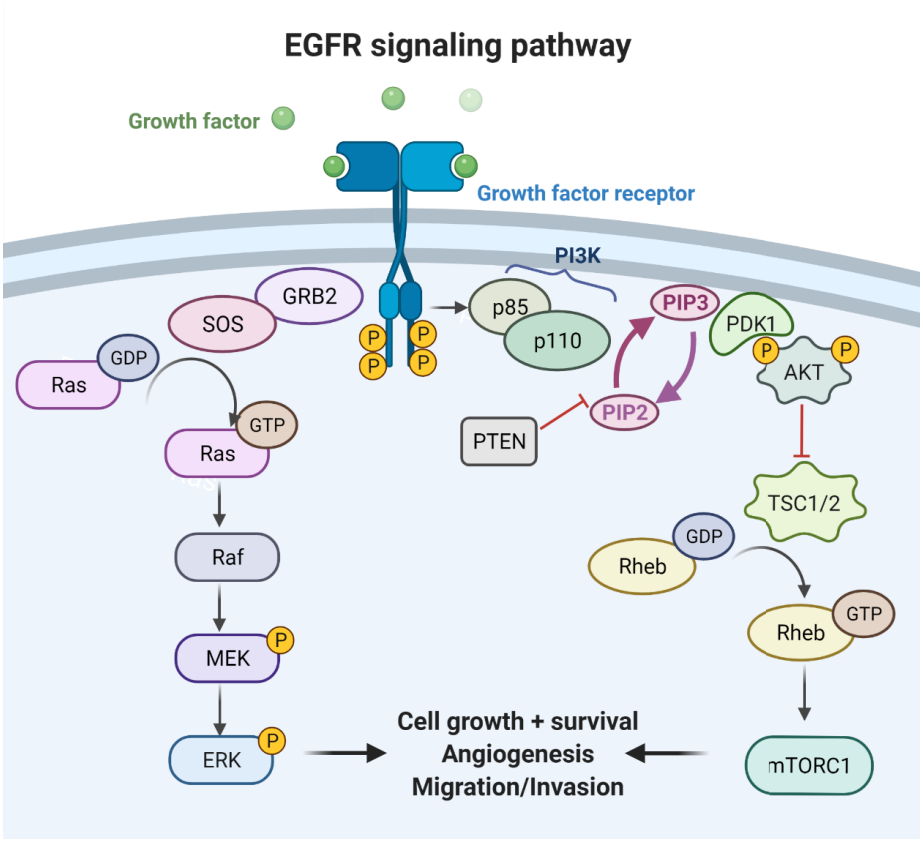

Figure 7. Overview of the EGFR signaling pathway regulating tumor growth and metastasis. Created with BioRender.com.

EGFR inhibitors

EGFR is an extensively investigated biomarker for HNSCC [133] and its inhibitors, such as cetuximab, afatinib, erlotinib and gefitinib have exhibited promising antitumor activity in preclinical studies both *in vitro* and *in vivo* [134-138]. However, most EGFR inhibitors have turned out to be clinically ineffective as a single agent and no predictive biomarkers for EGFR inhibitor responses have been established so far. Despite several novel drug candidates, cetuximab has remained the only FDA-approved EGFR-targeting drug for HNSCC.

Gefitinib (ZD1839; trade name Iressa) is a selective and reversible EGFR inhibitor that targets the intracellular ATP-binding site of the receptor [137]. Gefitinib is indicated in the first-line treatment of patients with metastatic non-small cell lung cancer (NSCLC) with specific EGFR mutations [139]. Studies report that gefitinib exhibits anticancer effects in several HNSCC cell lines [138,140]. However, in clinical investigations gefitinib has produced

disappointing results, since a phase III trial reported that gefitinib failed to significantly improve patients' outcome as compared to methotrexate [141]. Two doses of gefitinib (250 and 500 mg/day) resulted in only weak response rates, 2.7% and 7.6%, respectively. Additionally, the combination of gefitinib and docetaxel did not improve the outcome of HNSCC patients [142].

Erlotinib (trade name Tarceva) is another orally administered, reversible EGFR inhibitor. Erlotinib has been reported to possess only a modest objective response (4.3%) in R/M HNSCC patients [143]. Moreover, one phase II trial reported that erlotinib addition to cisplatin and RT did not increase the response rate or progression-free survival [144]. Moreover, several trials have been terminated due to low accrual (NCT00448240, NCT00412217).

Afatinib (BIBW 2992; tradename Gilotrif) is an irreversible EGFR, human epidermal growth factor receptor 2 (HER2) and HER4 inhibitor. Afatinib is approved as treatment for NSCLC, and has been reported to possess anticancer activity against HNSCC cell lines both *in vitro* and *in vivo* [134,136]. Additionally, *in vitro* studies report synergism between the afatinib–irradiation combination [145]. Afatinib has been actively studied in a clinical trial series called LUX-Head & Neck 1-4. In the phase III trial (LUX-Head&Neck 1) afatinib was compared with methotrexate after platinum-based CT for R/M HNSCC (NCT01345682). The study reported that afatinib was associated with significant improvement in PFS with a manageable safety profile [146]. However, in another phase III trial (LUX-Head&Neck 2; NCT01345669), afatinib administration after chemoradiotherapy did not improve disease-free survival (DFS) [147]. The trial was terminated prematurely due to futility. Still ongoing LUX-Head&Neck 3 is investigating afatinib versus methotrexate for treatment of R/M HNSCC after platinum-based chemotherapy (NCT01856478). The following phase III trial (LUX-Head & Neck 4), which investigated afatinib versus placebo for the treatment HNSCC after chemoradiotherapy, was also terminated due to futility (NCT02131155). Despite the disappointing monotherapy response, the combination of afatinib and RT is now under clinical investigation for HNSCC (NCT01783587).

2.4.2 PI3K/AKT/MTOR PATHWAY

The phosphoinositide 3-kinase (PI3K) pathway (or PI3K/Akt/mTOR) is one of the downstream signaling pathways of the EGFR receptor (Fig. 7) [148]. This pathway has a crucial role in cell differentiation, division, and apoptosis [149]. The PI3K/Akt/mTOR pathway is frequently altered in HNSCC [40,148]. The PI3K-pathway is reported to harbor mutations in 30.5% of analyzed HNSCC tumors (n=151), while only 9.3% of tumors harbored mutations in JAK/STAT and 8.0% in MAPK pathways [150]. Like EGFR, the

PI3K/Akt/mTOR signaling pathway has become an attractive target for the development of cancer therapies in HNSCC.

The PI3K/Akt/mTOR pathway can be activated by a range of signals, such as hormones, growth factors and components of the extracellular matrix. This pathway is stimulated by RTKs, such as EGFR, whose phosphorylation on tyrosine residues leads to phosphorylation and activation of PI3K (Fig. 7) [149]. PI3K is a heterodimer lipid kinase consisting of two subunits, p85 and p110. PI3K catalyzes phosphorylation of phosphatidylinositol-4, 5-bisphosphate (PIP2) into phosphatidylinositol-3, 4, 5-triphosphate (PIP3). The tumor suppressor protein PTEN can antagonize PI3K signaling by dephosphorylating PIP3. Plasma membrane bound PIP3 recruits and activates the serine/threonine-specific protein kinase AKT together with 3-phosphoinositide–dependent protein kinase-1 (PDK1). AKT-regulated target proteins control cell proliferation, growth, and survival [149]. One of the central AKT targets is the mammalian target of rapamycin (mTOR). mTOR is part of the mTOR complex 1 (mTORC1), which regulates cell cycle progression and cell growth by inhibiting and inducing catabolic and anabolic processes [151].

mTOR inhibitors: Temsirolimus and Sirolimus

Sirolimus, also known as rapamycin (trade name Rapamune), is an mTOR inhibitor, which also has immunosuppressive properties [152]. Sirolimus has been derived from the soil bacteria *Streptomyces hygrosopius* [152]. For decades, sirolimus has been used to treat lymphangioleiomyomatosis, coat coronary stents and prevent organ transplant rejection. Sirolimus inhibits T cell activation by reducing its sensitivity to IL-2, IL-4 and IL-15. Sirolimus binds to peptidyl-prolyl cis-trans isomerase (FKBP1B) to create an immunosuppressive complex, which inhibits the activation of mTOR, leading to inhibition of proliferation and cell growth [152]. Temsirolimus, also known as CCI-779 (trade name Torisel) is a soluble ester of sirolimus [153], which selectively inhibits mTOR by binding FKBP12. mTOR is involved in multiple tumor-promoting intracellular signaling pathways [153]. Temsirolimus is used as a first-line treatment for metastatic renal cell carcinoma and mantle cell lymphoma. Everolimus (RAD001, trade name Afinitor) and ridaforolimus (MK-8669) are other selective mTOR inhibitors. Similar to sirolimus, everolimus and ridaforolimus binds to FKBP12 thus inhibiting mTOR [154]. Everolimus is used to treat advanced renal cell carcinoma, pancreatic neuroendocrine tumors (PNET) and hormone receptor-positive advanced breast cancer [155]. Initial indications for ridaforolimus are soft-tissue and bone sarcomas, but it is also tested in clinical trials to treat hematologic malignancies and solid tumors [156].

Dual PI3K/mTOR inhibitors

Dactolisib (BEZ-235) is an imidazoquinoline derivative acting as a dual PI3K/mTOR inhibitor. Dactolisib has been investigated in various cancer types including advanced renal cell carcinoma; however, many trials were terminated due to toxicity and lack of clinical efficacy [157]. Other investigational orally bioavailable PI3K/mTOR inhibitors are apitolisib (GDC-0980), PF-04691502 and omipalisib. A study of apitolisib accessed the safety, tolerability, and modest antitumor effects in patients with solid tumors [158]. One phase I/II trial for apitolisib is recruiting prostate cancer patients (NCT01485861). PF-04691502 is studied as a treatment for many tumors but not yet for head and neck cancer. No clinical trials for omipalisib exist.

2.4.3 MAPK/ERK PATHWAY

Another attractive therapeutic target downstream of the EGFR signaling pathway is the MAPK/ERK pathway (also known as Ras-Raf-MEK-ERK pathway). Abnormal activation of this pathway is reported to occur in more than 30% of human cancers and one-fifth of HNSCCs [159,160]. No predictive biomarkers for MEK1/2-inhibitor responses are established to date, which reduces interest for further development of these inhibitors [159].

Mitogen-activated protein kinase (MAPK) is found in eukaryotic cells [161]. Several studies have categorized four different MAPKs: ERK1 and ERK2, c-Jun N-terminal kinase (JNK), ERK5, and p38 MAPK [161]. ERK activation can occur by various stimuli, such as activation of RTKs, which may lead to cell proliferation, differentiation or apoptosis [161]. The Ras/Raf/MEK/ERK cascade reaction has an important role in transmitting receptor signals from the cell surface to the nucleus, leading to activation of transcription factors and gene expression (Fig. 7) [161]. In brief, Ras recruits and activates the protein kinase Raf. Raf promotes activation of dual-specificity protein kinase MEK1/2 (MAPK/ERK kinase) as well as ERK1/2. Activated ERK1/2 phosphorylates several substrates leading to regulation of different transcription factors and gene expression changes [161]. In tumor cells, several mechanisms can activate the Ras/Raf/MEK/ERK cascade, such as overexpression of EGFR and mutations in genes encoding for cytokines, and receptors such as Fms and Kit [161].

MEK inhibitors

MEK 1 and 2 have become promising therapeutic targets due to their specific structure and substrate specificity [159]. Both MEKs have unique ATP-binding pockets, which allow highly specific targeting [161]. Inhibitor targeting leads to MEK conformational changes, which inactivate the molecule [161]. As an

ATP non-competitive inhibitor, unwanted inhibition of other kinases is reduced [161]. As a single agent, MEK inhibitors have achieved clinical success, however only in a limited number of tumor types with RAS or RAF mutations [159]. The MEK1/2 inhibitor Trametinib (trade name Mekinist) is FDA-approved for the treatment of *BRAF*-mutant melanoma and non-small cell lung cancer [162]. Additionally, it is under active clinical investigation for various other solid tumors. Another MEK1/2 inhibitor, binimetinib (trade names Mektovi), is accepted as treatment for unresectable or metastatic melanoma with BRAF mutations in combination with encorafenib [163]. Various clinical trials are recruiting patients for binimetinib treatment of different solid tumor types, but not yet for HNSCC. Selumetinib (trade name Koselugo) is also a MEK1/2 inhibitor, which was recently accepted by the FDA as a treatment for neurofibroma [164]. Selumetinib is under active clinical investigation. Selective oral MEK1/2 inhibitors, Pimasertib and Refametinib (BAY 86-9766), are under clinical investigation for treatment of solid tumors [165,166], but not for HNSCC. The MEK1/2 inhibitor TAK-733 has been investigated as a treatment for advanced solid tumors [167]. However, it demonstrated limited antitumor activity and further studies are not planned [167].

2.4.4 APOPTOTIC MODULATORS

Apoptosis is a normal process during development, aging and to maintain tissue homeostasis. Additionally, apoptosis occurs as a defense mechanism in immune reactions or when cells are damaged by disease or noxious agents [168]. One cancer hallmark is the ability to resist cell death [169], which is both critical in carcinogenesis and a major obstacle to effective treatment [170]. Radiotherapy is an effective treatment against cancer; however, resistance remains a clinical problem [171]. Irradiation-induced cell death depends on several factors, including dose and fractioning, hypoxia, p53 status, DNA repair capacity, cell cycle phase and the TME [171]. Ionizing radiation produces highly reactive OH• radicals, which induce double-strand DNA breaks (DSB) [172]. In normal cells, unsuccessful DNA repair halts the cell cycle or leads to apoptosis (Fig. 8) [172]. Unsuccessful DSB repair initiates the intrinsic apoptosis pathway [172,173], which is meditated via mitochondrial release of cytochrome c followed by apoptosome formation [173]. Additionally, reactive oxygen species (ROS) production induced by irradiation may lead to extrinsic apoptotic pathway activation via FAS death receptor-meditated caspase activation (Fig. 8) [172] .

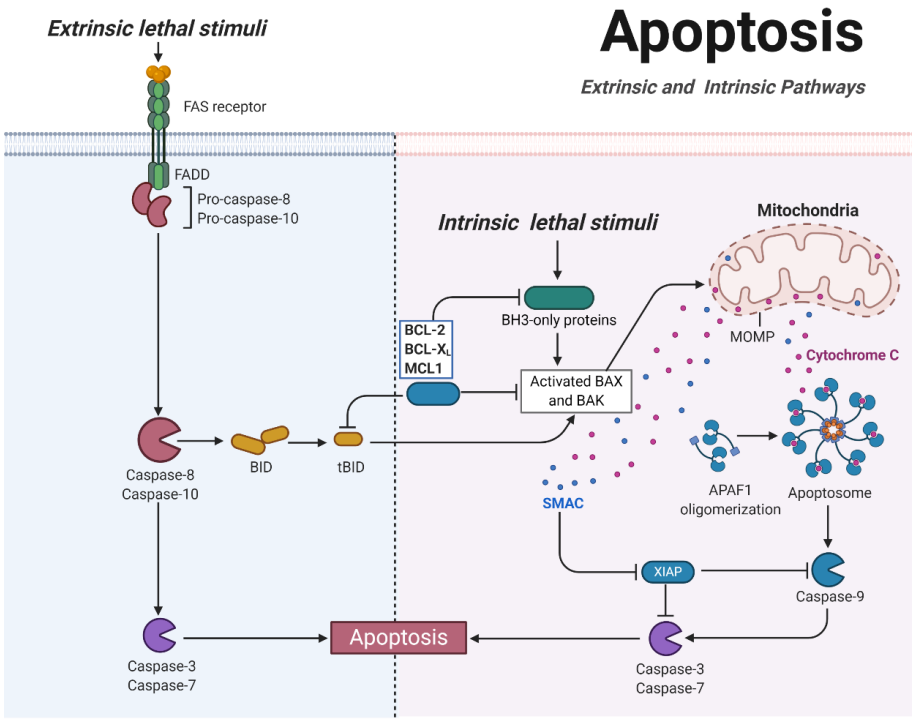

Figure 8. Two major apoptotic pathways; extrinsic and intrinsic pathway. The extrinsic lethal stimuli (ligand) and Fas receptor form the death-inducing signaling complex (DISC), which allows adaptor molecule FADD binding to DISC. This complex activates initiator caspases-8/10 leading to activation of effector caspases-3/7. The intrinsic lethal stimuli activates BH3-only proteins and BAX/BAK meditated cytochrome c release from the mitochondrial outer membrane. Adapted from "Apoptosis Extrinsic and Intrinsic Pathways," by BioRender.com (2021). Retrieved from https://app.biorender.com/biorender-templates.

One of the suggested mechanisms of resistance to anticancer treatments is the alteration in expression of B-cell lymphoma-2 (Bcl-2) family members [170]. The Bcl-2 family consists of three groups based on their functions: anti-apoptotic proteins (Bcl-2, Bcl-XL, Bcl-W, Mcl-1, Bfl-1/A1), pro-apoptotic pore formers (BAK, BAX and BOK) and pro-apoptotic BH3-only proteins (PUMA, NOXA and BIM) [174]. Bcl-2 family proteins control cell death by regulation of mitochondrial outer membrane permeabilization (MOMP), allowing the release of intermembrane proteins to the cytoplasm (cytochrome c) and caspase activation, which leads to apoptosis [174]. p53 promotes apoptosis by directly promoting transcription of pro-apoptotic BAX, PUMA and NOXA [175]. Cytoplasmic p53 may also inhibit anti-apoptotic activity by binding Bcl-2-family proteins [175]. An inactivating mutation of p53 is the most common mutation in HNSCC, accounting for approximately 50% of cases [130]. Based on the Cancer Genome Atlas (TCGA), encoding mutations of procaspase-8 occur in 9% of HNSCC tumors [176]. Caspase-8 plays plays a key role in the

extrinsic apoptosis pathway (Fig. 8). Another alteration in the apoptotic pathway in HNSCC is amplification of the FADD gene (25% of HNSCC), which is a component of the death-inducing signaling complex (DISC) (Fig. 8) [177].

Bcl-2 family inhibitors

Venetoclax (trade name Venclexta) is a selective Bcl-2 inhibitor, which has demonstrated clinical efficacy in hematological malignancies [178]. Venetoclax has been accepted as a treatment for acute myeloid leukemia in combination with other treatments [179]. The safety and efficacy of venetoclax as monotherapy is under active investigation for hematological malignancies. Another promising Bcl-2 family inhibitor is AT-101 (trade name Gossypol), which targets Bcl-2 and Mcl-1. AT-101 has shown a strong apoptotic response in preclinical trials [180]; however, in clinical trials it lacked the expected responses (NCT00286780). AT-101 has been later investigated in combination with other drugs to treat solid tumors, such as head and neck cancer, small-cell lung cancer and different carcinoma types [181-183]. However, these drug combinations did not demonstrate efficacy.

Navitoclax (ABT-263) is an orally active selective Bcl-2 and Bcl-xL inhibitor. Navitoclax has shown *in vitro* and *in vivo* activity against many tumor types alone and in combination with chemotherapy [178]. However, only a few Navitoclax *in vitro* studies exist for HNSCC [184,185], and only one study in combination with irradiation [186]. Navitoclax has been under clinical investigation for leukemia and solid tumors administered as a single agent or in combination with other anticancer drugs [178]. However, the navitoclax-radiotherapy combination remains clinically unexplored and no clinical trials for HNSCC exist.

2.4.5 INVESTIGATIONAL IMMUNOMODULATORS

Several immune checkpoints have been characterized related to cancer, such as indoleamine 2,3-dioxygenase 1 (IDO1), PD-L1, cytotoxic T-lymphocyte-associated protein 4 (CTLA-4) and B7–H3. All these checkpoints have different roles in cancer progression and modulation of immune responses. Immune checkpoint inhibitors, such as anti-PD-L1 monoclonal antibodies, avelumab and durvalumab and an anti-CTLA-4 antibody, tremelinumab, are under active clinical investigation for HNSCC treatment [187].

IDO1 has an important role in both cancer development and progression [188]. IDO1 is an intracellular enzyme that oxidizes tryptophan, which is required for cytotoxic T cell functions [189]. IDO1 secretion by cancer cells and regulatory T cells abrogates antitumor activity of cytotoxic T cells [188](Fig. 9). IDO1 is highly expressed in HNSCC and it is associated with a poor

prognosis and tumor chemoresistance [189,190]. Currently, several IDO1 inhibitors are under clinical development, such as epacadostat (INCB024360), linrodostat (BMS-986205), indoximod, IDO peptide vaccine, and NLG-919 (Navoximod, GDC-0919) [189]. One phase II trial combining nivolumab and epacadostat is recruiting HNSCC patients (NCT03854032), and one phase III trial is currently evaluating the efficacy and safety of pembrolizumab plus epacadostat for R/M HNSCC (NCT03358472). A phase II trial for a linrodostat–nivolumab combination is recruiting patients with stage II-IV HNSCC (NCT03854032). NLG-919, IDO1 vaccine and indoximod has been clinically evaluated as treatment for solid tumors, but not yet for HNSCC.

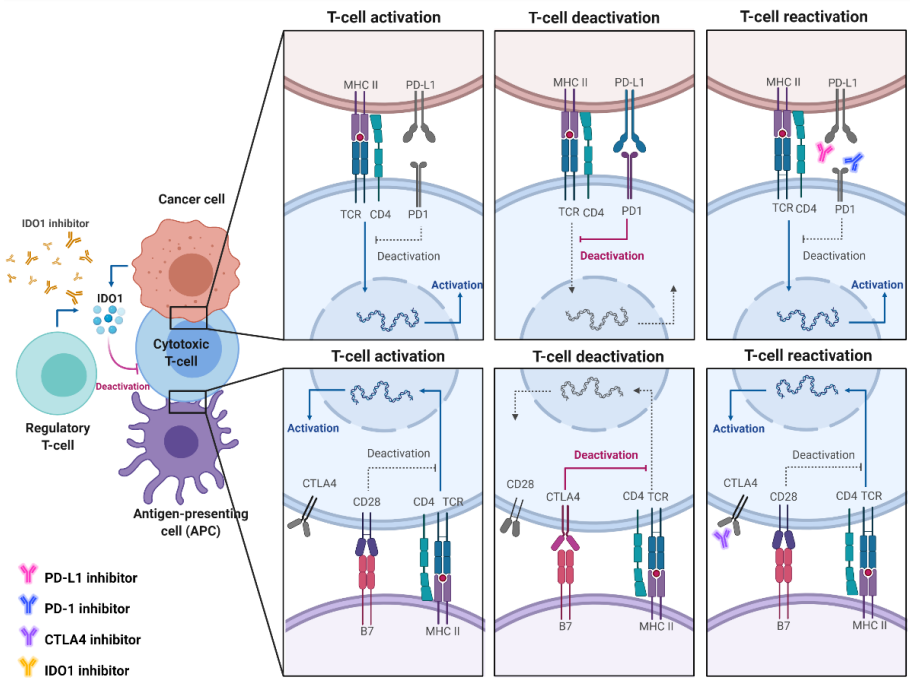

Figure 9. The immunosuppressive roles of IDO1, PD1, PD-L1 and CTLA4 in cancer, and the mechanism of immune checkpoint inhibitors targeting these molecules. Created with BioRender.com.

PD-L1 has been also shown to be highly expressed in HNSCC cells [191]. The engagement of upregulated PD-L1 and PD-1, found in activated T cells, protects the tumor cells from the host immune system through induction of T-cell apoptosis, anergy, exhaustion and expression of interleukin-10 [192]. In a phase I/II clinical trial of durvalumab, which included a group of HNSCC patients, ORR was 17%, and 25% in patients with high PD-L1 expression [187]. Additionally, patients with a high PD-L1 had a disease control rate 44.9%, which was much higher than PD-L1 low or negative patients (21.5%) [187].

Durvalumab has been investigated in HNSCC as a single agent (NCT02207530), in combination with TPF (NCT02997332), and with or without the CTLA-4 inhibitor tremelinumab (NCT02551159) [187]. Another promising anti-PD-L1 antibody is avelumab. Several clinical trials are currently recruiting HNSCC patients to investigate avelumab combined with other treatments [187]. A phase I study has evaluated the safely of avelumab and concurrent cetuximab-RT regimen in L/A SCCHN (NCT02938273). However, a phase III trial evaluating avelumab and standard care was terminated due to futility (NCT02952586) [193]. Recruitment of HNSCC patients for trials combining avelumab with other treatments such as radiotherapy with cyclophosphamide (NCT03844763) or cetuximab or palbociclib are ongoing (NCT03498378).

CTLA-4 is a surface protein expressed on T cells, and when bound to surface protein B7 of antigen-presenting cells (APC), it results in T-cell inactivation (Fig. 9) [194]. CTLA-4 is transported to the cell surface upon antigen stimulation. CTLA-4 has greater affinity to bind to B7 than T-cell activating receptor CD28 [194]. By limiting CD28-mediated signaling, CTLA-4 increases the T-cell activation threshold, lowering immune responses to weak antigens such as tumor antigens [194]. The CTLA4 antibody ipilimumab (trade name Yervoy) was the first tested immune checkpoint inhibitor, which is now approved as a treatment for melanoma, renal cell carcinoma, colorectal cancer and many other [195]. Currently, several clinical trials for another CTLA-4 targeting antibody, tremelimumab (ticilimumab), are ongoing for HNSCC [187].

B7-H3 (CD276) is a B7 family protein and immune checkpoint, which interacts with other immune checkpoint molecules such as PD-1, DC28 and CTLA4 [196]. B7-H3 is highly overexpressed in various solid cancers, such as colon, breast, and pancreatic cancers [197]. High B7-H3 expression is known to correlate with a poor clinical outcome and negative prognosis in patients. However, the mechanism underlying B7-H3 function in cancer has remained unclear [196,198]. B7-H3 expression is also significantly upregulated in oral cancer tissue and associated with poor survival [199]. However, a retrospective study reported significant association between high B7-H3 expression and poor survival with only immune hot tumors [200]. A B7-H3 inhibitor antibody called 8H9 is currently clinically investigated for peritoneal cancer (NCT01099644), and neuroblastoma and sarcoma (NCT00089245) [196]. The other antibody anti-B7.H3, enoblituzumab (MGA271), is under clinical investigation against various solid tumor types, such as melanoma, prostate ovarian and HNSCC [196].

AIM OF THE STUDY

The general aim of this thesis was to develop reliable *in vitro* models by providing ECM that recapitulates the human tumor tissue. These pre-clinical models are important for the development of a personalized medicine approach to cancer treatment.

The aims of this were:

1. To test whether the use of Myogel matrix derived from human tumor leiomyoma could improve the reliability of a drug screen compared to conventional 2D plastic or commonly used mouse sarcoma–derived Matrigel.
2. To identify effective synergistic compound–irradiation combinations for HNSCC cell lines cultured on Myogel matrix using high-throughput drug screening.
3. To introduce the first humanized *in vitro* microfluidic chip assay to test immunotherapeutic agents for HNSCC patient samples. This assay could be useful in predicting the efficacy of immunotherapeutic drugs for individual patients.

3 MATERIALS AND METHODS

3.1 CELLS AND CELL CULTURE

We used 12 HNSCC cell lines established at the University of Turku by Professor Reidar Grénman [201], one cell line established at the University of Oulu by Professor Tuula Salo's group (*Studies I and II*), and one commercial oral cancer cell line (HSC-3; Japan Health Sciences Foundation, Japan; Study III). The details of the HNSCC cell lines are presented in Table 5. Cell lines were cultured in Dulbecco's modified Eagle's medium (DMEM)/F-12 (Gibco, Paisley, UK) supplied with 10% heat-inactivated fetal bovine serum (FBS), 100 U/ml penicillin, 100 µg/ml streptomycin, 250 ng/ml fungizone (amphotericin b) and 50 µg/ml ascorbic acid (all from Sigma-Aldrich, St. Louis, MO, USA). Cell lines were tested for mycoplasma, using the PCR Mycoplasma Test Kit I/C (PromoKine, Heidelberg, Germany).

Table 5. Clinical and pathological characteristics of the HNSCC cell lines used in the original publications.

Cell line	Sex[a]	Age[b]	TNM	Specimen site	Type[c]	Grade	Study
UT-SCC-8	M	42	T2N0M0	larynx	pri	G1	I, II
UT-SCC-14	M	25	T3N1M0	tongue	pri(per)	G2	I, II
UT-SCC-24A	M	41	T2N0M0	tongue	pri	G2	I, II
UT-SCC-24B	M	41	T2N1M0	neck	met(per)	G2	I, II
UT-SCC-28	F	48	T2N0M0	floor of mouth	pri(per)	G1	I, II
UT-SCC-42A	M	43	T4N3M0	larynx	pri	G3	I, II
UT-SCC-42B	M	43	T4N3M0	neck	met	G3	I, II
UT-SCC-40	M	65	T3N0M0	tongue	pri	G1	I, II
UT-SCC-44	F	71	T4N2BM0	gingiva of mandibula	pri(per)	G3	I, II
UT-SCC-73	F	86	T1N0M0	tongue	pri	G2	I, II
UT-SCC-81	M	48	T2N0M0	tongue	pri	G1	I, II
UT-SCC-106A	M	37	T1AN0M0	larynx	pri	G1	I, II
OU-SCC-9B	M	55	T4N3M1a	neck*	met	G2	II
HSC-3	M	64		tongue	met		III

[a]M=male, F=female, [b] Age in years, [C]Pri=primary tumor, met=metastasis, per= persistent disease
***Primary tumor location: tongue**

3.2 PATIENT MATERIAL AND SAMPLE COLLECTION

Patient samples (Study III)

Patient volunteers donated samples after they signed the informed consent. Clinical and pathological characteristics of the patients are shown in Table 6. The fresh tumor samples were collected directly from the operating room and placed in ice-cold Hanks' Balanced Salt solution (HBSS; supplied with 100 U/ml penicillin, 100 µg/ml streptomycin and 250 ng/ml fungizone, Thermo Fisher Scientific, Waltham, MA, USA). The samples were taken from the vital tumor tissue area close to the center of the tumor to ensure a high proportion of live carcinoma cells and some cancer associated fibroblasts. Tissue samples were transferred to a Petri dish containing HBSS and placed on ice. Necrotic tissue and blood clots were cut out using a scalpel. The remaining vital tissue was transferred to a new Petri dish containing fresh HBSS and cut into small tissue pieces (1-2 mm) using a scalpel. The tissue pieces were transferred to a 15 ml falcon tube using a 1000 µl pipette and centrifuged for 5 min at 1000 rpm at 4°C. The tissue pieces were washed by discarding the supernatant and replacing it with fresh HBSS followed by another centrifugation round. The washing step was repeated twice. After the last centrifugation, the supernatant was replaced with 5 ml HBSS buffer containing 1 mg/ml collagenase type I from Clostridium histolyticum (Sigma-Aldrich) and placed on a rocker platform at 37°C for 2 h. After collagenase digestion, the tube was centrifuged, and the supernatant replaced with a fresh HBSS. The washing step was repeated twice and the digested sample filtered using a 100 µm cell strainer (Falcon CellStrainer, FisherScientific, NH, USA). The flow-through, containing single cells and small cell aggregates, was centrifuged. The supernatant was removed, and single cells were mixed with DMEM/F-12.

Table 6. Clinical and pathological characteristics of the HNSCC patients.

Patient	Sex[a]	Age[b]	TNM	Specimen site	Grade	Study
1	F	73	T3N0M0	Gingiva	G3	III
2	F	80	T2N0M0	Buccal mucosa	G2	III
3	F	68	T4aN0M0	Overlapping lesion of unspecified parts of mouth	G1	III
4	M	61	T2N0M0	Mobile tongue	G3	III
5	M	53	T3N0M0	Mobile tongue	G2	III

[a]M=male, F=female, [b] Age in years

Isolation of serum and human peripheral blood mononuclear cells (PBMCs) from the buffy coat (III)

For the serum collection, blood was collected into the collection tubes (BD Vacutainer, Franklin Lakes, NJ, USA, ref 367624) and allowed to clot at room temperature without disturbance for 30 min. The tubes were then centrifuged

at 2000 rpm for 10 min at 4°C, and the supernatant (serum) was carefully transferred into new tube.

Human peripheral blood mononuclear cells (PBMCs) were separated from a buffy coat of three healthy blood donors provided by the Finnish Red Cross Blood Transfusion Service and from blood samples of two HNSCC patients. We used a Ficoll–Paque PLUS (GE Healthcare, Piscataway, NJ, USA) density gradient technique to separate PBMCs. PBMCs consist of lymphocytes (T cells, B cells, NK cells) and monocytes.

3.3 THREE-DIMENSIONAL MATRICES AND CULTURING CONDITIONS

Study I: We designed five culturing conditions (Fig. 10) for each clear-bottom 384-well plate (Corning #3764, NY, USA). For 3D cell culture, we ensured proper gelation of Myogel by mixing type I rat collagen (500 μg/ml; Corning) and 1 N sodium hydroxide with Myogel (500 μg/ml). Before use, matrices (Myogel and Matrigel; Corning; cat no. 354234) were thawed overnight on ice (+4 ◦C). Pipette tips and other equipment were precooled in a freezer (-20 ° C) and 384-well plates on ice before use. Matrices were diluted with a serum-free culture medium to 500 μg/ml. The matrices were added to the plates with an electronic pipette (5 μL, VIAFLO II, Integra, Zizers, Switzerland) followed by brief centrifugation for 2 min at 300 rpm at 4 °C. In control plates, the matrix was replaced with a serum-free culture media. The plates were incubated overnight (+37 ◦C). On the next day, the cells were counted using a Scepter cell counter (Merck Millipore, Burlington, MA, USA) and suspended at the desired density (500 cells per well). The cell density was optimized based on previous studies to avoid confluence on the last day [202,203]. For the 2D culture wells, cell seeding was performed using a MultiFlo FX automated reagent dispenser (20 μL, 25 000 cell/ml, 500 cell/well). For the 3D cultures, cells were first mixed with the matrix (Myogel + collagen or Matrigel) and administered with a Viaflo II electronic pipette (10 μL, 50 000 cells/ml, 500 cell/well). After 60 min incubation, culture medium was pipetted on top of the solidified matrix and the plates were placed back into the incubator. On the following day, the plates were ready for the drug screen.

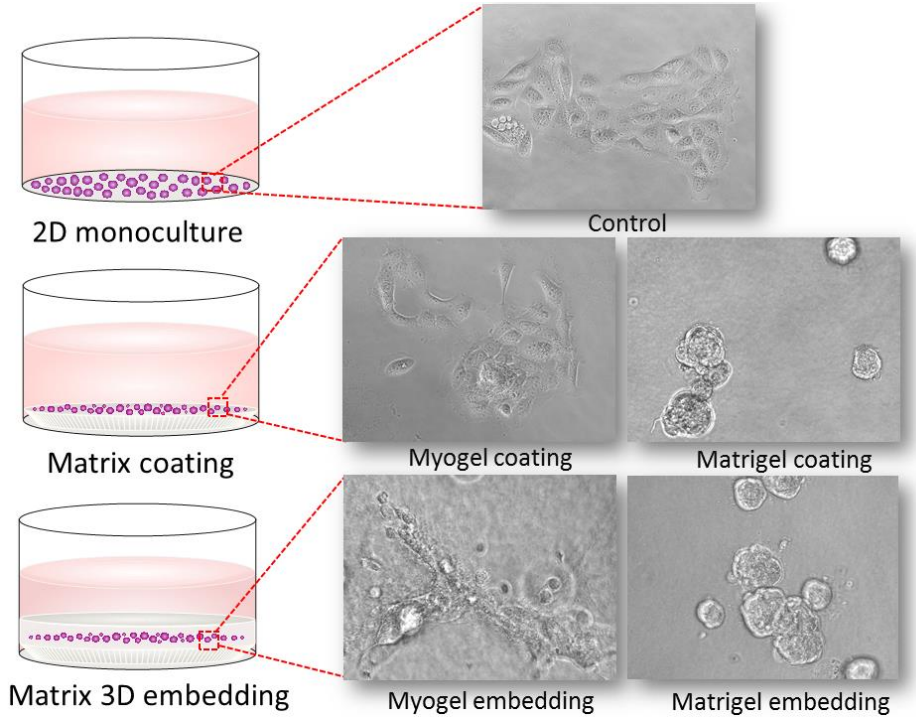

Figure 10. Cells were cultured in five conditions plastic (2D), Myogel coated (2D) and embedded (3D) and Matrigel coated (2D) and embedded (3D). Within Matrigel, UT-SCC-8 cells formed spheroids, while within Myogel, cells form invasive branches.

Study II: We used Myogel (5 µl, 500 µg/ml) coated wells. All the matrix addition was performed by a HighRes Biosystems automation platform (HighRes Biosolutions, Beverly, MA, United States).

Study III: In order to provide a fully human 3D matrix for cancer cells, we replaced the previously used type I rat collagen with human fibrinogen (Merck, Darmstadt, Germany). Fibrinogen (0.5 mg/ml) and thrombin (Merck, final concentration: 0.3 U/ml) was combined to form a fibrin hydrogel.

Like all biological matrices, Myogel varies between lots. To minimize this variation, we have pooled together several myomas from different patients for Myogel production. Different lots are uniquely coded. The same Myogel lot (270117) was used throughout all projects (I-III). The lot was a combination of 14 different myomas (total volume 280 ml).

3.4 HIGH-THROUGHPUT SCREENING

We performed drug sensitivity and resistance testing (DSRT) to quantitatively profile drug responses of HNSCC cells cultured in different matrices (*Study I*), and to identify the synergy between ionizing radiation and 396 anticancer compounds (*Study II*). The DSRT protocol was previously adapted from a method for leukemia cells designed by the High Throughput Biomedicine Unit (HTB) at the Institute for Molecular Medicine Finland (FIMM) [203].

Compound libraries

Study I: We used 19 anticancer compounds, targeting the epidermal growth factor receptor (EGFR), MEK, and PI3K/mTOR (Table 7). The HTB unit designed the custom plates for DSRT and provided all drugs except cetuximab (Erbitux, Merck KGaA, Darmstadt, Germany). For DSRT, drugs were tested over five tenfold concentrations in three replicate wells, and normalized against positive (100 µl benzoyl chloride, BzCl) and negative (0.1% dimethyl sulfoxide, DMSO) controls. Drug plates were stored in pressurized inert nitrogen gas–filled storage pods (Roylan Developments Ltd., Surrey, UK). Cetuximab was added to the plates using an Echo525 acoustic dispenser (Labcyte, San Jose, CA, USA).

Table 7. List of the anticancer compounds screened in Study I.

Compound	Class	Mechanism/Targets	Min (nM)[a]	Max (nM)[b]
Afatinib	Kinase inhibitor	EGFR inhibitor	0.099	989.011
Canertinib	Kinase inhibitor	pan-HER inhibitor	0.989	9890.110
Gefitinib	Kinase inhibitor	EGFR inhibitor	0.989	9890.110
Erlotinib	Kinase inhibitor	EGFR inhibitor	0.989	9890.110
Refametinib	Kinase inhibitor	MEK1/2 inhibitor	0.989	9890.110
Binimetinib	Kinase inhibitor	MEK1/2 inhibitor	0.099	989.011
Selumetinib	Kinase inhibitor	MEK1/2 inhibitor	0.989	9890.110
Trametinib	Kinase inhibitor	MEK1/2 inhibitor	0.025	247.253
Pimasertib	Kinase inhibitor	MEK1/2 inhibitor	0.989	9890.110
TAK-733	Kinase inhibitor	MEK1/2 inhibitor	0.099	989.011
Dactolisib	Kinase inhibitor	PI3K/mTOR inhibitor	0.099	989.011
PF-04691502	Kinase inhibitor	PI3K/mTOR inhibitor	0.989	9890.110
Apitolisib	Kinase inhibitor	PI3K/mTOR inhibitor	0.989	9890.110
Omipalisib	Kinase inhibitor	PI3K/mTOR inhibitor	0.099	989.011
Everolimus	Rapalog	mTOR inhibitor	0.010	98.901
Temsirolimus	Rapalog	mTOR inhibitor	0.010	98.901
Ridaforolimus	Rapalog	mTOR inhibitor	0.010	98.901
Sirolimus	Rapalog	mTOR inhibitor	0.010	98.901
Cetuximab	Monoclonal antibody	EGFR inhibitor	0.005*	49.451*

***µg/ml, a=lowest drug concentration, b=highest drug concentration**

Study II: We utilized a drug library of 396 experimental and FDA-approved compounds (Fig. 11). Most compounds were dissolved in DMSO; however, 19 drugs (metabolic modifiers and platinum-based drugs) were diluted in water due to stabilization issues and poor solubility. The majority of compounds were classified as kinase inhibitors (n=208), differentiating/epigenetic modifiers (n = 73) or chemotherapeutic agents (n = 50). The compound library contained also hormone therapy drugs (n = 19), apoptotic modulators (n = 10), immunomodulatory drugs (n = 9), metabolic modifiers (n=7) and mTOR inhibitors (n = 4, Fig. 11). In one drug set, compounds were applied in six plates (384-well plate, Corning, #3764) in five ten-fold concentrations. Drug sets were stored in pressurized inert nitrogen gas–filled storage pods (Roylan Developments Ltd). DMSO (0.1%) was used as a negative control and BzCl (100 µM) as a positive control.

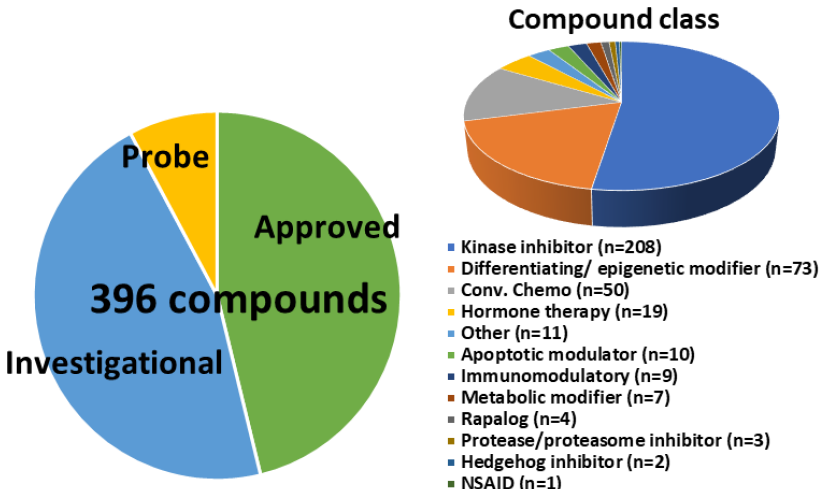

Figure 11. The library of 396 FDA-approved and experimental agents used in Study II. The majority of compounds were investigational (46%) and FDA-approved (46%), whereas 8% were probes. The library contained kinase inhibitors and other signaling pathway modulators.

High-throughput screen workflow

Study I: Anticancer compounds were added on cultures 24 h after cell seeding. First, a culture medium was added into the drug-containing plates by the MultiFlo FX automated reagent dispenser and the plates placed on a shaker for 60 min at 1000 rpm. Diluted compounds were added onto the cell culture plates using a Biomek FX pipetting robot (10 µl/well, Beckman Coulter, Brea, CA, USA). After the compound administration, the final well volume was 35 µl. After 72 h of culturing, the CellTiter-Glo 2.0 (CTG, Promega, Madison, WI, USA) luminescent viability assay was used to determine the efficacy of the drugs (Fig. 12). Before the viability determination, the plates were imaged

using an Incucyte live cell imaging system (Sartorius, Göttingen, Germany). For the viability assay, the plates were placed at room temperature for 15 min and CTG was added to the assay plates using a MultiFlo FX automated reagent dispenser (30 µl/well). The plates were placed on a shaker for 10 min at 450 rpm and centrifuged for 5 min at 1000 rpm. The viability (luminescence) was recorded using the PheraStar plate reader (BMG Labtech GmbH, Ortenberg, Germany).

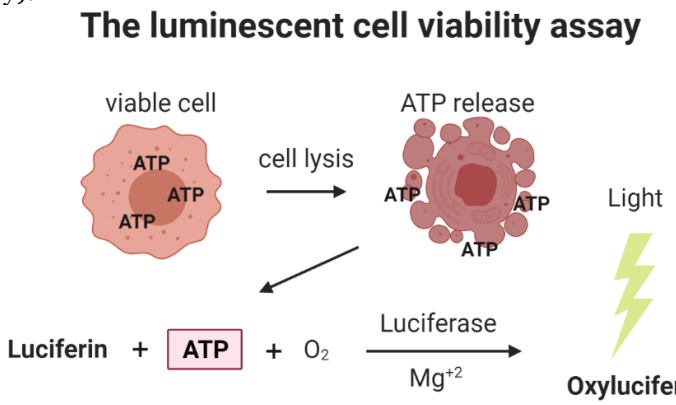

Figure 12. Illustration of CellTiter-Glo (CTG) luminescent cell viability assay. The CTG assay is a homogenous method resulting in cell lysis and generation of a luminescent signal proportional to the amount of ATP present. The method relies on the luciferase reaction, which catalyzes the mono-oxygenation of luciferin in the presence of Mg^{2+}, oxygen and ATP. Created with BioRender.com.

Study II: We utilized the HighRes Biosystems automation platform (HighRes Biosolutions), a benchtop robot (ACell, HighRes Biosolutions), an ambient storage hotel (Cytomat 24, Thermo Fisher Scientific) and an automated incubator (Cytomat 10C, Thermo Fisher Scientific). First, Myogel was diluted to 500 µg/ml concentration with a serum-free culture medium. Myogel dilution was applied to previously manufactured 384-well compound plates using a reagent dispenser (MultiFlo FX, BioTEK). The plates were centrifuged for 20 sec at 1000 rpm at room temperature (Agilent VSpin, Santa Clara, CA, United States) and placed in an automated incubator. On the next day, Scepter 2.0 was used to count the cells and the cells were diluted to the desired density (500-750 cell/well). Cells were seeded to previously coated drug plates utilizing an automated system and reagent dispenser (MultiFlo FX, 20 µl/well). On the following day, the plates were irradiated by a gamma irradiator OB29/4 (STS, Braunschweig, Germany) using EC20 irradiation doses. To ensure similar handling of control and irradiated plates, control plates were also transported to the irradiator room. After irradiation exposure, all plates were moved back to an incubator. After two days, the CTG assay was performed using an automated system. The plates were cooled (to room temperature) for 15 minutes and 25 µl of CTG was applied to the assay plates with a Certus flex dispenser (Fritz Gyger AG, Gwatt, Switzerland). Signal was detected using the PheraStar FS HT plate reader.

DSRT Data Analysis

For profiling the drug responses, we calculated the drug sensitivity score (DSS) using the Breeze software developed at HTB FIMM (available at https://breeze.fimm.fi) [204]. DSS improves the identification of drug response vulnerabilities in cell lines and among patients [203], capturing several parameters (IC50, the curve slope and the minimum and maximum responses) into a single metric [205]. The drug effect was normalized against negative (DMSO) and positive (BzCl) controls to generate the dose–response curves for each drug in each cell line and condition (Study I: matrix and Study II: ±irradiation) separately. The high data quality was confirmed by Z'-factor (should be ≥0.5), which is a typical quality control measurement for an HTS screen [206]. Z'-factor is defined in terms of four parameters: the standard deviations (σ) and means (μ) of both the positive (c+) and negative (c-) controls:

$$Z' = 1 - \frac{(3\sigma_{c+} + 3\sigma_{c-})}{|\mu_{c+} - \mu_{c-}|}$$

Study I: The pipeline and scripts were created using the R programming language. Based on DSS values, we divided the drug response into four activity groups based on a previous study (Table 8) [205].

Table 8. Drug responses divided into four activity groups based on drug sensitivity score (DSS).

DSS value	Drug response
< 5	inactive
5≥ DSS < 10	low activity
10≥ DSS < 15	moderate activity
DSS≥15	high activity

Study II: Cell lines were screened with two drug sets. One set represented control (a single agent) and the other set was irradiated with the EC20 dose optimized previously (compound–irradiation combination). To determine the synergistic and antagonistic effects, selective DSS (ΔDSS) was calculated by subtracting the DSS for the compound–irradiation combination from a single agent DSS (Fig. 13a). A positive ΔDSS value was classified as a synergistic and a negative ΔDSS value as an antagonistic compound, respectively. Based on ΔDSS values, the fifteen most promising synergistic and antagonistic compounds were further validated in a dose–response matrix analysis (Fig. 13b).

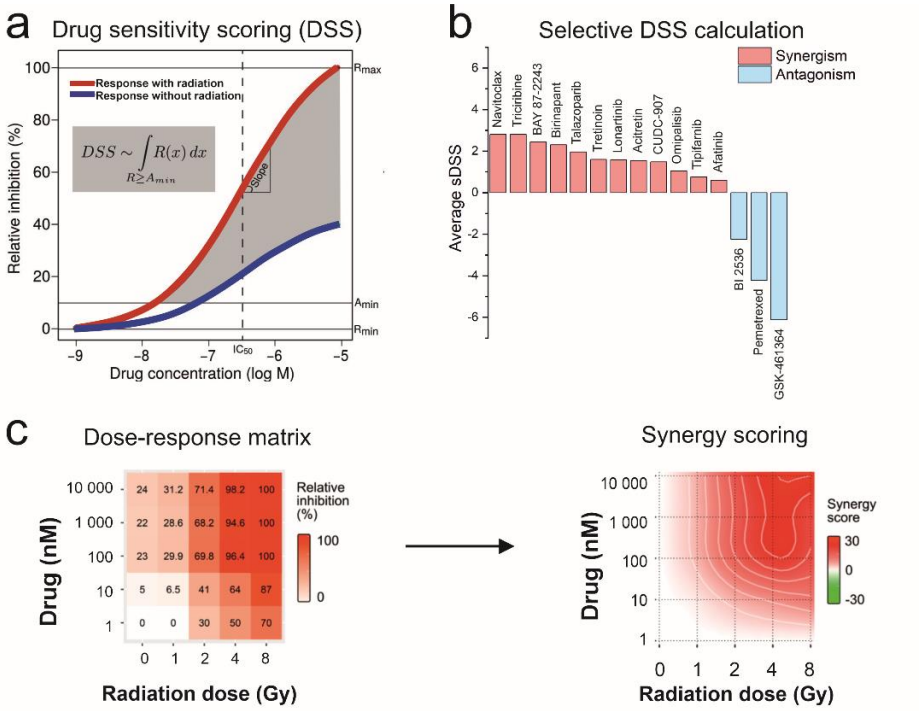

Figure 13. (a) Synergistic and antagonistic irradiation–compound combinations for HNSCC cells cultured on Myogel were first detected by calculating drug sensitivity score (DSS) and selective ΔDSS. (b) Based on average ΔDSSs, the most synergistic and antagonistic drugs were further investigated with multiple irradiation doses using the Synergy Finder web application, https://synergyfinder.fimm.fi (c).

Dose–response matrix analysis and synergy scoring (Study II)

For the synergy validation, we used custom-made 384-well plates with 15 compounds in five ten-fold concentrations in three replicate wells for the five HNSCC cell lines used previously. Each cell line was seeded onto five plates, which were irradiated with different doses: 0, 1, 2, 4 and 8 Gy. Otherwise, we used the same HTS workflow as described previously. To test synergism and antagonism, the observed responses were compared with the expected combination responses. Expected combination responses were calculated and the dose–response matrices were created using the ZIP reference model with the SynergyFinder 2.0 web application (Fig.13c) [207,208]. Based on the ZIP synergy scores, the compound–irradiation combinations were classified as noninteractive, antagonistic or synergistic (Table 9).

Table 9. The classification of drug-irradiation combination based on the synergy score values.

Synergy score (S)	Drug response
S≤ -10	strong antagonism
-5> S < -10	moderate antagonism
-5 > S < 5	noninteractive
5≥ S < 10	moderate synergy
S ≥ 10	strong synergy

The Western blot analysis of EGFR, ERK1/2 and pERK1/2 expression in cells cultured on plastic, Matrigel and Myogel (Study I)

For protein expression analysis, we seeded cells on 25 cm^2 non-coated, Myogel or Matrigel (1.0 mg/ml) coated flasks (750,000 cell/flask). We used five cell lines (UT-SCC-24A, UT-SCC-24B, UT-SCC-42A, UT-SCC-42B, UT-SCC-81), which showed different efficacy of EGFR and MEK inhibitors in Myogel as compared to the other culturing conditions. After culturing cells in normal culture medium for 48 hours, the flasks were washed three times with PBS and serum-free Opti-MEM (Gibco) was added. The cells were washed twice with PBS after 24 hours of culturing and lysed with a lysis buffer (50 mM TrisHCl, pH 7.5, 10 mM CaCl2, 150 mM NaCl, 0.05% Brij35; Sigma-Aldrich) containing complete protease inhibitor cocktail (Roche, Basel, Switzerland) and PhosSTOPTM phosphatase inhibitor (Roche).

The cell debris was removed using centrifugation and a DC Protein assay (Bio-Rad Hercules, CA, USA) was used to measure the protein concentrations. 30 µg of soluble protein was separated by 12% sodium dodecyl sulfate polyacrylamide gel electrophoresis (SDS-PAGE) and transferred to an Immobilon P membrane (Merck Millipore). Odyssey Blocking Buffer (LI-COR Biosciences, Lincoln, NE, USA) was used to block the membrane, followed by overnight incubation in +4◦C with 1:1000 rabbit anti-EGFR (D38B1; Cell Signaling Technology, Danvers, MA, USA), 1:1000 rabbit anti-p44/42 MAPK (Erk1/2, 9102; Cell Signaling Technology), 1:2000 rabbit anti-Phospho-p44/42 MAPK (Erk1/2, Thr202/Tyr204, 9106; Cell Signaling Technology) or 1:2000 mouse anti-β-Actin (8226; Abcam, Cambridge, UK) antibodies [209]. On the following day, the membrane was washed three times with TBS-Tween20 (0.05%) and 1:10000 IRDye 680RD Goat anti-Rabbit IgG or IRDye 800CW Goat anti-Mouse IgG secondary antibody (Licor Biosciences) was added for 50 min at room temperature. The membrane was washed three times for 5 min after incubation in the secondary antibody. The membrane was imaged using The Odyssey scanner (LI-COR Biosciences) and protein levels were quantified using Fiji software [210]. β-Actin level was used to normalize the results.

Collection of clinical trial data (Study I)

We collected clinical trial data for 19 anticancer compounds in HNSCC patients until 17 March 2018, from a website https://clinicaltrials.gov (Maintained by the National Library of Medicine) and PubMed. Only complete monotherapy trials with reported results were included. Information of the objective response rates (ORRs, RECIST), number of monotherapy-treated patients and responding patients were collected in one table.

Meta-analysis of clinical data (Study I)

We graphically presented the comparison of the ORRs of collected clinical trials and response rates obtained in this study under all culturing conditions by conducting a meta-analysis using RStudio, version3.6.0. For more specific analysis and plotting, the Rpackage meta, ggplot2, and ggthemes were used. The metaprop function from the meta package was used for calculation of the ORRs, and ggplot functionalities were used to obtain the confidence intervals and the figures.

3.5 A LIVE CELL APOPTOSIS ASSAY

First, two 96-well plates (Perkin Elmer, #6005182, Waltham, MA, USA) were coated with 50 µl of Myogel (0.5 mg/ml) and left overnight in the incubator. On the next day, cells (UT-SCC-42A and UT-SCC-24B) were detached using trypsin/EDTA and labeled with CellTrace Far Red (Invitrogen, Carlsbad, CA, USA) following the manufacturer's instructions. For both cell lines, one million cells were mixed with 1-µl CellTrace Far Red in 1 ml of PBS in a 15 ml falcon tube and incubated for 20 min in an incubator. After incubation, 5 ml culture medium was added to the tube and incubation was continued for 5 min. After incubation, the cells were centrifuged 5 min at 1000 rpm at room temperature and mixed with fresh culture medium. The cells were counted using a Scepter cell counter and diluted to 10 000 cells /ml concentration. The cells were mixed with either 0.1% DMSO or navitoclax (100, 1000 or 10 000 nM). Additionally, the IncuCyte Caspase-3/7 Apoptosis Assay Reagent (Sartorius; 1:1000) was used to detect the apoptotic cells (Fig. 14). The cells were seeded into the wells (1000 cells per well, 100 µl) in six replicates per condition. The plates were imaged every second hour with a 20x objective (9 images per well) using an Incucyte S3 live cell analysis system (Sartorius). After 24 h, one plate was irradiated with 8 Gy using a gamma irradiator OB29/4. Imaging was continued for 48 hours. Cancer cell proliferation (red) and apoptotic cells (green) were determined using the Incucyte analysis system. The percentage of apoptotic cells (apoptotic index) was determined by summing apoptotic cells (green and red objects) divided by total cell count (red objects) multiplied by 100.

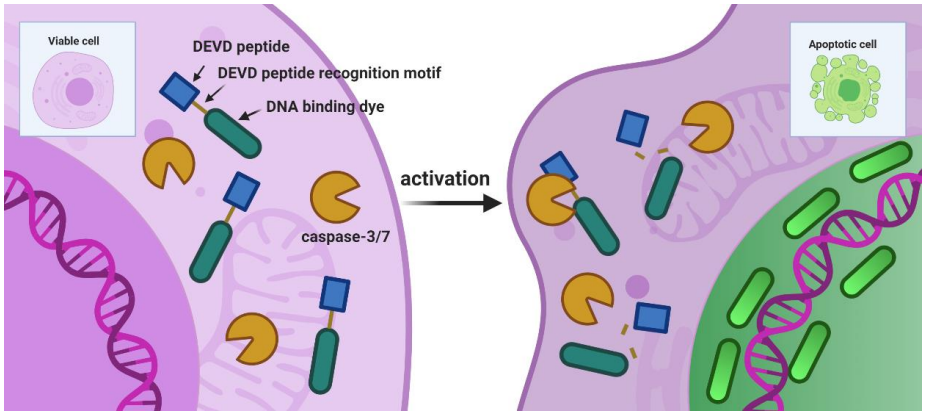

Figure 14. Illustration of the Incucyte Caspase-3/7 apoptosis assay. A Caspase-3/7 green reagent passes freely through the cell membrane and is non-fluorescent in healthy cells. In apoptotic cells, activated caspase-3/7 cleaves the Caspase-3/7 green reagent at the DEVD recognition motif, releasing a DNA binding fluorescent dye that labels the nucleus of apoptotic cells. Created with BioRender.com.

3.6 MICROFLUIDIC CHIP

Design and fabrication process of the microfluidic chip

We designed a microfluidic chip based on a previously published model [211]. For microfluidic chip production, we utilized a standard soft lithography process for fabrication of polydimethylsiloxane (PDMS). We designed microchannel patterns, demonstrated in Figure 15, which were then plotted on high resolution polymer films, and subsequently applied as photomasks for the photolithography steps using CAD software. Microchannels were created by applying master mold and two layered SU8 negative photoresist structures on a silicon wafer following the MicroChem Nano protocol. The microfluidic chip included a central chamber (16 mm x 1.2 mm x 150 µm) for the immune cells and chambers for cancer cells (150 µm x 600 µm). The immune cell and cancer cell chambers were connected by microchannels along a 10 mm section from both sides (200 µm x 10 µm x 12 µm; Fig. 15).

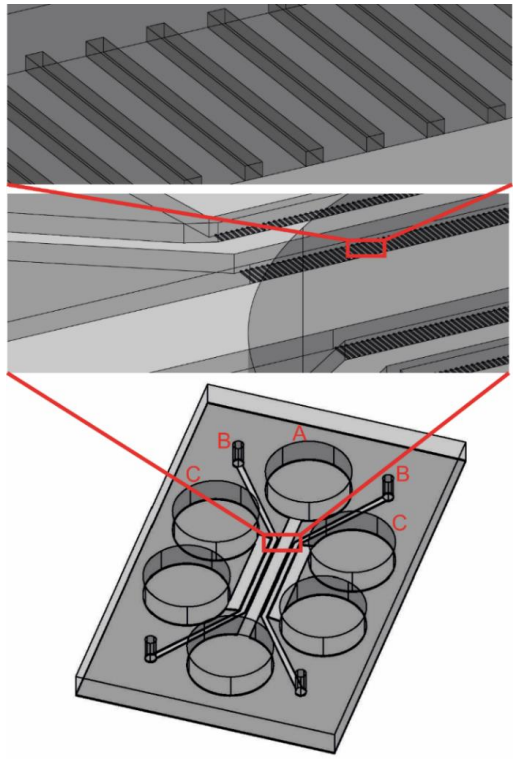

Figure 15. The design of microfluidic chip. Chamber A is filled with immune cells and cancer cells are injected into chamber B. C chambers are filled with a culture medium.

The PDMS replicas were prepared by mixing Sylgard 184 (Dow Corning) with a crosslinking agent (10:1) and poured over the master mould template. Air bubbles were eliminated by keeping the PDMS replicas in a vacuum for 45 min, after which they were placed in a preheated oven and incubated for 2 h at +70 °C.
During the cool down (to room temperature), the PDMS replicas were removed, and template and the chips were cut out and all the inlets and outlets were opened. A nitrogen gun and pressure-sensitive tape were used to remove dust from the PDMS surface. The glass microscope slides were cleaned with ethanol and dried with the nitrogen gun. The slides and PDMS replicas were exposed to oxygen plasma in a PVA TePla 400 plasma system for 1 min (power: 60 W, O2 flow rate: 500 ml/min) and immediately bonded together to cover the microchannels. Before use, chips were autoclaved for 30 min at +120 °C.

Microfluidic chip assay workflow

The cell suspension for the chip assay was prepared using trypsin/EDTA to detach cells from the flask. For patient samples the preparation process is described in paragraph 3.2. The cell suspension (cell line or freshly isolated tumor cells) was labeled according to the manufacturer's instructions with

CellTrace Far Red (Invitrogen) similar to the labeling described in paragraph 3.5. Labeled cells were mixed with a Myogel/fibrin mixture. The Myogel/fibrin mix was prepared according to the following concentrations: 2.4 mg/ml Myogel, 0.5 mg/ml fibrinogen (Merck), 0.3 U/ml thrombin (Sigma-Aldrich), and 33.3 µg/ml aprotinin (Sigma-Aldrich). DMEM/F12 medium with 10% FBS was used for dilution of the reagents for all experiments. Immediately after preparation, a cell-gel mixture (20 000 cells in 3 µl) was loaded in the chip through small channels shown in Figure 15 (chamber B). Chips were placed in the incubator for 30 min to ensure fibrinogen gelation.

Immune cells were isolated using a density gradient technique described in paragraph 3.2. Immune cells were labeled according to the manufacturer's instructions with CellTrace Violet (Invitrogen) and mixed with DMEM/F12 medium with 10% serum. FBS was used for the oral cancer cell line (HSC-3) and the patient's own serum for the freshly isolated patient cells. The immune cell suspension was divided into three groups: control with no drug, PDL-1 antibody (9.6 µg/ml, Bio X Cell, Hanover, NH, USA) and IDO1 inhibitor (5 µg/ml, NLG-919, Cayman Chemical, Ann Arbor, MI, USA). Two microfluidic chips were used per each drug group for HSC-3 and one microfluidic chip per drug groups for patient samples. For each chip, immune cell suspension (1 million cells in 150 µl) was loaded in the large chamber shown in Figure 15 (chamber A). To mimic the *in vivo* situation, where the patients receive immunomodulators as intravenous therapy, PD-L1 and IDO1 inhibitors were mixed with immune cells, and not with cancer cells. Side chambers (chamber C) were filled with a cell culture medium to ensure proper hydration for the cells. Chips were placed in the incubator for three days and imaged once a day under a fluorescence microscope using a Leica DM6000 B/M light microscope with a digital camera (DFC420 and DFC365FX; Leica Microsystems, Wetzlar, Germany).

Cell recognition and counting

An algorithm for analyzing the number of immune and cancer cells was built using Matlab's (Mathworks, MA, USA). We used a semiautomated algorithm with manual threshold to identify labeled cells from the background [212]. In addition, Matlab's built-in functions were used to recognize the boundaries of cells and objects and the identity of tumor-associated immune cells based on their size and morphology. Objects smaller than a typical cancer cell area were excluded from cancer cell quantification using a manual threshold setting. The cancer cell proliferation rate was defined by normalizing a cell number of each time point to the number on day one.

3.7 STATISTICAL ANALYSIS

Study I: The Friedman test was conducted to discover differences in drug efficacy on 12 cell lines comparing the five culturing conditions (control, Myogel 2D, Myogel 3D, Matrigel 2D, and Matrigel 3D) using SPSS software (version 25, 2017, IBM Corporation, NY, USA). We selected the non-parametric Friedman test because this test does not rely on a normal distribution of the data and is suitable to test differences between several related samples. We performed pair-wise comparisons with the Bonferroni correction for multiple comparisons [213]. One-way non-parametric ANOVA (Kruskal-Wallis test) was used to detect statistical significance between protein expressions (EGFR, ERK1/2 and pERK1/2) of cell lines cultured in five matrices using SPSS software.

We set the statistical significance to $p < 0.05$. P values are presented as follows: *=$P \leq 0.05$, ** = $P \leq 0.01$, *** = $P \leq 0.001$. OriginLab software was used to create the figures.

3.8 ETHICAL PERMISSIONS

The patient sample collection protocol (*Studies II and III*) was approved by the institutional Research Ethics Board (statement number 31/2016) and all methods were performed in accordance with the relevant guidelines and regulations. The Ethics Committees of Oulu and Tampere approved the use of human leiomyoma (statement number 2/2017).

4 RESULTS

4.1 DRUG SENSITIVITY AND RESISTANCE TESTING OF HNSCC CELL LINES CULTURED IN DIFFERENT CULTURING CONDITIONS (I)

A high-throughput drug screen on 12 HNSCC cell lines revealed a remarkable variation in EGFR and MEK inhibitor sensitivity under different culturing conditions (Fig. 16 and 17). Based on DSS values, drug responses were graded into four activity groups (inactive, low, moderate, and high; Table 8).

EGFR inhibitor response

Most cell lines cultured on plastic, on top of and embedded in Matrigel showed a moderate or high sensitivity to EGFR inhibitors (Fig. 16). However, EGFR inhibitors were inactive or showed only low activity in HNSCC cell lines cultured in Myogel (Fig. 16).

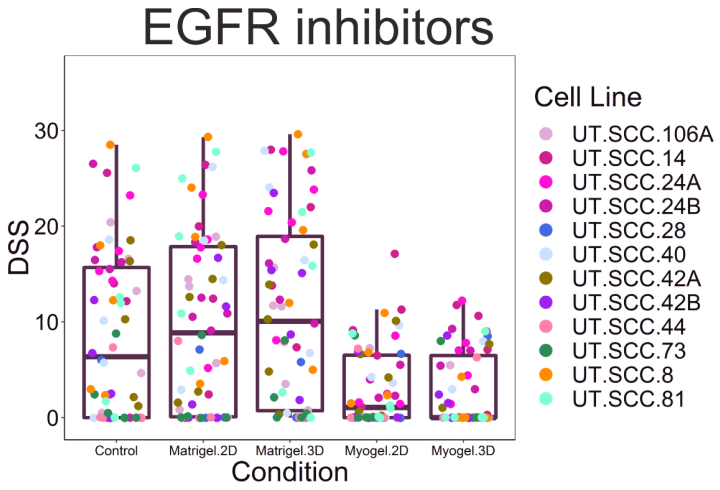

Figure 16. The drug-sensitivity scores (DSS) for each cell line grouped according to culturing conditions shown in box plots. Cancer cells in 2D and 3D Myogel were less responsive to EGFR inhibitors compared to control and Matrigel cultures. Dot represents the DSS of one EGFR inhibitor (cetuximab, gefitinib, erlotinib, afatinib or ganertinib) in each of 12 cell lines. Box plot represents the first (lower) quartile, median and third (upper) quartile.

The Friedman test was conducted to discover differences in drug response across five culturing conditions. The test revealed significant differences between culturing conditions and the EGFR inhibitor response (Table 10). The significant difference was seen in Myogel and Matrigel 3D cultures for cetuximab, gefitinib, afatinib and canertinib (Table 10).

Table 10. EGFR inhibitor responses in different culturing conditions compared to each other using Friedman test. Adjusted p-values are shown, and significant cases appear in bold.

Matrix comparison		Cetuximab	Gefitinib	Erlotinib	Afatinib	Canertinib
Myogel 2D	**Myogel 3D**	1	0.098	1	1	1
Myogel 2D	**Control**	0.118	1	1	0.118	0.118
Myogel 3D	**Control**	0.081	0.814	1	0.118	**0.019**
Myogel 3D	**Matrigel 2D**	0.081	0.055	0.454	**0.008**	**0.002**
Myogel 3D	**Matrigel 3D**	**0.003**	**0.012**	0.142	**0.001**	**0.003**
Myogel 2D	**Matrigel 3D**	**0.005**	0.098	0.142	**0.001**	**0.024**
Myogel 2D	**Matrigel 2D**	0.118	0.332	0.454	**0.008**	**0.019**
Control	**Matrigel 3D**	1	1	1	1	1
Control	**Matrigel 2D**	1	1	1	1	1
Matrigel 2D	**Matrigel 3D**	1	1	1	1	1

MEK inhibitor response

Most HNSCC cell lines cultured on plastic, on top of and embedded in Matrigel showed a moderate or high MEK inhibitor activity (Fig. 17). However, MEK inhibitors exhibited a low activity in cells cultured in Myogel (Fig. 17). According to the Friedman test, all six MEK inhibitors exhibited a significantly higher response in cell lines cultured in Matrigel than in Myogel (Table 11).

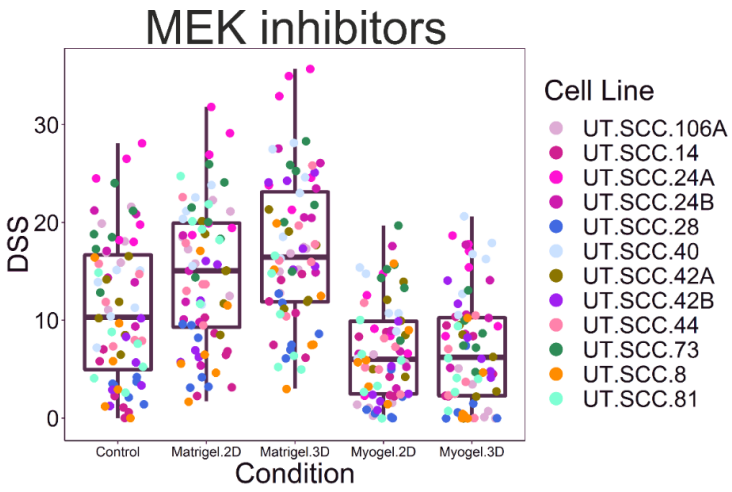

Figure 17. MEK inhibitor DSSs for each cell line grouped according to culturing conditions shown in box plots. Cancer cells in 2D and 3D Myogel were less responsive to MEK inhibitors Dot represents the DSS of one MEK in each of 12 cell lines. Box plot represents the first (lower) quartile, median and third (upper) quartile.

Table 11. The Friedman test comparison for MEK inhibitor responses of cells cultured in different conditions. Adjusted p-values are shown and significant cases appear in bold.

Matrix		Pimasertib	Trametinib	Refametinib	Binimetinib	TAK-733	Selumetinib
Myogel 2D	**Myogel 3D**	1	1	1	1	1	1
Myogel 2D	**Control**	1	0.707	1	1	0.707	1
Myogel 3D	**Control**	1	1	1	1	1	0.707
Myogel 3D	**Matrigel 2D**	**0.012**	**0.03**	**0.012**	**0.004**	**0.012**	**0.004**
Myogel 3D	**Matrigel 3D**	**0**	**0**	**0**	**0**	**0**	**0**
Myogel 2D	**Matrigel 3D**	**0**	**0**	**0**	**0**	**0**	**0.002**
Myogel 2D	**Matrigel 2D**	**0.005**	**0.003**	**0.008**	**0.004**	**0.003**	**0.019**
Control	**Matrigel 3D**	**0.008**	**0.019**	**0.019**	**0.005**	**0.019**	0.169
Control	**Matrigel 2D**	0.282	0.707	0.707	0.389	0.528	0.814
Matrigel 2D	**Matrigel 3D**	1	1	1	1	1	1

PI3K/mTOR inhibitor response

Interestingly, the response to PI3K/mTOR and mTOR inhibitors were relatively similar across different conditions in HNSCC cell lines (Fig. 18). In most cell lines, temsirolomus and ridaforolimus (mTOR inhibitors) showed low activity, whereas everolimus was inactive (I: Fig. S2). However, all cell lines, regardless of the culturing conditions, were sensitive to PI3K/mTOR inhibitor omipalisib (a moderate-to-high activity; I: Fig. S2). PI3K/mTOR inhibitor dactolisib was inactive in all cell lines except one (UT-SCC-24B; I: Fig. S2). PI3K/mTOR inhibitor PF-04691502 and mTOR inhibitor sirolimus exhibited varying activity across the cell lines (I: Fig. S2). Another PI3K/mTOR inhibitor, apitolisib, showed low-to-moderate activity (I: Fig. S2).

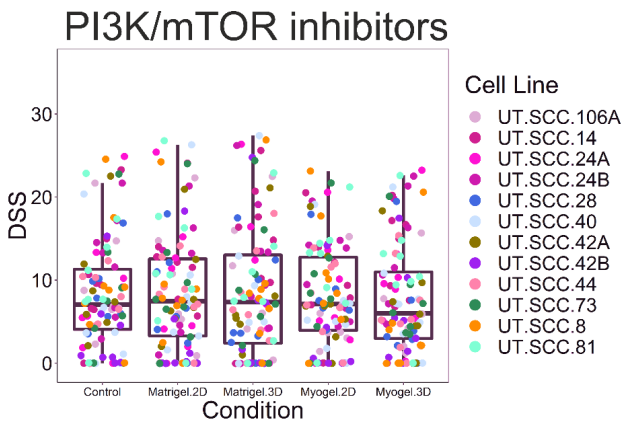

Figure 18. PI3K/ mTOR inhibitor DSSs for each cell line grouped according to growing environments shown in box plots. No clear differences between culturing conditions were seen for the PI3K/ mTOR inhibitors. Box plot represents first quartile, median and third quartile.

According to the Friedman test, PI3K/mTOR inhibitors omipalisib and PF-04691502 showed significantly less activity in Myogel cultures compared to Matrigel 3D cultures (Table 12 and I: Figure S2). However, mTOR inhibitor everolimus exhibited a higher response in Myogel cultures compared to Matrigel, although the overall response was weak (Table 12 and I: Figure S2). No significant differences between any culturing conditions were observed in other mTOR inhibitors (temsirolimus, sirolimus and ridaforolimus) and PI3K/mTOR inhibitors dactolisib and apitolisib, and therefore pairwise comparisons could not be performed (N/A; Table 12).

Table 12. The Friedman test comparison for PI3K/mTOR inhibitor responses of cells cultured in different conditions. Adjusted p-values are shown, and the number and percentage of significant cases appear in bold. (N/A, not applicable).

Matrix		Everolimus	Temsirolimus	Sirolimus	Ridaforolimus	Dactolisib	Apitolisib	Omipalisib	PF-04691502
Myogel 2D	**Myogel 3D**	1	N/A	N/A	N/A	N/A	1	1	1
Myogel 2D	**Control**	1	N/A	N/A	N/A	N/A	0.707	0.814	1
Myogel 3D	**Control**	1	N/A	N/A	N/A	N/A	1	1	1
Myogel 3D	**Matrigel 2D**	0.142	N/A	N/A	N/A	N/A	0.528	0.201	0.332
Myogel 3D	**Matrigel 3D**	**0.01**	N/A	N/A	N/A	N/A	0.067	**0.004**	**0.008**
Myogel 2D	**Matrigel 3D**	**0.008**	N/A	N/A	N/A	N/A	**0.008**	**0**	**0.003**
Myogel 2D	**Matrigel 2D**	0.118	N/A	N/A	N/A	N/A	0.098	**0.012**	0.169
Control	**Matrigel 3D**	0.612	N/A	N/A	N/A	N/A	1	0.067	0.332
Control	**Matrigel 2D**	1	N/A	N/A	N/A	N/A	1	1	1
Matrigel 2D	**Matrigel 3D**	1	N/A	N/A	N/A	N/A	1	1	1

Comparison of drug screen and clinical trial responses

Only cetuximab, erlotinib, afatinib, and gefitinib had reached phase III in HNSCC clinical trials. Moreover, the widely studied erlotinib was applied only as a combination therapy for head and neck cancer. Only one MEK inhibitor, trametinib, had reached a phase I clinical trial for head and neck cancer, but the study was terminated by the sponsor's decision. Cetuximab monotherapy was assessed in 7 clinical trials for head and neck cancer, and reported ORRs were between 3.7% and 14.5% (Table 13). Based on a meta-analysis, a pooled ORR of head and neck cancer clinical trials was 10.0% (confidence interval, CI 7.0–14.0).

Table 13. Clinical trial ORR for cetuximab monotherapy for HNSCC patients, and the pooled ORR. Data from https://clinicaltrials.gov.

Trial No.	Phase	Completion Year	Monotherapy Treated Patients	ORR%*	Notes:
NCT01040832	2	2012	53	5.7	
NCT00671437	2	2015	27	3.7	Based on CT scan
NCT00661427a	2	2012	30	13.3	Drug dose 500 mg/m2
NCT00661427b			19	10.5	Drug dose 750 mg/m2
NCT00514943	2	2013	62	9.7	Based on independent central review
NCT01602315	2	2016	35	5.7	
NCT00939627	2	2014	22	4.5	
NCT01577173	2	2015	62	14.5	
NCT01696955	2	2017	38	7.9	
The pooled ORR				**10.0%**	**(CI 7.0–14.0)**

*Objective response rate (ORR) based on Response Evaluation Criteria in Solid Tumors (RECIST).

Across 12 cell lines, only 17% (2/12) of cell lines cultured on Myogel 2D and 25% (3/12) embedded in Myogel responded to cetuximab treatment (Fig. 19). However, 67% (8/12) of cell lines cultured on plastic responded to cetuximab. Elevated response rates were observed in Matrigel 2D (67%; 8/12) and 3D cultures (75%; 9/12).

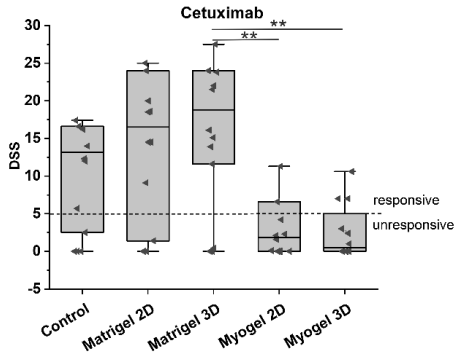

Figure 19. HNSCC cancer cell lines (n=12) cultured in 2D and 3D Myogel were less responsive to cetuximab compared to control and Matrigel cultures. DSS ≥5 was used as the cut-off point for response for each drug. Box plot represents first quartile, median and third quartile. ** P ≤ 0.01.

Afatinib was assessed as a single agent in three head and neck clinical trials for HNSCC and reported ORRs were between 7.3% and 10.3% (Table 14). A pooled ORR was a modest 10% (CI 7.0–13.0). Once again, cells cultured in Myogel (2D and 3D) exhibited a low response rate to afatinib treatment (17%;2/12), while on plastic and Matrigel (2D and 3D) the cells showed a high response rate of 75% (9/12; Fig. 20). Gefitinib was assessed as a single agent on four clinical trials, where it exhibits only a weak response with a pooled ORR of 6% (CI 3.0–9.0). Across all cell lines, in both Myogel cultures (2D and 3D), cells showed only a weak response to gefitinib (8.3%; 1/12). Gefitinib response rates of other conditions were elevated on plastic 16.7% (2/12), Matrigel 2D 41.7% (5/12) and 3D 50% (6/12; Fig. 20).

Table 14. Clinical trial objective response rates of afatinib and gefitinib monotherapy in HNSCC patients, and the pooled ORR. Data from https://clinicaltrials.gov.

Drug	Trial No.	Phase	Completion Year	Monotherapy Treated Patients	ORR %*	Notes:
Afatinib	NCT01345682	3	2016	322	10.2	
	NCT00514943	2	2013	62	8.1	Based on independent central review
	NCT01415674	2	2006	41	7.3	The neoadjuvant treatment
	The pooled ORR				**10**	**CI 7.0–13.0**
Gefitinib	NCT00206219a	3	2007	158	2.7	Drug dose 250 mg/day
	NCT00206219b			166	7.6	Drug dose 500 mg/day
	NCT00015964	2	2005	47	10.6	
	NCT01185158	2	2004	70	1.4	
	NCT00519077	2	2013	44	6.81	
	The pooled ORR				**6**	**CI 3.0–9.0**

*Objective response rate (ORR) based on Response Evaluation Criteria in Solid Tumors (RECIST).

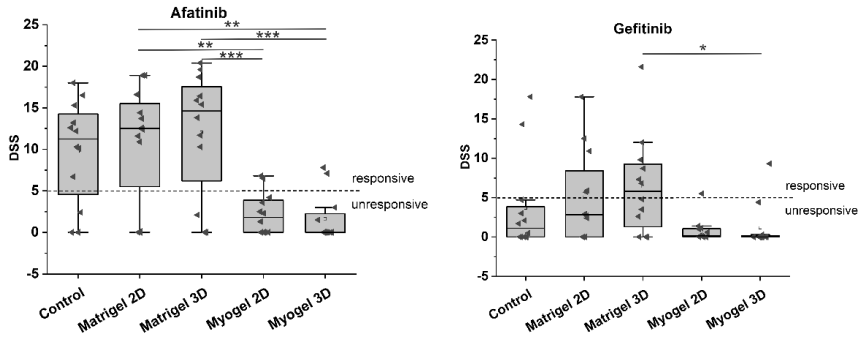

Figure 20. HNSCC cancer cell lines (n=12) in 2D and 3D Myogel were less responsive to afatinib and gefitinib compared to control and Matrigel cultures. DSS ≥5 was used as the cut-off point for response for each drug. Box plot represents first quartile, median and third quartile. *P≤ 0.05, ** P ≤ 0.01, ***P ≤ 0.001.

Temsirolimus as a single agent was assessed in two phase II head and neck cancer clinical trials and the reported ORRs were between 0% and 2.5%. One trial resulted in promising tumor shrinkage in 39.4% of patients, but unfortunately lacked ORR (Table 15) [214]. Another trial reported only a 2.5% ORR (Table 15). The pooled ORR for temsirolimus was 2% (CI 0–10.0). One window-of-opportunity trial for sirolimus (phase I and II) showed clinical response with an ORR of 25% including one complete response (Table 15)[215]. As mentioned above, no significant differences between any culturing conditions were seen in temsirolimus and sirolimus (Table 12). However, the overall DDSs were higher for sirolimus than temsirolimus (Fig. 21).

Table 15. Clinical trial ORRs of temsirolimus and sirolimus monotherapy in HNSCC patients. Data from https://clinicaltrials.gov.

	Trial No.	Phase	Completion Year	Monotherapy Treated Patients	ORR%*	Notes:
Temsirolimus	NCT01172769	2	2012	33	0	
	NCT01256385	2	2013	40	2.5	
	The pooled ORR				**2**	**CI 0–10.0**
Sirolimus	NCT01195922	1 & 2	2015	16	25.0	The neoadjuvant treatment

*Objective response rate (ORR) based on Response Evaluation Criteria in Solid Tumors (RECIST)

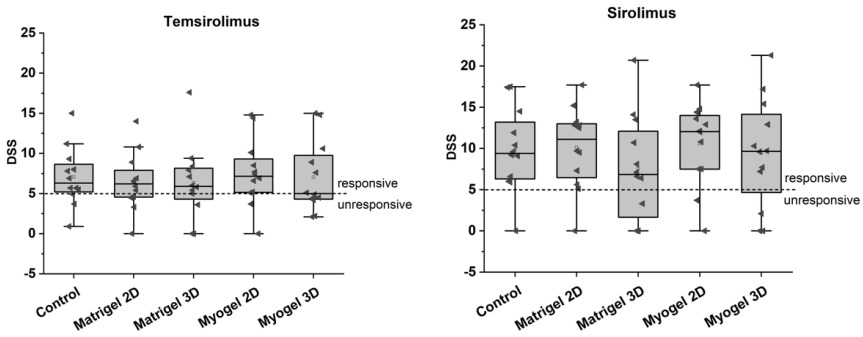

Figure 21. HNSCC cell lines (n=12) showed no significant differences in response to temsirolimus or sirolimus between culturing conditions. DSS ≥5 was used as the cut-off point for response for each drug. Box plot represents first quartile, median and third quartile.

4.2 MATRIX EFFECT ON PROTEIN EXPRESSION AND VIABILITY OF HNSCC CELLS (I, III)

Matrix effect on protein expression

The matrix effect on protein expression of five HNSCC cell lines was investigated with a western blot analysis. The Kruskal-Wallis test was conducted to discover differences in EGFR, ERK1/2, and pERK1/2 protein levels in five HNSCC cell lines. The cell lines showed varying protein expression, however no statistically significant differences in the protein levels between culturing conditions were observed (Fig. 22).

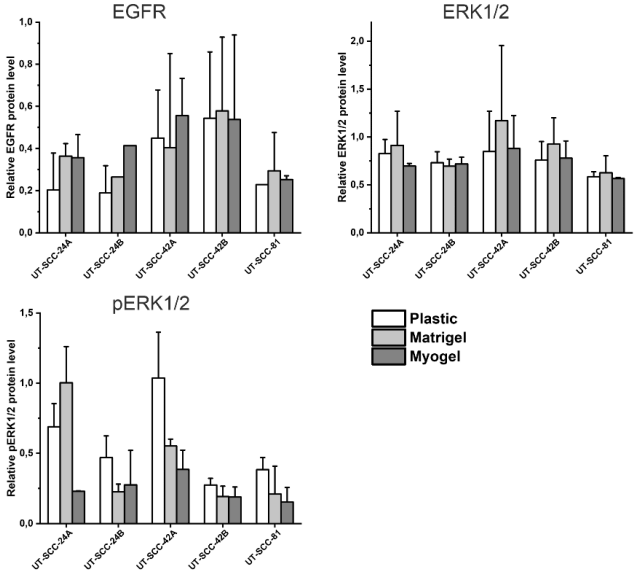

Figure 22. EGFR, ERK1/2 and p-ERK1/2 expressions of five HNSCC cell lines growing on plastic, Matrigel and Myogel. β-Actin was used to normalize the levels of proteins.

Matrix effect on the cell viability across patient–derived cells

In the Study III, freshly isolated patient–derived cancer cells were cultured on plastic, Myogel and Matrigel coated wells and viability was measured using a CTG-assay after three days. The viability assay revealed that Myogel increased the viability of patient-derived cancer cells compared with Matrigel or uncoated wells (Fig. 23.

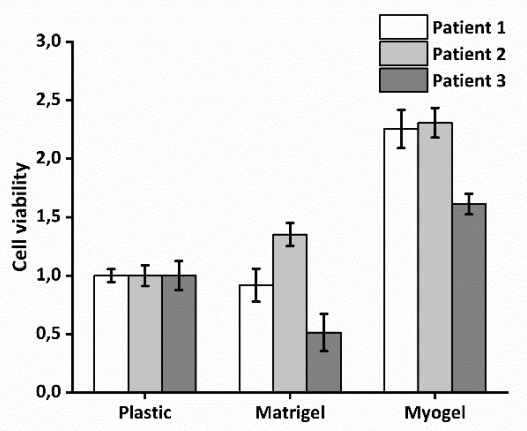

Figure 23. Freshly isolated cancer cells cultured in Myogel have a higher proliferation rate compared with other culturing conditions, plastic and Matrigel. Cancer cells were isolated from three patients and cultured in different conditions for three days. The proliferation rate was measured using a CTG luminescent viability assay. The results are presented as mean ± SD for three replicate wells. No statistical significances were calculated since the assay was done once for each patient's freshly isolated cells.

4.3 COMBINATION SCREEN OF COMPOUNDS AND IRRADIATION FOR HNSCC CELL LINES (II)

In the study II, we used a compound library of 396 FDA-approved drugs and experimental compounds and ionizing radiation to identify synergistic and antagonistic combinations for five HNSCC cell lines cultured on Myogel. The initial HTS screen revealed variation among cell lines in their drug response and synergism and antagonism with irradiation (Fig. 24). Some drugs appeared completely inactive (n=39) with or without irradiation. A fraction of the drugs were highly effective across all cell lines but lacked interaction with irradiation (n=28). The majority of the drugs' responses were influenced by irradiation (n= 357), but in most of them irradiation had only a weak effect or the effect was inconsistent across cell lines. However, clear synergistic and antagonistic patterns were observed between some drugs and irradiation across cell lines. The most promising drug candidates (n=15) were further validated using multiple irradiation doses (Fig. 25). Among 15 drugs, 12 were synergistic and 3 antagonistic. Interestingly, seven synergistic drugs were

epigenetic modifiers (acitretin, BAY 87-2243, CUDC-907, lonartinib, talazoparib, tipifarnib and tretinoin). The rest of the synergistic drugs were kinase inhibitors (afatinib, omipalisib and triciribine) and apoptotic modulators (birinapant and navitoclax). Two PLK1 kinase inhibitors (BI 2536 and GSK-461364) and one metabolic modifier, pemetrexed, were selected for further validation due to their strong antagonistic properties.

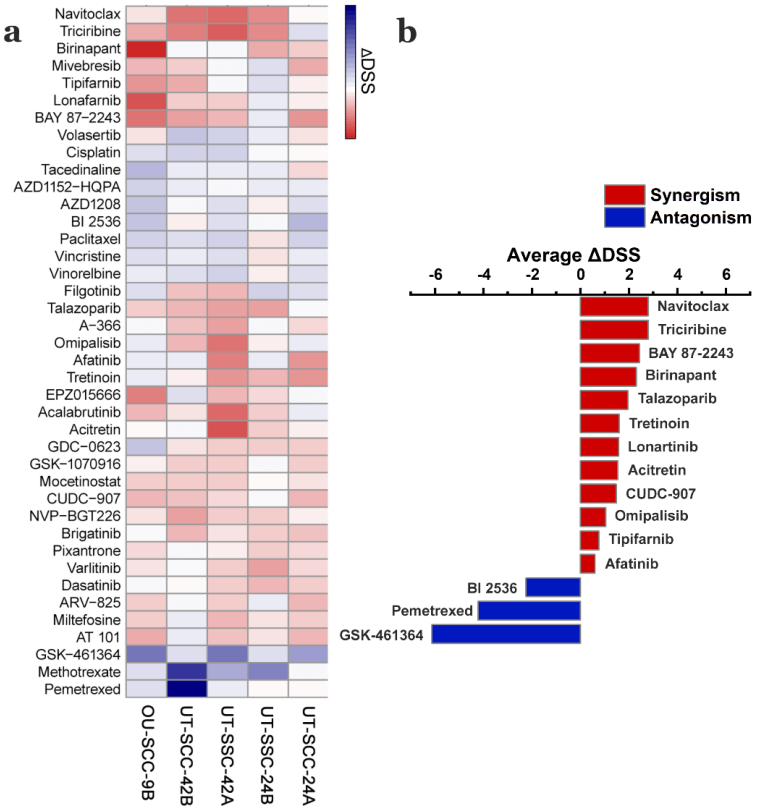

Figure 24. A high-throughput screen with an EC20 irradiation dose reveals synergistic and antagonistic properties of the compounds. (a) A library of 396 FDA-approved and experimental compounds and radiation were tested against five HNSCC cell lines (top 40 compounds with the highest absolute median values are shown). The CTG assay was used to determine relative cell viability after 72 hours and presented as a heat map of selective drug sensitivity scores (ΔDSS). (b) Average ΔDSS of five cell lines of the most promising compounds with synergistic and antagonistic properties.

The dose-response matrix data analysis revealed strong antagonism and synergy in several drug–irradiation combinations

The dose-response matrix data analysis showed strong synergism and antagonism with 15 compound-irradiation combinations (Fig. 25). Combination screen and synergy scoring was calculated using five drug

concentrations and four irradiation doses (1, 2, 4 and 8 Gy) on five cell lines. The same protocol was used as in the initial screen. The analysis was performed using a ZIP reference model with the SynergyFinder 2.0 web application [207]. Based on the obtained synergy scores, we classified the compound–irradiation combinations as noninteractive, antagonistic or synergistic (Table 9).

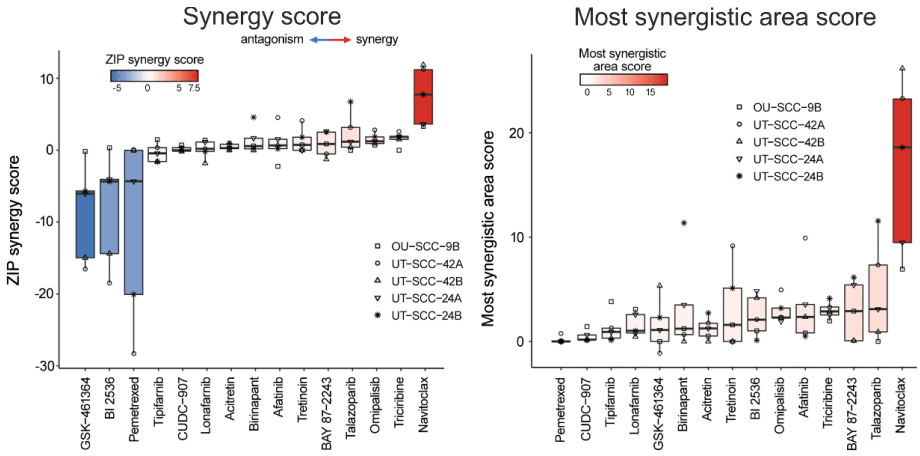

Figure 25. The synergy validation for the 15 most promising combinations tested in five HNSCC cell lines grown on Myogel. The cells were tested using five drug concentrations and four radiation doses. Quantification of combination synergy across the five HNSCC cell lines using two synergy metrics, the synergy score and the most synergistic area score in SynergyFinder software. Each bar contains scores from each cell line, and box plot represents first quartile, median and third quartile, and whiskers represent minimum and maximum score.

The dose-response analysis verified that, among seven tested epigenetic modifiers, only talazoparib and tretinoin exhibited a promising synergy (Fig. 25). The PARP inhibitor, talazoparib, showed a promising radiosynergism in two cell lines (UT-SCC-42A and UT-SCC-24B; Fig. 25). Afatinib acted synergistic in one cell line, although the overall effect was modest (Fig. 25 and 26). Tretinoin exhibit moderate radiosynergism in the same cell lines, although as a single agent it was ineffective (Fig. 25). Both apoptotic modulators (birinapant and navitoclax) acted synergistically similar to the initial screen. However, SMAC mimetic, birinapant acted synergistically with radiation only in one cell line (UT-SCC-24B), while the Bcl-2/Bcl-xL inhibitor, navitoclax, acted synergistically in all tested cell lines (Fig. 25). Navitoclax exhibited a strong synergy (the most synergistic are score > 10) in three cell lines (UT-SCC-42A, UT-SCC-42B and UT-SCC-24B) and a moderate synergy (the most synergistic are score 5 – 10) in the other two cell lines (UT-SCC-24A and UT-SCC-9B; Fig. 25 right panel).

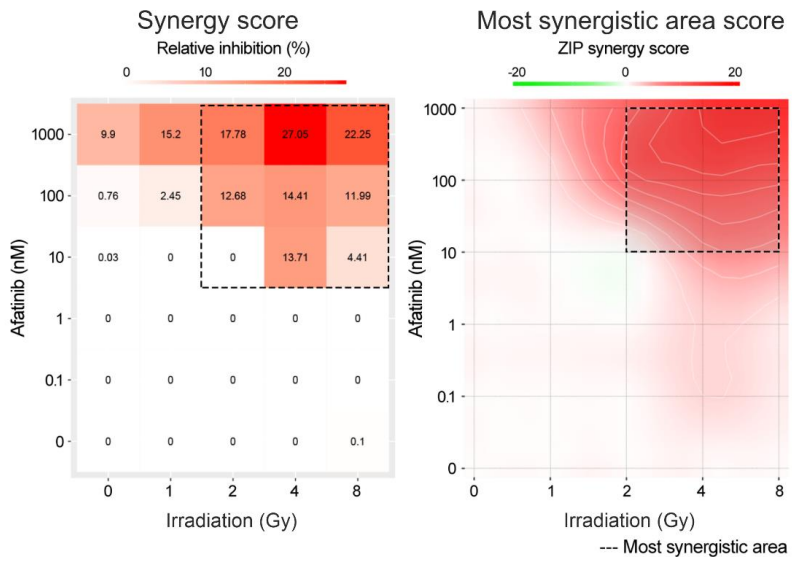

Figure 26. The dose–response matrix showing synergistic afatinib–irradiation combination of representative cell line (UT-SCC-42A).

The metabolic modifier pemetrexed and PLK1 inhibitors BI 2536 and GSK-461364 showed a strong antagonism together with irradiation similar to the initial screen (Fig. 25). BI 2536 and irradiation had strong antagonism in two cell lines (UT-SCC-42A and UT-SCC-42B; Fig. 25). Pemetrexed showed a strong antagonism in three cell lines (UT-SCC-42A, UT-SCC-24A and UT-SCC-24B; Fig. 25 and 27).

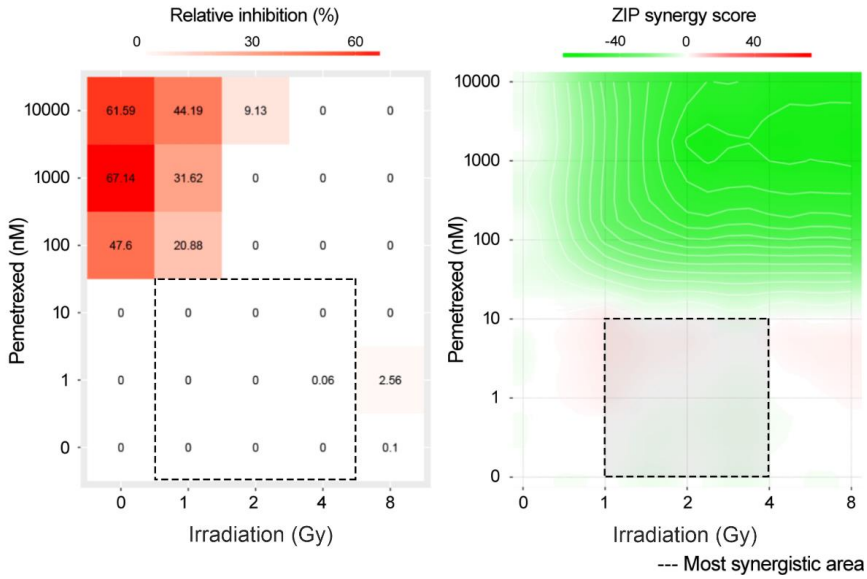

Figure 27. The dose–response matrix showing antagonistic pemetrexed–irradiation combination of representative cell line (UT-SCC-42A).

Navitoclax exhibits strong synergism with irradiation

An extended navitoclax–irradiation dose–response screen was performed on eight UT-SCC cell lines (Fig. 28). Mutation profiles of the UT-SCC cell lines were previously characterized [202]. In total, we tested six p53-mutated and six wild-type cell lines. Navitoclax and irradiation synergy was detected in cell lines regardless of the p53 mutation status. Ten cell lines exhibited a strong synergy, and three cell lines had a moderate synergistic effect (Fig. 28a). In some cell lines, navitoclax exhibited a strong effect on cancer cell viability even as a single agent (Fig. 28b).

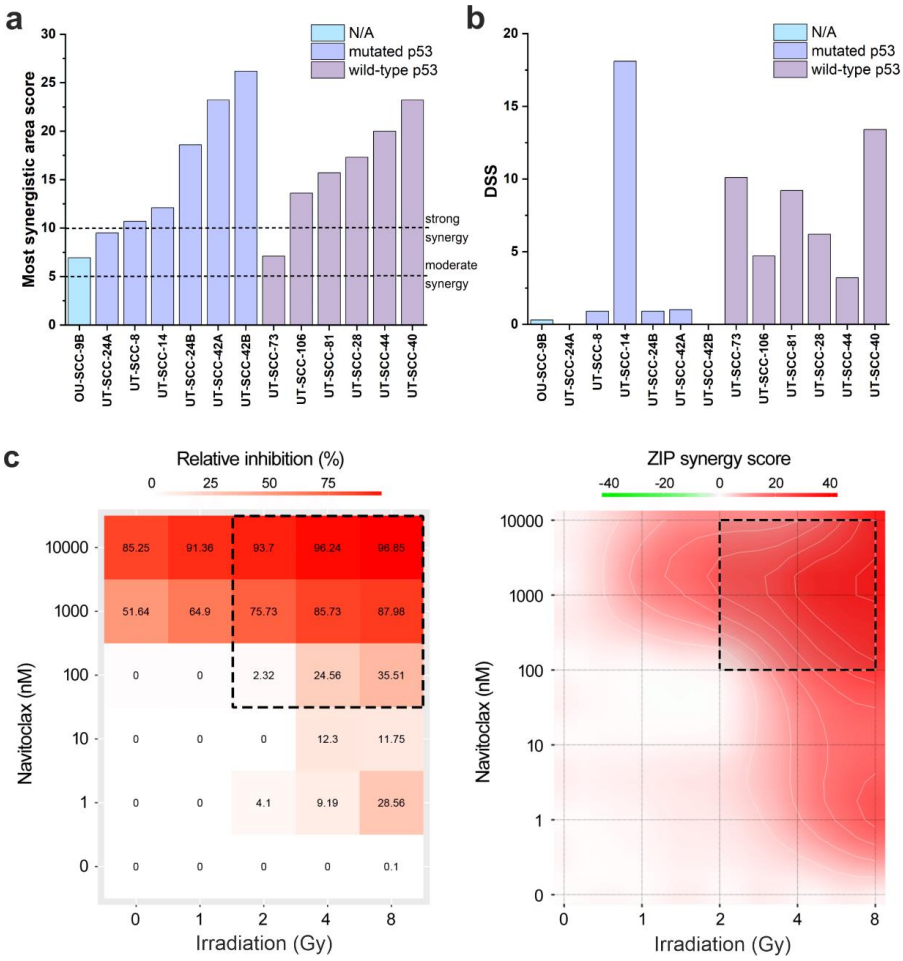

Figure 28. The combination of navitoclax and irradiation exhibited a strong synergy regardless of the p53 mutation status. (a) The most synergistic area scores of navitoclax–irradiation combination and (b) the DSSs of Navitoclax as a single agent across 13 HNSCC cell lines. (c) The dose–response matrix showing antagonistic pemetrexed–irradiation combination of representative cell line (UT-SCC-40).

Navitoclax induced apoptosis alone and with irradiation

Since we demonstrated that navitoclax decreased cancer cell viability as a single agent and with radiotherapy, we further examined the effects of navitoclax on cell death. We applied a live cell apoptosis assay for two HNSCC cell lines (UT-SCC-42A and UT-SCC-24B). Interestingly, as a single agent, navitoclax triggered apoptosis and induced apoptosis dose-dependently in both cell lines (Fig. 29). The combination of navitoclax and radiotherapy increased the apoptosis rate compared to radiotherapy alone, arrested cancer cell proliferation and led to high apoptosis percentage (40–50%) within 48 hours in both cell lines (Fig. 29).

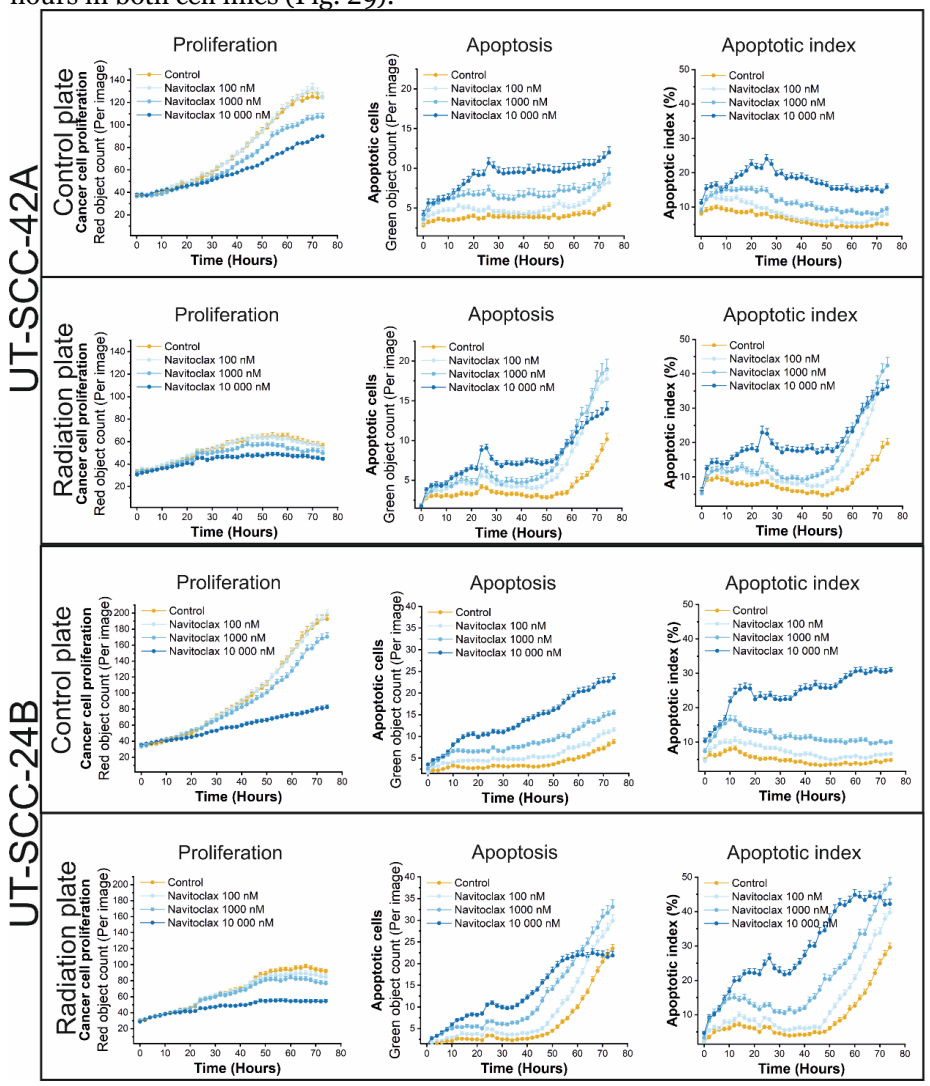

Figure 29. Navitoclax and irradiation induce apoptosis and arrest proliferation in HNSCC cells. A live cell apoptosis assay was conducted for two UT-SCC cell lines (42A and 24B). Caspase-3/7

Apoptosis Assay Reagent (green) was applied to detect apoptotic cells. Cancer cells were labeled with CellTrace Far Red and seeded into two identical plates (1000 cell per well) treated with Navitoclax (100, 1 000 and 10 000 nM). DMSO (0.1%) served as control. One plate was irradiated (8 Gy) after 24 hours. Using Incucyte S3 analysis software, green objects (apoptotic cells), red objects (cancer cells) and the percentage of apoptotic cells were quantified. Analysis showed that Navitoclax reduced proliferation in both cell lines, and with irradiation proliferation was arrested. Navitoclax triggered apoptosis as a single agent and after irradiation exposure the number of apoptotic cells were significantly increased. Navitoclax raised the apoptotic index in both cell lines. A day after irradiation exposure, a large proportion of cancer cells were apoptotic. The navitoclax–irradiation combination led to 40 to 50% of cells in apoptosis within two days. Average ± SEM (n = 6).

4.4 *IN VITRO* MICROFLUIDIC CHIP ASSAY FOR TESTING PERSONALIZED IMMUNOTHERAPEUTICS FOR HEAD AND NECK CANCER PATIENTS (III)

Cancer cell density affects migration of immune cells towards cancer cells

We used two chips to observe migration of immune cells (peripheral blood mononuclear cells, PBMCs) towards tongue cancer cells (HSC-3). In the first chip, (Fig. 30) both immune and cancer cells were applied (chambers A and B, respectively). The second chip contained only immune cells and a Myogel/fibrin coating without the cancer cells (Fig. 30). Immune cells in chip 1 migrated towards cancer cells continuously during all three days. However, in chip 2 such migration was not seen, and immune cells did not enter chamber B (Fig. 30).

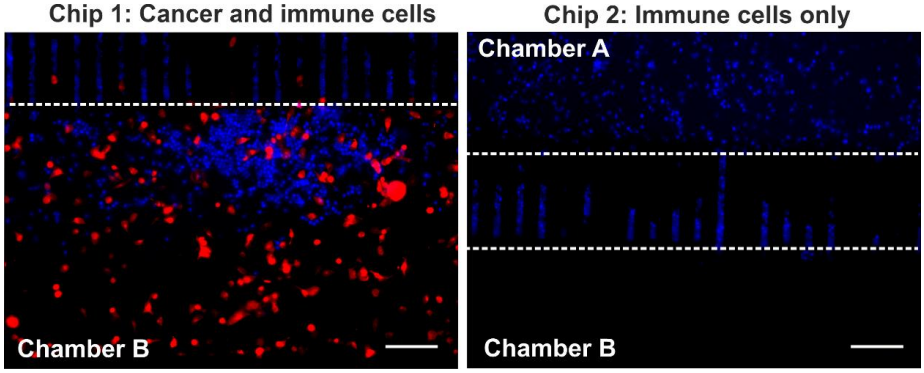

Figure 30. Cancer cell presence affects migration of the immune cells**.** In chip 1, cell trace far red labeled cancer cells were mixed with Myogel/fibrin and injected in chamber B. Cell trace violet labeled immune cells were mixed with cell culture medium and loaded in chamber A in Chip 1 and 2. Immune cell migration occurred only in Chip 1. Scale bar represents 100 µm.

To study whether the number of cancer cells affects the migration of immune cells, we used two different cell densities (20 000 and 10 000 cells). In this experiment, we used immune cells from three healthy donors. In all chips, the migration of the immune cells was cancer cell density dependent. With higher cancer density, more immune cells migrated towards the cancer cells (Fig. 31).

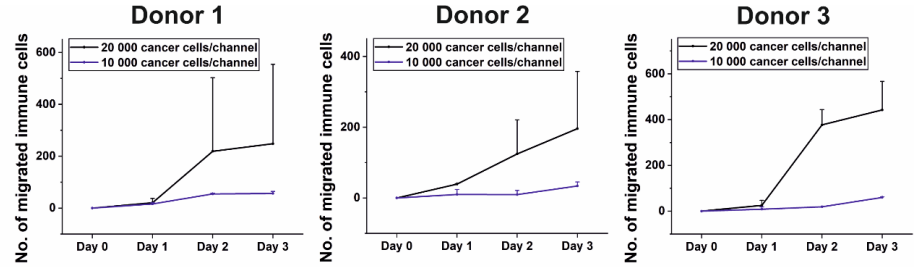

Figure 31. Cancer cell density affects migration of the immune cells. Immune cell migration was dependent on the number of the injected cancer cells. Data are presented as means with standard deviation of two technical replicates. Both cancer cell concentrations were tested on two microfluidic chips and therefore statistical analysis was not performed.

IDO1 inhibitor enhances the migration of immune cells towards cancer cells

The HSC-3 cell line and immune cells isolated from three healthy donors were applied to investigate the effect of the IDO1 inhibitor and PD-L1 antibody on immune cell migration. The IDO1 inhibitor enhanced the immune cell migration for all three donors (Fig. 32). However, the PD-L1 antibody did not enhance migration but, on the contrary, it reduced migration in two donors (Donor 1 and 3; Fig. 32).

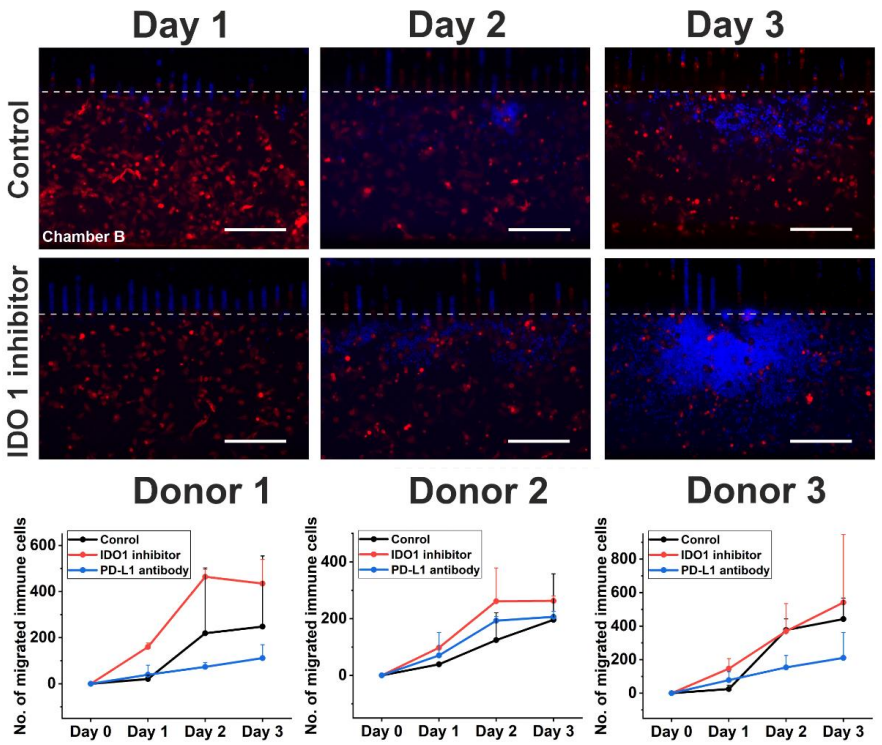

Figure 32. IDO1 inhibitor activates migration of immune cells (blue) toward cancer cells (red). Immune cells isolated from three healthy donors were loaded in separate microfluidic chips to study PD-L1 antibody and IDO1 inhibitor responses. Control chips were filled with drug-free culture medium. The number of migrated cancer cells were counted from Chamber B for three days. Data are presented as means with standard deviation of two technical replicates. Each drug was tested on two microfluidic chips and therefore statistical analysis was not performed. Scale bar represents 200 µm.

In the next step, we used HNSCC cancer cells isolated from the patients and their own immune cells (PBMCs) and serum to study the effect of IDO1 inhibitor and PD-L1 antibody on the immune cell migration. As in previous cell line results, the IDO1 inhibitor increased the migration of immune cells, whereas the PD-L1 antibody failed to increase the migration (Fig. 33).

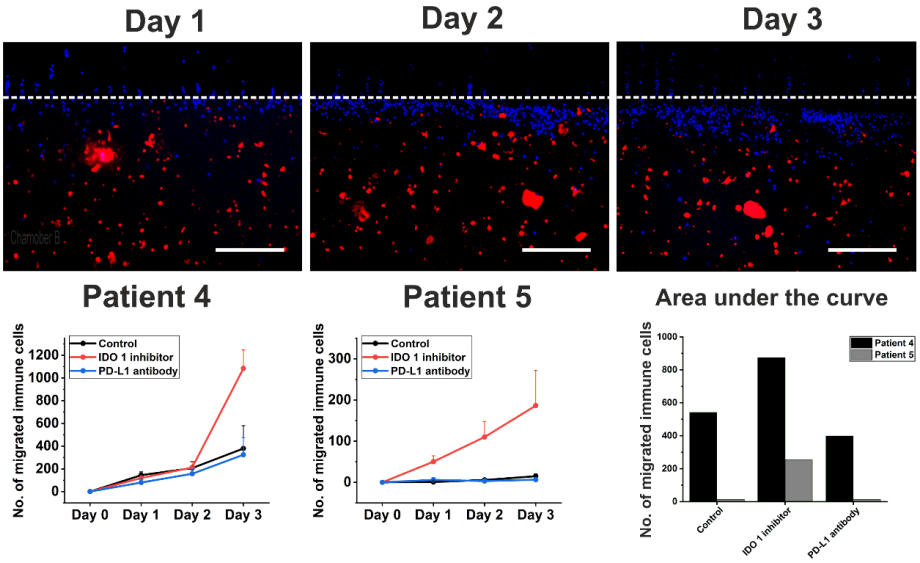

Figure 33. Infiltration of the patient–derived immune cells to the chamber B filled with patient–derived cancer cells. Cell trace far red and violet dye were used for labeling HNSCC patient–derived cancer and immune cells, respectively. Cancer cells were loaded into the chamber B with or without PD-L1 antibody or IDO1 inhibitor. Data are presented as means with standard deviation of three images from different locations on the chip. Scale bar represents 200 μm.

We studied the effect of the IDO1 inhibitor and PD-L1 antibody on tumor cell proliferation using two patient samples. For patient four, PD-L1 antibody had the highest effect on cancer cell proliferation, but for patient five both inhibitors appeared promising (Fig. 34).

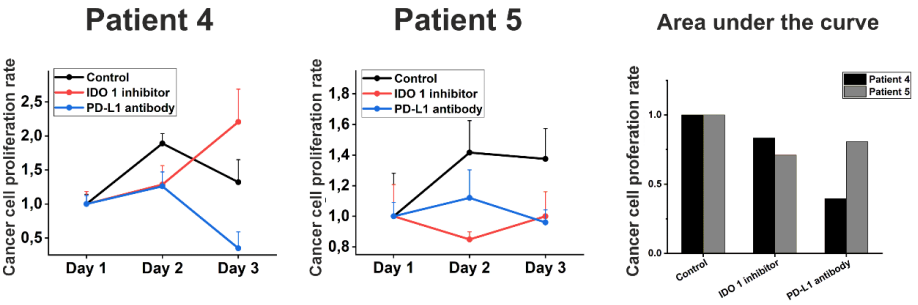

Figure 34. Proliferation rates of patient–derived cancer cells measured over three days. Data are presented as means with standard deviation of three images from different locations on the chip.

5 DISCUSSION

In the first project, we showed that matrix (Matrigel vs Myogel) affects the drug responses of HNSCC cells. Myogel cultured cells were less responsive to the EGFR and MEK inhibitors than cells cultured on Matrigel or plastic. However, PI3K/mTOR inhibitors exhibited similar efficacy under all culturing conditions. Another approach was to compare clinical trial ORRs to our *in vitro* responses. Based on our results, Myogel cultured cells best mirrored the EGFR inhibitor response rates reported in clinical trials. In the second project, we applied Myogel in HTS to identify synergistic drug–radiation combinations using a compound library (n=396) and ionizing radiation. Our screen detected several compounds with strong synergistic and antagonistic effects. The most promising compound, navitoclax, was validated in extended HTS and apoptosis assays. In the third project, we applied Myogel in the first humanized *in vitro* microfluidic chip assay to test immune checkpoint inhibitors against HNSCC cell lines and patient samples. Our findings revealed that an IDO1 inhibitor, but interestingly not a PD-L1 antibody, activated migration of the immune cells toward cancer cells. Moreover, we showed that the response of patient cancer and immune cells to the IDO1 inhibitor and PD-L1 antibody differed between the two patients tested.

5.1 MYOGEL IMPROVES THE PREDICTABILITY OF HNSCC *IN VITRO* ANTICANCER DRUG TESTING

Current *in vitro* cancer research is moving towards 3D cell culture models to better reflect the *in vivo* situation [78]. Several matrices are available for 3D cultures, such as Matrigel, rat tail collagen, fibrinogen and synthetic hydrogels [216]. However, all these matrices lack the broad spectrum of human tumor–derived matrix and signaling molecules. Based on this observation, we hypothesized that Myogel, originating from human TME would provide a more natural cell culture environment for cancer cells and, therefore, more reliable drug testing data. Numerous studies have reported that 3D culturing and the presence of ECM affect the sensitivity to chemotherapeutic agents [3,79]. In this PhD project, we investigated the anticancer compound response of 12 HNSCC cell lines between five different culturing dimensions (2D vs 3D), and matrices by applying mouse and human TME–derived matrices.

Our results showed a significantly lower EGFR and MEK inhibitor sensitivity in Myogel cultured cells than in Matrigel cultured cells. However, PI3K/mTOR inhibitors exhibited similar sensitivity under all culturing conditions. This indicates that extracellular matrix has a greater effect on drugs targeting receptors, such EGFR than those that target enzymes in the cytosol, such as mTOR. Surprisingly, no significant differences in drug response were observed between cells cultured on top of the matrix (2D) and cells embedded

in matrix (3D). This indicates that ECM components and cell-ECM junctions have a greater effect on drug sensitivity than the shift from 2D to 3D cultures. This finding emphasizes the importance of the use of the appropriate matrix in *in vitro* anticancer compound testing.

In typical preclinical studies, anticancer compounds are tested on cancer cells cultured on a 2D plastic surface, on mouse-derived matrix and later in xenografts prior to clinical investigations. However, clearly this practice has been unsuccessful due to the low predictive value of anticancer activity in clinical testing [73]. We have previously demonstrated that Myogel's protein content differs 66% from mouse sarcoma derived Matrigel, although they preserve same basic ECM components, such as laminin, type IV collagen, EGF and proteoglycans [4]. Moreover, the mouse degradome is larger and more complex, as it contains 75 more proteases and protease homologues than in the human degradome [217]. We have previously reported that matrix affects HNSCC cell behavior, such as proliferation and invasion [7]. Therefore, we hypothesized that the high failure rate of preclinical investigation might partially be caused by the lack of human TME.

In the human body, cancer cells are surrounded by the TME comprising many components, such as cytokines and growth factors secreted by immune and stromal cells, such as CAFs [218]. This unique niche clearly affects cancer cell behavior and drug sensitivity against anticancer compounds [78]. Due to the enormously large number of such proteins, a precise identification of all the factors interfering in the drug screen is extremely difficult. Unfortunately, this is also the case in our drug screen matrix, Myogel, which contains TME components.

The EGFR inhibitors have been widely investigated as a promising treatment for HNSCC. However, in clinical trials these inhibitors have been shown to elicit only a modest response [2]. To date, cetuximab remains the only FDA-approved EGFR inhibitor treatment for HNSCC patients. Unfortunately, the efficacy of cetuximab has remained relatively low, and patients rapidly develop drug resistance [2,133]. Despite promising *in vitro* and *in vivo* animal studies, other EGFR inhibitors, such as gefitinib, have had poor efficacy in clinical trials as a single agent [133,134,136-138]. In our study, both plastic and Matrigel cell cultures exhibited higher EGFR inhibitor response rates than are reflected in clinical outcomes. Interestingly, EGFR inhibitors have not yet achieved the desired clinical effects [72]. Nevertheless, EGFR inhibitors tested in Myogel showed a response rate similar to the results of 16 monotherapy clinical trials (1258 patients). However, we included only clinical trials where drugs were given as a single agent. These trials usually include metastatic and recurrent HNSCC patients, who are resistant to the first-line treatments, which make comparison of *in vitro* results less than ideal. Moreover, we had to exclude combination therapy trials, because we could not reliably

distinguish the separate effects of the co-administered drugs. Additionally, the direct comparison between clinical and *in vitro* results is not ideal. To provide a more reliable comparison, drugs should be tested as parallel trials in patients and patient-derived *in vitro* cultures.

Several genomic alterations are found to affect the PI3K/AKT/mTOR pathway activation in HNSCC [150], which plays an important role in initiation and progression of cancer [150]. Preclinical studies and early clinical trials of mTOR inhibitors have yielded modest results [219]. Temsirolimus has shown tumor shrinkage in two phase II clinical trials, but no objective response was observed [214]. Thus far, another mTOR inhibitor, sirolimus has only one completed monotherapy trial in HNSCC (n=16) [215]. This trial reported ORR 25% including one complete response [215]. In our drug screen, no significant differences in drug response between any culturing conditions were seen for temsirolimus or sirolimus. However, overall, cell lines were more sensitive to sirolimus than temsirolimus. In the human body, temsirolimus converts to sirolimus via enzymatic hydrolysis [220]. Temsirolimus is an ester analog of sirolimus that is reported to retain its mTOR inhibitory activity while exhibiting better solubility than sirolimus [220]. However, our results indicate that the activity of temsirolimus may be more attributed to its metabolites.

To better understand how the matrix affects cell responses to EGFR and MEK inhibitors, we examined the protein levels of EGFR, ERK1/2, and pERK1/2 in five cell lines that revealed the most diverse EGFR- and MEK-inhibitor effects. Unfortunately, after repeating the experiments three times, we found no significant difference in protein levels of EGFR and ERK1/2 between culture conditions. Therefore, we could not draw any conclusions of EGFR and ERK1/2 protein expression levels in relation to EGFR or MEK inhibitor response. Previous studies have shown that EGFR protein expression and gene copy number alteration have failed to predict an EGFR inhibitor response [221]. Furthermore, a previous study on a large HNSCC cell line panel showed only a weak association between EGFR overexpression and amplification and its inhibitor response [202]. EGFR overexpression in HNSCC is reported in many studies, although supporting data are limited and contradictory [130]. According to Shaznabar *et al.*, the EGFR protein overexpression is more common in established HNSCC cell lines than in clinical samples [222]. Moreover, no EGFR overexpression was observed in HNSCC samples when normalized to healthy mucosal samples [222]. Some studies have suggested that EGFR-mediated autophagy and overexpression of other receptor tyrosine kinases might play a role in the therapeutic resistance [42,223-225].

5.2 HTS REVEALS SYNERGISTIC AND ANTAGONISTIC EFFECTS OF COMPOUND– IRRADIATION COMBINATIONS

In the first project, we concluded that drug screens using Myogel cultured cells better reflect the response rates of EGFR inhibitor clinical trials compared to control and Matrigel cultures. Moreover, no significant differences in drug sensitivity were detected between Myogel coating (2D) and embedding (3D). We concluded that 2D-coated culture is sufficient for drug testing purposes if it provides the human TME elements. Therefore, we used only Myogel for the following drug screen. The response rates of targeted monotherapies in HNSCC clinical trials have turned out low, and therefore we used combination therapy in the following drug screening. We tested five HNSCC cell lines cultured on Myogel coating with 396 drugs, including investigational and clinically approved compounds, and irradiation to find synergistic and antagonistic combinations. Our data showed substantial variability in drug and irradiation responses between all five cell lines. The majority of the drugs lacked interaction with irradiation, but some drugs possessed strong synergism or antagonism. The most promising candidates were further validated using a dose–response matrix analysis using multiple irradiation doses. We examined the most synergistic agent, navitoclax, further using an additional dose-response analysis for eight cell lines. Additionally, we performed a live cell apoptosis assay for two representative cell lines.

Many *in vitro* studies have reported that a combination therapy schedule has a crucial role in the treatment response. Unfortunately, our screen features only one schedule, which was designed based on a typical HNSCC chemoradiation schedule, whereby radiotherapy begins simultaneously with drug administration or on the next day. In our screen, we irradiated cells 24 hours after cell seeding and drug exposure to ensure that cells were completely attached before irradiation.

Drug screen detected promising synergistic agents

Afatinib exhibited promising synergy with irradiation, similar to previous *in vitro* studies [136,145]. Moreover, the combination of afatinib and radiotherapy is now under clinical investigation for HNSCC (NCT01783587). Our data indicated that tretinoin enhances the effect of radiotherapy. This is in line with published data in which tretinoin was reported to modulate radiosensitivity in HNSCC cell lines [226]. We observed a moderate synergism between talazoparib and irradiation in HNSCC cells. Such radiosynergism has been observed in several solid tumors, but for the first time for HNSCC in our drug screen [227]. Patient recruitment for clinical trials using talazoparib and radiotherapy for several cancer types, such as lung, gynecologic and breast cancer is ongoing.

Antagonistic compounds

Two PLK1 inhibitors (BI 2536 and GSK-461364) exhibited strong antagonism when administered 24 hours before radiation. A previous study has demonstrated both synergistic and antagonistic effects of PLK1 inhibitors when combined with irradiation depending on treatment schedule in colorectal cancer and osteosarcoma cell lines [228]. To date, BI 2536 is underexplored in HNSCC both clinically and *in vitro*. BI 2536 clinical trials are focusing on leukemia and solid tumors, such as breast, pancreatic, prostate and lung cancer. One phase II trial for BI 2536 included an unspecified number of HNSCC patients but also patients with many other types of solid tumors (NCT00526149). *In vitro* and clinical antitumor effects of GSK-461364 on HNSCC has remained underexplored. To date, GSK-461364 is investigated clinically only in one trial for non-Hodgkin's lymphoma (NCT00536835).

Pemetrexed is a FDA-approved drug for pleural mesothelioma and NSCLC [229]. Although pemetrexed has been widely investigated as a treatment for HNSCC patients, the benefit of pemetrexed in HNSCC treatment remains unclear [230]. Despite various antitumor effects reported, the pemetrexed–irradiation combination has been shown to obtain both antagonistic and synergistic effects in a schedule-dependent manner in HNSCC cells [229]. Similar to our findings, Wouters *et al.* reported that drug administration 24 hours before irradiation resulted in moderate antagonism in HNSCC cell lines (CAL-27). Our data showed strong antagonism of pemetrexed and irradiation in all cell lines, which were sensitive to pemetrexed as a single agent. This brings up concerns regarding the combination treatment of pemetrexed and radiotherapy in HNSCC.

Navitoclax–radiation combination exhibits strong synergistic anticancer effects on cell viability, proliferation, and apoptosis

The Bcl-2/Bcl-xL inhibitor navitoclax has been reported to have *in vitro* antitumor effects across various tumor types alone and in combination with chemotherapeutic agents [178]. However, only a few navitoclax *in vitro* studies have been published for HNSCC and only one has investigated navitoclax together with irradiation [186]. In that study navitoclax was reported to obtain only modest benefit in two HNSCC cell lines. However, only one irradiation dose and two navitoclax concentrations were used. Navitoclax has been under active clinical investigation for leukemia and solid tumors as a single agent and in combination with other drugs. However, the combination of navitoclax and irradiation is still underutilized. No clinical trials for HNSCC have been performed.

For the first time, we report a clear synergism between navitoclax and irradiation in HNSCC. The dose-response matrix analysis revealed significant synergism in ten cell lines and moderate synergism in three cell lines. Surprisingly, in the drug library, other Blc-2 family inhibitors were ineffective (II: Fig. S1). The Blc-2 selective inhibitor venetoclax lacked efficacy as a single

agent and when combined with irradiation in all five cell lines. The Bcl-2 and Mcl-1 inhibitor AT 101 had modest, however not as convincing synergism as the Bcl-2/Bcl-xL inhibitor navitoclax. This indicates that dual Bcl-2 and Bcl-xL inhibition is crucial for inducing synergy with irradiation in HNSCC cells. To investigate the role of Bcl-xL in radiosynergy, further analysis could be conducted using newly discovered selective Bcl-xL inhibitors, such as WEHI-539 and A-1331852.

To our knowledge, these investigational compounds are not yet tested on HNSCC cell lines or with radiotherapy. The most common genomic alteration in HNSCC is an inactivating p53 mutation, which occurs in 50% of cases [130]. p53 promotes transcription of pro-apoptotic BAX, PUMA and NOXA and inhibits anti-apoptotic Bcl-2-family proteins [175]. To investigate whether p53 mutation status has an effect on navitoclax-induced radiosensitivity, we screened six wild-type and six mutated p53 HNSCC cell lines. Our data showed that both status, wild-type and mutated p53 HNSCCs exhibited a strong synergism and therefore, we concluded that p53 mutation status had no role in navitoclax radiosynergism. This indicates that navitoclax has the ability to overcome the tumor protective mechanisms of mutated p53 after irradiation damage (Fig. 35). However, navitoclax alone seemed to have a greater effect on HNSCC cell lines with wild-type p53 than mutated p53.

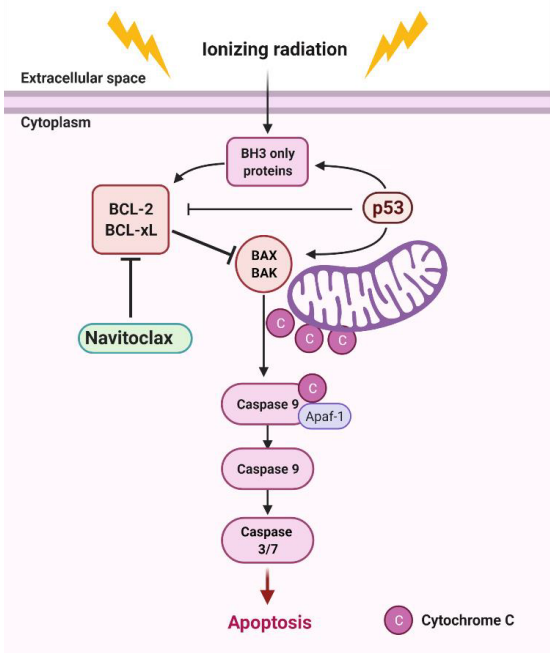

Figure 35. A possible mechanism underlying the navitoclax–irradiation combination induced apoptosis. Created with BioRender.com.

Bcl-2 family proteins control mitochondria-dependent apoptosis by releasing mitochondrial proteins into the cytosol leading to caspase activation [178]. Navitoclax has been reported to trigger mitochondria-dependent apoptosis in small-cell lung cancer (SCLC) and acute lymphoblastic leukemia cells *in vitro* and *in vivo* [231]. Our live cell apoptosis assay results demonstrated that this occurs also in HNSCC cells. The irradiation-induced apoptosis was remarkably increased in the presence of navitoclax in both tested cell lines. In addition, as a single agent navitoclax decreased proliferation of cancer cells and when combined with irradiation completely halted the cell cycle. This indicates that navitoclax might possess therapeutic potential in HNSCC as a single agent and together with irradiation.

5.3 MICROFLUIDIC CHIP ASSAY REVEALS VARYING IMMUNOTHERAPY RESPONSES BETWEEN PATIENTS

In recent years, immunotherapy has revolutionized cancer research and treatment and it has been investigated in several different cancers including HNSCC. Despite promising results, only a small proportion of patients respond to therapy [9,68]. Due to the small percentage of responders, the majority of patients will receive ineffective treatment with unwanted adverse effects. So far, no markers to predict the patients' response are available.

We manufactured a 3D *in vitro* microfluidic chip suitable for testing immunotherapeutic drugs' efficacy on HNSCC cancer patient samples (cancer and immune cells and serum). We improved the existing chip method by providing a fully human TME for the cancer cells by embedding them in a Myogel/fibrin matrix. The system was first validated using a human oral squamous carcinoma cell line (HSC-3) and next applied for two HNSCC patient samples.

The crosstalk between immune and cancer cells is commonly studied using immune cell migration assays [232]. These assays have been also used to determine the effectiveness of immunotherapy [90,91]. However, testing immunomodulators appears more complex than conventional drug testing since it requires co-culture of cancer and immune cells. Available co-culturing models still require improvements due to different adherent properties of cancer and immune cells. The microfluidic chip, designed by Businaro *et al.,* provides different chambers for the cells, which are connected by microchannels [211]. Immune and cancer cells are injected in different chambers and cancer cells are embedded in matrix. Since we previously showed that Myogel is superior to Matrigel in drug testing (*Study I*) for HNSCC cell lines, we replaced Matrigel with Myogel. To confirm that Myogel is suitable for patient–derived cells, we measured the viability of HNSCC

patient–derived cancer cells cultured on plastic, Matrigel and Myogel. Our viability assay revealed that patient–derived cells exhibit higher viability on Myogel compared to other culturing conditions in three patients. Additionally, we replaced commonly used FBS isolated from bovine fetuses with the patient's own serum. In this way, we provided immune and cancer cells with the most *in vivo* mimicking environment.

In this study, we targeted two immune checkpoints, IDO1 and PD-1. IDO1 is upregulated in HNSCC and it has been reported to suppress functions of effector T and natural killer cells and activate differentiation of regulatory T cells via tryptophan metabolism [189,190,233]. However, the exact mechanism of IDO1 on immunomodulation on TME of HNSCC have remained unclear [234]. PD-L1 is also shown to be highly expressed in HNSCC [235]. The PD-L1 upregulation allows cancer cells to escape from the immune system via induction of T-cell apoptosis, anergy, exhaustion and expression of interleukin-10 [192].

Our results demonstrated that an IDO1 inhibitor, but interestingly not a PD-L1 antibody, activates the migration of the immune cells toward cancer cells. To our knowledge, this is the first study to demonstrate that inhibition of IDO1 induces infiltration of the immune cells. Unfortunately, since we used a mixture of peripheral blood mononuclear cells, we were not able to specify an immunotherapy effect on specific immune cell groups. However, our findings indicate that IDO1 inhibitors might convert the tumor from cold to hot. In theory, this could improve the effectiveness of immunotherapeutic agents, like PD-1 and PD-L1 antibodies, when co-administered with an IDO1 inhibitor. In the future, we will explore immunotherapeutic combination therapy and investigate immunotherapy effects on specific immune cell populations, such as regulatory and cytotoxic T-cells.

In our study, differences in drug responses were observed between two HNSCC patient samples. For patient number five, the IDO1 inhibitor was the most effective, while patient number four benefited the most from the PD-L1 antibody. Additionally, we detected altered antiproliferative effects between patient samples of both immune checkpoint inhibitors. However, immune cell migration did not correlate with the proliferation results. Therefore, we concluded that immune cell migration alone is not a sufficient parameter to assess the response to immunotherapeutic drugs, as previously suggested [91]. Additionally, the use of an apoptotic reagent would improve determination of the immune cell mediated cytotoxicity. Moreover, isolation and separate testing of the different immune cell populations would be essential for better understanding the effects of immune therapy.

6 CONCLUSIONS AND FUTURE PROSPECTIVES

Our study revealed significant differences in drug sensitivity between HNSCC cancer cells cultured in Myogel and Matrigel. We concluded that a drug screen using Myogel cultured cells better reflects the response rates of EGFR inhibitor clinical trials compared with those obtained with control and Matrigel cultures. Therefore, we propose that applying Myogel in the preclinical phase could reveal the false-positive drug responses, decrease drug development expenses, and minimize exposure of patients to the adverse effects of ineffective treatments in clinical trials.

Our second drug screen, applying only Myogel, revealed both synergistic and antagonistic drug-irradiation combinations for HNSCC cells. In agreement with previous studies, pemetrexed and PLK1 inhibitors (BI 2536 and GSK-461364) exhibited a strong antagonism, whereas the combinations of irradiation with afatinib, talazoparib or tretinoin resulted a promising synergy. As the most promising finding, we reported that the navitoclax–irradiation combination resulted in a strong synergy resulting in cell cycle arrest and apoptosis in HNSCC cells. Our findings encourage clinical investigation of the navitoclax–irradiation combination as treatment for HNSCC. However, further *in vitro* and *in vivo* studies are needed to determine the toxicity and efficacy testing of this combination before initiating clinical trials.

In the third project, we introduced a novel *in vitro* microfluidic chip assay designed for testing immunotherapeutic agents on HNSCC patient samples. Hopefully in the future, using this method, we could provide preliminary data of the patient response to immunotherapy. By applying Myogel and patient serum in a microfluidic chip assay, we provided a fully human culturing condition for HNSCC cells and ensured a high viability of patient–derived cells. We showed that the IDO1 inhibitor induced immune cell infiltration towards cancer cells. We hypothesized, that this might indicate transformation of immune cell phenotypes, which might enhance the efficacy of the other immunotherapeutic drugs, such as PD-1 and PD-L1 antibodies. Therefore, our next move is to apply our microfluidic chip assay to investigate the combinations of immune checkpoint inhibitors.

We have actively continued development of the microfluidics assay, and currently the chip has been improved to have three testing systems instead of one (unpublished data). Additionally, we have succcessfully optimized the imaging and analysis system to identify apoptotic cells using the caspase-3/7 apoptosis reagent. Next, we will broaden our understanding of immunotherapeutic effects on specific immune cell populations by testing isolated lymphocytes (CD8, CD4 and natural killer cells) separately and together using different dyes. Our assay will be applied also for

immunotherapeutics used in clinics for HNSCC (nivolumab and pembrolizumab). Our chip assay will allow simultaneous immunotherapy testing in patients and patient–derived cells (co-clinical trials) to prospectively test the value of personalized cancer medicine in HNSCC patients.

This PhD project emphasizes the importance of applying extracellular matrix – especially a human tumor–derived matrix – in anticancer drug discovery and preclinical evaluation. The future goal is to introduce Myogel for a broad panel of patient–derived cancer samples and personalized medicine applications.

ACKNOWLEDGEMENTS

The studies presented in this thesis were performed during 2017-2021 at Department of Oral Maxillofacial Diseases, Faculty of Medicine, University of Helsinki. The projects was funded by the Doctoral Program in Clinical Research (KLTO), the The Emil Aaltonen Foundation, Cancer Society Finland, the Sigrid Juselius Foundation, the Jane and Aatos Erkko Foundation and the Helsinki University Central Hospital research funds.

My deepest gratitude belongs to my supervisors, Professor Tuula Salo, Docent Outi Monni and Professor Antti Mäkitie. First, I wish to thank my primary supervisor Tuula for her comprehensive guidance and support throughout my PhD project. Her enthusiasm for science, broad knowledge in cancer research and brilliant ideas have been truly inspirational. Without her expertise, innovations and collaborative skills, these projects would not have been possible. Next, I would like to thank Outi for her guidance and kindness. I have the deepest respect for her broad knowledge of cancer genetics. I wish to acknowledge Antti for his positive attitude and encouragement that have given me the motivation and self-confidence over the years. I highly respect his expertise in head and neck cancer research and its treatments.

I acknowledge my thesis committee members Professor David Rice and Docent Pia Vahteristo for their support and encouraging feedback. I am grateful to Professor Klaus Elenius and Professor Sara Zanivan for agreeing to be my official pre-examiners. Their constructive comments proved valuable and improved this thesis. I am deeply thankful to Professor Jukka Westermarck for kindly accepting invitation to serve as my dissertation opponent. I am thankful to Vilja Pietiäinen for agreeing to be faculty representative in my public examination.

This PhD project would not have happened without the assistance of my wonderful co-workers from the Salo group, who have spent their precious time helping me with these projects. First, I would like to thank my co-worker and friend Docent Ahmed Al-Samadi for always helping and supporting me. Without his guidance and expertise, my journey would had been much more difficult. I wish also to thank Ahmed and our co-author Benedek Poor for their leading role in the third article. I have been extremely lucky to work with great colleague and best friend Erika Naakka. I am grateful for her support in life, work and graphic design. I wish to thank Meri Sieviläinen and Krista Juurikkala for being excellent travel company at international conferences. I wish to thank Erika Naakka, Meri Sieviläinen, Ilida Suleymanova, Aini Hyytiäinen and Wafa Wabhi for peer support and joyful moments both in and outside the lab. I acknowledge Aini Hyytiäinen, Maija Risteli, Pirjo Åström, Ilida Suleymanova and Wafa Wabhi for their expertise and assistance in lab experiments and analysis. My gratitude extends to all current and former

group members; Krista Laurila, Johanna Peltonen, Tuulia Onali, Abdelhakim Salem, Rabeia Mustafa, Awais Wahab, Douwe Hoornstra, Sakhr Al-Kubati, Professor Fabricio Passador-Santos and many other.

I warmly thank my co-authors Piia-Riitta Karhemo, Reidar Grénman, Krister Wennerberg, Minna Turunen, Paula Bergman, Riia Tiikkaja, Karri Mesimäki, Tommy Wilkman, Ville Liu, Benedek Poor and Päivi Saavalainen for their valuable expertise and assistance during this project. Special thanks to Jani Saarela, Laura Turunen and Sergey Kuznetsov from the FIMM HTB unit for their excellent drug testing expertise and Swapnil Potdar, Philipp Ianevski and Aleksandr Ianevski for their great bioinformatic skill.

Many thanks to Deborah Kaska and Vanessa Fuller for their excellent language editing. I thank Professor Peeter Karihtala, Professor Matthias Nees and Professor Hannu Sariola for their valuable comments. I would like to thank Prson Gautam and Hazem Ibrahim for their technical support and Satu Manninen for data collection.

Thanks to all my dear friends with whom I spent much-needed time outside the lab. I am grateful to have you in my life. I warmly thank my soul sisters Elina, Erika, Linda, Henna and Noora for always listening and supporting me. Special thanks goes also to my childhood friends Aino, Henna, Ellu and Sussu for sharing ups and downs in life.

My sincerest gratitude goes to the most important people in my life, my mother and father, who unfortunately are no longer with us. Without their love and support, I would not have made this far. I am forever grateful to my father for his great life advice and genuine interest in my research. I am so very grateful to my siblings Toni, Julius and Linda for sharing the joys and sorrows of life with me. Linda, you are my rock. Thank you for being the best sister and friend.

Finally, I thank Perttu for all his love, patience and support during difficult times. I thank also my loyal furry friends Milli and Vinski for the refreshing walks during the writing process and for bringing joy into our lives.

Helsinki, November 2021
Katja Tuomainen

REFERENCES

1. Sung H, Ferlay J, Siegel RL *et al.* (2021) Global Cancer Statistics 2020: GLOBOCAN Estimates of Incidence and Mortality Worldwide for 36 Cancers in 185 Countries. CA Cancer J Clin. *71*, 209-2493.

2. Wen Y; Grandis JR. (2015) Emerging Drugs for Head and Neck Cancer. Expert Opin Emerg Drugs. *20*, 313-3292.

3. Hickman JA, Graeser R, de Hoogt R *et al.* (2014) Three-Dimensional Models of Cancer for Pharmacology and Cancer Cell Biology: Capturing Tumor Complexity in Vitro/Ex Vivo. Biotechnol J. *9*, 1115-11289.

4. Salo T, Sutinen M, Hoque Apu E *et al.* (2015) A Novel Human Leiomyoma Tissue Derived Matrix for Cell Culture Studies. BMC Cancer. *15*, 981.

5. Salo T, Dourado MR, Sundquist E *et al.* (2018) Organotypic Three-Dimensional Assays Based on Human Leiomyoma-Derived Matrices. Philos Trans R Soc Lond B Biol Sci. *373*1737.

6. Naakka E, Tuomainen K, Wistrand H *et al.* (2019) Fully Human Tumor-Based Matrix in Three-Dimensional Spheroid Invasion Assay. J Vis Exp. 147.

7. Wahbi W, Naakka E, Tuomainen K *et al.* (2020) The Critical Effects of Matrices on Cultured Carcinoma Cells: Human Tumor-Derived Matrix Promotes Cell Invasive Properties. Exp Cell Res. *389*, 1118851.

8. Seiwert TY, Burtness B, Mehra R *et al.* (2016) Safety and Clinical Activity of Pembrolizumab for Treatment of Recurrent Or Metastatic Squamous Cell Carcinoma of the Head and Neck (KEYNOTE-012): An Open-Label, Multicentre, Phase 1b Trial. Lancet Oncol. *17*, 956-9657.

9. Ferris RL, Blumenschein G, Fayette J *et al.* (2016) Nivolumab for Recurrent Squamous-Cell Carcinoma of the Head and Neck. N Engl J Med. *375*, 1856-186719.

10. *Head and Neck Cancers - National Cancer Institute.* Available at: https://www.cancer.gov/types/head-and-neck/head-neck-fact-sheet. Accessed Mar 1, 2021.

11. Vigneswaran N; Williams MD. (2014) Epidemiologic Trends in Head and Neck Cancer and Aids in Diagnosis. Oral Maxillofac Surg Clin North Am. *26*, 123-1412.

12. Shah JP; Lydiatt W. (1995) Treatment of Cancer of the Head and Neck. CA Cancer J Clin. *45*, 352-3686.

13. Brierley JD. *TNM Classification of Malignant Tumours*, 8th ed.; Wiley Blackwell: Chichester, England, 2017.

14. Gandini S, Botteri E, Iodice S *et al.* (2008) Tobacco Smoking and Cancer: A Meta-Analysis. Int J Cancer. *122*, 155-1641.

15. Blot WJ, McLaughlin JK, Winn DM *et al.* (1988) Smoking and Drinking in Relation to Oral and Pharyngeal Cancer. Cancer Res. *48*, 3282-328711.

16. Hashibe M, Brennan P, Benhamou S *et al.* (2007) Alcohol Drinking in Never Users of Tobacco, Cigarette Smoking in Never Drinkers, and the Risk of Head and Neck Cancer: Pooled Analysis in the International Head and Neck Cancer Epidemiology Consortium. J Natl Cancer Inst. *99*, 777-78910.

17. Chaturvedi AK, Engels EA, Pfeiffer RM *et al.* (2011) Human Papillomavirus and Rising Oropharyngeal Cancer Incidence in the United States. J Clin Oncol. *29*, 4294-430132.

18. Gillison ML, D'Souza G, Westra W *et al.* (2008) Distinct Risk Factor Profiles for Human Papillomavirus Type 16-Positive and Human Papillomavirus Type 16-Negative Head and Neck Cancers. J Natl Cancer Inst. *100*, 407-4206.

19. de Martel C, Plummer M, Vignat J *et al.* (2017) Worldwide Burden of Cancer Attributable to HPV by Site, Country and HPV Type. Int J Cancer. *141*, 664-6704.

20. Jouhi L, Halme E, Irjala H *et al.* (2018) Epidemiological and Treatment-Related Factors Contribute to Improved Outcome of Oropharyngeal Squamous Cell Carcinoma in Finland. Acta Oncol. *57*, 541-5514.

21. Ho P, Ko Y, Yang YC *et al.* (2002) The Incidence of Oropharyngeal Cancer in Taiwan: An Endemic Betel Quid Chewing Area. J Oral Pathol Med. *31*, 213-2194.

22. Yu MC; Yuan J. (2002) Epidemiology of Nasopharyngeal Carcinoma. Semin Cancer Biol. *12*, 421-4296.

23. Guha N, Boffetta P, Wünsch Filho V *et al.* (2007) Oral Health and Risk of Squamous Cell Carcinoma of the Head and Neck and Esophagus: Results of Two Multicentric Case-Control Studies. Am J Epidemiol. *166*, 1159-117310.

24. Chien YC, Chen JY, Liu MY *et al.* (2001) Serologic Markers of Epstein-Barr Virus Infection and Nasopharyngeal Carcinoma in Taiwanese Men. N Engl J Med. *345*, 1877-188226.

25. Horn-Ross PL, Ljung BM; Morrow M. (1997) Environmental Factors and the Risk of Salivary Gland Cancer. Epidemiology. *8*, 414-4194.

26. Luce D, Leclerc A, Bégin D *et al.* (2002) Sinonasal Cancer and Occupational Exposures: A Pooled Analysis of 12 Case-Control Studies. Cancer Causes Control. *13*, 147-1572.

27. Perloy A, Maasland DHE, van den Brandt, Piet A. *et al.* (2017) Intake of Meat and Fish and Risk of Head-Neck Cancer Subtypes in the Netherlands Cohort Study. Cancer Causes Control. *28*, 647-6566.

28. Pavia M, Pileggi C, Nobile CGA *et al.* (2006) Association between Fruit and Vegetable Consumption and Oral Cancer: A Meta-Analysis of Observational Studies. Am J Clin Nutr. *83*, 1126-11345.

29. Ganesh D, Sreenivasan P, Öhman J *et al.* (2018) Potentially Malignant Oral Disorders and Cancer Transformation. Anticancer Res. *38*, 3223-32296.

30. Aghbari SMH, Abushouk AI, Attia A *et al.* (2017) Malignant Transformation of Oral Lichen Planus and Oral Lichenoid Lesions: A Meta-Analysis of 20095 Patient Data. Oral Oncol. *68*, 92-102.

31. Warnakulasuriya S; Ariyawardana A. (2016) Malignant Transformation of Oral Leukoplakia: A Systematic Review of Observational Studies. J Oral Pathol Med. *45*, 155-1663.

32. Abadie WM, Partington EJ, Fowler CB *et al.* (2015) Optimal Management of Proliferative Verrucous Leukoplakia: A Systematic Review of the Literature. Otolaryngol Head Neck Surg. *153*, 504-5114.

33. Bray F, Ferlay J, Soerjomataram I *et al.* (2018) Global Cancer Statistics 2018: GLOBOCAN Estimates of Incidence and Mortality Worldwide for 36 Cancers in 185 Countries. CA Cancer J Clin. *68*, 394-4246.

34. Siegel RL, Miller KD; Jemal A. (2017) Cancer Statistics, 2017. CA Cancer J Clin. *67*, 7-301.

35. Linge A, Lohaus F, Löck S *et al.* (2016) HPV Status, Cancer Stem Cell Marker Expression, Hypoxia Gene Signatures and Tumour Volume Identify Good Prognosis Subgroups in Patients with HNSCC After Primary Radiochemotherapy: A Multicentre Retrospective Study of the German Cancer Consortium Radiation Oncology Group (DKTK-ROG). Radiother Oncol. *121*, 364-3733.

36. *Global Cancer Observatory – Cancer Today.* Available at: https://gco.iarc.fr/today/online-analysis-table?v=2018&mode=cancer&mode_population=continents&population=900&populations=900&key=asr&sex=0&cancer=39&type=0&statistic=5&prevalence=0&population_group=0&ages_group%5B%5D=0&ages_group%5B%5D=17&group_cancer=1&include_nmsc=1&include_nmsc_other=1. Accessed Mar 1, 2021.

37. Hussein AA, Helder MN, de Visscher JG *et al.* (2017) Global Incidence of Oral and Oropharynx Cancer in Patients Younger than 45 Years Versus Older Patients: A systematic Review. Eur J Cancer. *82*, 115-127.

38. Lawrence MS, Sougnez C, Lichtenstein L *et al.* (2015) Comprehensive Genomic Characterization of Head and Neck Squamous Cell Carcinomas. Nature (London). *517*, 576-5827536.

39. Leemans CR, Snijders PJF; Brakenhoff RH. (2018) The Molecular Landscape of Head and Neck Cancer. Nat Rev Cancer. *18*, 269-2825.

40. Iglesias-Bartolome R, Martin D; Gutkind JS. (2013) Exploiting the Head and Neck Cancer Oncogenome: Widespread PI3K-mTOR Pathway Alterations and Novel Molecular Targets. Cancer Discov. *3*, 722-7257.

41. Squarize CH, Castilho RM, Abrahao AC *et al.* (2013) PTEN Deficiency Contributes to the Development and Progression of Head and Neck Cancer. Neoplasia. *15*, 461-4715.

42. Johnson DE, Burtness B, Leemans CR *et al.* (2020) Head and Neck Squamous Cell Carcinoma. Nat Rev Dis Primers. *6*, 921.

43. Ang KK, Harris J, Wheeler R *et al.* (2010) Human Papillomavirus and Survival of Patients with Oropharyngeal Cancer. N Engl J Med. *363*, 24-351.

44. Homer JJ; Fardy MJ. (2016) Surgery in Head and Neck Cancer: United Kingdom National Multidisciplinary Guidelines. The Journal of Laryngology & Otology. *130*, S68-S70S2.

45. van der Veen J; Nuyts S. (2017) Can Intensity-Modulated-Radiotherapy Reduce Toxicity in Head and Neck Squamous Cell Carcinoma? Cancers (Basel). *9*10.

46. Machiels J-, René Leemans C, Golusinski W *et al.* (2020) Squamous Cell Carcinoma of the Oral Cavity, Larynx, Oropharynx and Hypopharynx: EHNS-ESMO-ESTRO Clinical Practice Guidelines for Diagnosis, Treatment and Follow-Up. Ann Oncol. *31*, 1462-147511.

47. Mallick S, Benson R, Julka PK *et al.* (2016) Altered Fractionation Radiotherapy in Head and Neck Squamous Cell Carcinoma. Journal of the Egyptian National Cancer Institute. *28*, 732.

48. *Drugs Approved for Head and Neck Cancer - National Cancer Institute.* Available at: https://www.cancer.gov/about-cancer/treatment/drugs/head-neck. Accessed Mar 1, 2021.

49. Dasari S; Tchounwou PB. (2014) Cisplatin in Cancer Therapy: Molecular Mechanisms of Action. Eur J Pharmacol. *0*, 364-378.

50. Pazdur R, Kudelka AP, Kavanagh JJ *et al.* (1993) The Taxoids: Paclitaxel (Taxol®) and Docetaxel (Taxotere®). Cancer Treat. Rev. *19*, 351-3864.

51. Price KAR; Cohen EE. (2012) Current Treatment Options for Metastatic Head and Neck Cancer. Curr Treat Options Oncol. *13*, 35-461.

52. *TPF - National Cancer Institute.* Available at: https://www.cancer.gov/about-cancer/treatment/drugs/tpf. Accessed Mar 1, 2021.

53. Browman GP; Cronin L. (1994) Standard Chemotherapy in Squamous Cell Head and Neck Cancer: What we have Learned from Randomized Trials. Semin Oncol. *21*, 311-3193.

54. Brockstein B, Haraf DJ, Rademaker AW *et al.* (2004) Patterns of Failure, Prognostic Factors and Survival in Locoregionally Advanced Head and Neck Cancer Treated with Concomitant Chemoradiotherapy: A 9-Year, 337-Patient, Multi-Institutional Experience. Ann Oncol. *15*, 1179-11868.

55. Chandana SR; Conley BA. (2009) Neoadjuvant Chemotherapy for Locally Advanced Squamous Cancers of the Head and Neck: Current Status and Future Prospects. Curr Opin Oncol. *21*, 218-2233.

56. Qin H, Luo J, Zhu Y *et al.* (2012) Combination of Taxanes, Cisplatin and Fluorouracil as Induction Chemotherapy for Locally Advanced Head and Neck Cancer: A Meta-Analysis. PLoS One. *7*, e5152612.

57. Lazzari G, De Cillis MA, Buccoliero G *et al.* (2019) Competing Morbidities in Advanced Head and Neck Squamous Cell Carcinoma Concurrent Chemoradiotherapy: A Strong Implication of A Multidisciplinary Team Approach. Cancer Manag Res. *11*, 9771-9782.

58. Blanchard P, Baujat B, Holostenco V *et al.* (2011) Meta-Analysis of Chemotherapy in Head and Neck Cancer (MACH-NC): A Comprehensive Analysis by Tumour Site. Radiother Oncol. *100*, 33-401.

59. Forastiere AA, Goepfert H, Maor M *et al.* (2003) Concurrent Chemotherapy and Radiotherapy for Organ Preservation in Advanced Laryngeal Cancer. N Engl J Med. *349*, 2091-209822.

60. Vermorken JB, Mesia R, Rivera F *et al.* (2008) Platinum-Based Chemotherapy Plus Cetuximab in Head and Neck Cancer. N Engl J Med. *359*, 1116-112711.

61. Bonner JA, Harari PM, Giralt J *et al.* (2006) Radiotherapy Plus Cetuximab for Squamous-Cell Carcinoma of the Head and Neck. N Engl J Med. *354*, 567-5786.

62. Cohen MH, Chen H, Shord S *et al.* (2013) Approval Summary: Cetuximab in Combination with Cisplatin Or Carboplatin and 5-Fluorouracil for the First-Line Treatment of Patients with Recurrent Locoregional Or Metastatic Squamous Cell Head and Neck Cancer. Oncologist. *18*, 460-4664.

63. Ang KK, Zhang Q, Rosenthal DI *et al.* (2014) Randomized Phase III Trial of Concurrent Accelerated Radiation Plus Cisplatin with Or without Cetuximab for Stage III to IV Head and Neck Carcinoma: RTOG 0522. J Clin Oncol. *32*, 2940-295027.

64. Vermorken JB, Herbst RS, Leon X *et al.* (2008) Overview of the Efficacy of Cetuximab in Recurrent and/Or Metastatic Squamous Cell Carcinoma of the Head and Neck in Patients Who Previously Failed Platinum-Based Therapies. Cancer. *112*, 2710-271912.

65. Taberna M, Oliva M; Mesía R. (2019) Cetuximab-Containing Combinations in Locally Advanced and Recurrent Or Metastatic Head and Neck Squamous Cell Carcinoma. Frontiers in oncology. *9*, 383.

66. Alfieri S, Cavalieri S; Licitra L. (2018) Immunotherapy for Recurrent/Metastatic Head and Neck Cancer. Curr Opin Otolaryngol Head Neck Surg. *26*, 152-1562.

67. Cramer JD, Burtness B; Ferris RL. (2019) Immunotherapy for Head and Neck Cancer: Recent Advances and Future Directions. Oral Oncol. *99*, 104460.

68. Larkins E, Blumenthal GM, Yuan W *et al.* (2017) FDA Approval Summary: Pembrolizumab for the Treatment of Recurrent Or Metastatic Head and Neck Squamous Cell Carcinoma with Disease Progression on Or After Platinum-Containing Chemotherapy. Oncologist. *22*, 873-8787.

69. Cohen EEW, Soulières D, Le Tourneau C *et al.* (2019) Pembrolizumab Versus Methotrexate, Docetaxel, Or Cetuximab for Recurrent Or Metastatic Head-and-Neck Squamous Cell Carcinoma (KEYNOTE-040): A Randomised, Open-Label, Phase 3 Study. Lancet. *393*, 156-16710167.

70. Mohs RC; Greig NH. (2017) Drug Discovery and Development: Role of Basic Biological Research. Alzheimers Dement (N Y). *3*, 651-6574.

71. *FDA - Step 1: Discovery and Development.* Available at: https://www.fda.gov/patients/drug-development-process/step-1-discovery-and-development. Accessed Mar 12, 2021.

72. Hutchinson L; Kirk R. (2011) High Drug Attrition Rates--Where are we Going Wrong? Nat Rev Clin Oncol. *8*, 189-1904.

73. Maeda H; Khatami M. (2018) Analyses of Repeated Failures in Cancer Therapy for Solid Tumors: Poor Tumor-Selective Drug Delivery, Low Therapeutic Efficacy and Unsustainable Costs. Clin Transl Med. *7*, 111.

74. *FDA - Step 3: Clinical Research.* Available at: https://www.fda.gov/patients/drug-development-process/step-3-clinical-research. Accessed Mar 1, 2021.

75. Kelm JM, Timmins NE, Brown CJ *et al.* (2003) Method for Generation of Homogeneous Multicellular Tumor Spheroids Applicable to a Wide Variety of Cell Types. Biotechnol Bioeng. *83*, 173-1802.

76. Vinci M, Gowan S, Boxall F *et al.* (2012) Advances in Establishment and Analysis of Three-Dimensional Tumor Spheroid-Based Functional Assays for Target Validation and Drug Evaluation. BMC Biol. *10*, 29.

77. Hagemann J, Jacobi C, Hahn M *et al.* (2017) Spheroid-Based 3D Cell Cultures Enable Personalized Therapy Testing and Drug Discovery in Head and Neck Cancer. Anticancer Res. *37*, 2201-22105.

78. Langhans SA. (2018) Three-Dimensional in Vitro Cell Culture Models in Drug Discovery and Drug Repositioning. Front Pharmacol. *9*, 6.

79. Correia AL; Bissell MJ. (2012) The Tumor Microenvironment is a Dominant Force in Multidrug Resistance. Drug Resist Updat. *15*, 39-491-2.

80. Nath S; Devi GR. (2016) Three-Dimensional Culture Systems in Cancer Research: Focus on Tumor Spheroid Model. Pharmacol Ther. *163*, 94-108.

81. Lee J, Cuddihy MJ; Kotov NA. (2008) Three-Dimensional Cell Culture Matrices: State of the Art. Tissue Eng Part B Rev. *14*, 61-861.

82. Gasiorowski JZ, Murphy CJ; Nealey PF. (2013) Biophysical Cues and Cell Behavior: The Big Impact of Little Things. Annu Rev Biomed Eng. *15*, 155-176.

83. Hughes CS, Postovit LM; Lajoie GA. (2010) Matrigel: A Complex Protein Mixture Required for Optimal Growth of Cell Culture. Proteomics. *10*, 1886-18909.

84. Nyström ML, Thomas GJ, Stone M *et al.* (2005) Development of a Quantitative Method to Analyse Tumour Cell Invasion in Organotypic Culture. J Pathol. *205*, 468-4754.

85. Mao Y; Schwarzbauer JE. (2005) Stimulatory Effects of a Three-Dimensional Microenvironment on Cell-Mediated Fibronectin Fibrillogenesis. J Cell Sci. *118*, 4427-4436Pt 19.

86. Ho W, Tawil B, Dunn JCY *et al.* (2006) The Behavior of Human Mesenchymal Stem Cells in 3D Fibrin Clots: Dependence on Fibrinogen Concentration and Clot Structure. Tissue Eng. *12*, 1587-15956.

87. Sontheimer-Phelps A, Hassell BA; Ingber DE. (2019) Modelling Cancer in Microfluidic Human Organs-on-Chips. Nat Rev Cancer. *19*, 65-812.

88. Hassell BA, Goyal G, Lee E *et al.* (2017) Human Organ Chip Models Recapitulate Orthotopic Lung Cancer Growth, Therapeutic Responses, and Tumor Dormancy In Vitro. Cell Rep. *21*, 508-5162.

89. Choi Y, Hyun E, Seo J *et al.* (2015) A Microengineered Pathophysiological Model of Early-Stage Breast Cancer. Lab Chip. *15*, 3350-335716.

90. Parlato S, De Ninno A, Molfetta R *et al.* (2017) 3D Microfluidic Model for Evaluating Immunotherapy Efficacy by Tracking Dendritic Cell Behaviour Toward Tumor Cells. Sci Rep. *7*, 10931.

91. Lucarini V, Buccione C, Ziccheddu G *et al.* (2017) Combining Type I Interferons and 5-Aza-2'-Deoxycitidine to Improve Anti-Tumor Response Against Melanoma. J Invest Dermatol. *137*, 159-1691.

92. Paterson K, Zanivan S, Glasspool R *et al.* (2021) Microfluidic Technologies for Immunotherapy Studies on Solid Tumours. Lab Chip. *21*, 2306-232912.

93. Drost J; Clevers H. Organoids in Cancer Research. Nature Reviews Cancer **2018**, *18*, 407-418.

94. Weeber F, Ooft SN, Dijkstra KK *et al.* (2017) Tumor Organoids as a Pre-Clinical Cancer Model for Drug Discovery. Cell Chem Biol. *24*, 1092-11009.

95. Driehuis E, Spelier S, Beltrán Hernández I *et al.* (2019) Patient-Derived Head and Neck Cancer Organoids Recapitulate EGFR Expression Levels of Respective Tissues and are Responsive to EGFR-Targeted Photodynamic Therapy. J Clin Med. *8*11.

96. Yang H, Sun L, Liu M *et al.* (2018) Patient-Derived Organoids: A Promising Model for Personalized Cancer Treatment. Gastroenterol Rep (Oxf). *6*, 243-2454.

97. Affolter A, Lammert A, Kern J *et al.* (2021) Precision Medicine Gains Momentum: Novel 3D Models and Stem Cell-Based Approaches in Head and Neck Cancer. Front Cell Dev Biol. *9*.

98. Driehuis E, Kolders S, Spelier S *et al.* (2019) Oral Mucosal Organoids as a Potential Platform for Personalized Cancer Therapy. Cancer Discov. *9*, 852-8717.

99. Galuschka C, Proynova R, Roth B *et al.* (2017) Models in Translational Oncology: A Public Resource Database for Preclinical Cancer Research. Cancer Res. *77*, 2557-256310.

100. Barriuso J, Nagaraju R; Hurlstone A. (2015) Zebrafish: A New Companion for Translational Research in Oncology. Clin Cancer Res. *21*, 969-9755.

101. Wu J, Zhai J, Li C *et al.* (2017) Patient-Derived Xenograft in Zebrafish Embryos: A New Platform for Translational Research in Gastric Cancer. J Exp Clin Cancer Res. *36*, 1601.

102. Al-Samadi A, Tuomainen K, Kivimäki A *et al.* (2019) PCR-Based Zebrafish Model for Personalised Medicine in Head and Neck Cancer. J Transl Med. *17*, 2351.

103. Fior R, Póvoa V, Mendes RV *et al.* (2017) Single-Cell Functional and Chemosensitive Profiling of Combinatorial Colorectal Therapy in Zebrafish Xenografts. Proc Natl Acad Sci U S A. *114*, E8234-E824339.

104. Nicoli S; Presta M. (2007) The Zebrafish/Tumor Xenograft Angiogenesis Assay. Nat Protoc. *2*, 2918-292311.

105. Teng Y, Xie X, Walker S *et al.* (2013) Evaluating Human Cancer Cell Metastasis in Zebrafish. BMC Cancer. *13*, 453.

106. Shultz LD, Goodwin N, Ishikawa F *et al.* (2014) Human Cancer Growth and Therapy in Immunodeficient Mouse Models. Cold Spring Harb Protoc. *2014*, 694-7087.

107. Anderson RT, Keysar SB, Bowles DW *et al.* (2013) The Dual Pathway Inhibitor Rigosertib is Effective in Direct Patient Tumor Xenografts of Head and Neck Squamous Cell Carcinomas. Mol Cancer Ther. *12*, 1994-200510.

108. Hidalgo M, Amant F, Biankin AV *et al.* (2014) Patient-Derived Xenograft Models: An Emerging Platform for Translational Cancer Research. Cancer Discov. *4*, 998-10139.

109. *Clinical Trial Endpoints for the Approval of Cancer Drugs and Biologics.* Available at: https://www.fda.gov/regulatory-information/search-fda-guidance-documents/clinical-trial-endpoints-approval-cancer-drugs-and-biologics. Accessed Mar 24, 2021.

110. Schwartz LH, Litière S, de Vries E *et al.* (2016) RECIST 1.1-Update and Clarification: From the RECIST Committee. Eur J Cancer. *62*, 132-137.

111. Seymour L, Bogaerts J, Perrone A *et al.* (2017) iRECIST: Guidelines for Response Criteria for use in Trials Testing Immunotherapeutics. Lancet Oncol. *18*, e143-e1523.

112. Cox TR. (2021) The Matrix in Cancer. Nat Rev Cancer. *21*, 217-2384.

113. Baghban R, Roshangar L, Jahanban-Esfahlan R *et al.* (2020) Tumor Microenvironment Complexity and Therapeutic Implications at a Glance. Cell Commun Signal. *18*, 591.

114. Winkler J, Abisoye-Ogunniyan A, Metcalf KJ *et al.* (2020) Concepts of Extracellular Matrix Remodelling in Tumour Progression and Metastasis. Nat Commun. *11*, 1-191.

115. Theocharis AD, Skandalis SS, Gialeli C *et al.* (2016) Extracellular Matrix Structure. Adv Drug Deliv Rev. *97*, 4-27.

116. Kalluri R. (2016) The Biology and Function of Fibroblasts in Cancer. Nat Rev Cancer. *16*, 582-5989.

117. Jang I; Beningo KA. (2019) Integrins, CAFs and Mechanical Forces in the Progression of Cancer. Cancers (Basel). *115*.

118. Hu JL, Wang W, Lan XL *et al.* (2019) CAFs Secreted Exosomes Promote Metastasis and Chemotherapy Resistance by Enhancing Cell Stemness and Epithelial-Mesenchymal Transition in Colorectal Cancer. Mol Cancer. *18*, 911.

119. Hsu H, Wall NR, Hsueh C *et al.* (2014) Combination Antiangiogenic Therapy and Radiation in Head and Neck Cancers. Oral Oncology. *50*, 19-261.

120. Seiwert TY; Cohen EEW. (2008) Targeting Angiogenesis in Head and Neck Cancer. Semin Oncol. *35*, 274-2853.

121. Vassilakopoulou M, Psyrri A; Argiris A. (2015) Targeting Angiogenesis in Head and Neck Cancer. Oral Oncology. *51*, 409-4155.

122. Hinshaw DC; Shevde LA. (2019) The Tumor Microenvironment Innately Modulates Cancer Progression. Cancer Res. *79*, 4557-456618.

123. Kim J; Bae J. (2016) Tumor-Associated Macrophages and Neutrophils in Tumor Microenvironment. Mediators Inflamm. *2016*, 6058147.

124. O'Donnell JS, Teng MWL; Smyth MJ. (2019) Cancer Immunoediting and Resistance to T Cell-Based Immunotherapy. Nat Rev Clin Oncol. *16*, 151-1673.

125. Schreiber RD, Old LJ; Smyth MJ. (2011) Cancer Immunoediting: Integrating Immunity's Roles in Cancer Suppression and Promotion. Science. *331*, 1565-15706024.

126. Ayers M, Lunceford J, Nebozhyn M *et al.* (2017) IFN-Γ-Related mRNA Profile Predicts Clinical Response to PD-1 Blockade. J Clin Invest. *127*, 2930-29408.

127. Chen DS; Mellman I. (2017) Elements of Cancer Immunity and the Cancer-Immune Set Point. Nature. *541*, 321-3307637.

128. Sharma P, Hu-Lieskovan S, Wargo JA *et al.* (2017) Primary, Adaptive and Acquired Resistance to Cancer Immunotherapy. Cell. *168*, 707-7234.

129. Herbst RS. (2004) Review of Epidermal Growth Factor Receptor Biology. Int J Radiat Oncol Biol Phys. *59*, 21-262 Suppl.

130. Leemans CR, Braakhuis BJM; Brakenhoff RH. (2011) The Molecular Biology of Head and Neck Cancer. Nat Rev Cancer. *11*, 9-221.

131. Lee JW, Soung YH, Kim SY *et al.* (2005) Somatic Mutations of EGFR Gene in Squamous Cell Carcinoma of the Head and Neck. Clin Cancer Res. *11*, 2879-28828.

132. Loeffler-Ragg J, Witsch-Baumgartner M, Tzankov A *et al.* (2006) Low Incidence of Mutations in EGFR Kinase Domain in Caucasian Patients with Head and Neck Squamous Cell Carcinoma. Eur J Cancer. *42*, 109-1111.

133. Cohen EEW. (2006) Role of Epidermal Growth Factor Receptor Pathway-Targeted Therapy in Patients with Recurrent and/Or Metastatic Squamous Cell Carcinoma of the Head and Neck. J Clin Oncol. *24*, 2659-266517.

134. Young N, Soneru C, Liu J *et al.* (2015) Afatinib Efficacy Against Squamous Cell Carcinoma of the Head and Neck Cell Lines in Vitro and in Vivo. Targ Oncol. *10*, 501-5084.

135. Huang SM, Bock JM; Harari PM. (1999) Epidermal Growth Factor Receptor Blockade with C225 Modulates Proliferation, Apoptosis, and Radiosensitivity in Squamous Cell Carcinomas of the Head and Neck. Cancer Res. *59*, 1935-19408.

136. Schütze C, Dörfler A, Eicheler W *et al.* (2007) Combination of EGFR/HER2 Tyrosine Kinase Inhibition by BIBW 2992 and BIBW 2669 with Irradiation in FaDu Human Squamous Cell Carcinoma. Strahlenther Onkol. *183*, 256-2645.

137. Wakeling AE, Guy SP, Woodburn JR *et al.* (2002) ZD1839 (Iressa). Cancer Res. *62*, 5749-575420.

138. Magné N, Fischel JL, Dubreuil A *et al.* (2002) Influence of Epidermal Growth Factor Receptor (EGFR), p53 and Intrinsic MAP Kinase Pathway Status of Tumour Cells on the Antiproliferative Effect of ZD1839 ("Iressa"). Br J Cancer. *86*, 1518-15239.

139. Kazandjian D, Blumenthal GM, Yuan W *et al.* (2016) FDA Approval of Gefitinib for the Treatment of Patients with Metastatic EGFR Mutation-Positive Non-Small Cell Lung Cancer. Clin Cancer Res. *22*, 1307-13126.

140. Sebastian S, Azzariti A, Accardi R *et al.* (2008) Validation of Gefitinib Effectiveness in a Broad Panel of Head and Neck Squamous Carcinoma Cells. Int J Mol Med. *21*, 809-8176.

141. Stewart JSW, Cohen EEW, Licitra L *et al.* (2009) Phase III Study of Gefitinib Compared with Intravenous Methotrexate for Recurrent Squamous Cell Carcinoma of the Head and Neck [Corrected]. J Clin Oncol. *27*, 1864-187111.

142. Argiris A, Ghebremichael M, Gilbert J *et al.* (2013) Phase III Randomized, Placebo-Controlled Trial of Docetaxel with Or without Gefitinib in Recurrent Or Metastatic Head and Neck Cancer: An Eastern Cooperative Oncology Group Trial. J Clin Oncol. *31*, 1405-141411.

143. Soulieres D, Senzer NN, Vokes EE *et al.* (2004) Multicenter Phase II Study of Erlotinib, an Oral Epidermal Growth Factor Receptor Tyrosine Kinase Inhibitor, in Patients with Recurrent Or Metastatic Squamous Cell Cancer of the Head and Neck. J Clin Oncol. *22*, 77-851.

144. Martins RG, Parvathaneni U, Bauman JE *et al.* (2013) Cisplatin and Radiotherapy with Or without Erlotinib in Locally Advanced Squamous Cell

Carcinoma of the Head and Neck: A Randomized Phase II Trial. J Clin Oncol. *31*, 1415-142111.

145. Macha MA, Rachagani S, Qazi AK *et al.* (2017) Afatinib Radiosensitizes Head and Neck Squamous Cell Carcinoma Cells by Targeting Cancer Stem Cells. Oncotarget. *8*, 20961-2097313.

146. Machiels JH, Haddad RI, Fayette J *et al.* (2015) Afatinib Versus Methotrexate as Second-Line Treatment in Patients with Recurrent Or Metastatic Squamous-Cell Carcinoma of the Head and Neck Progressing on Or After Platinum-Based Therapy (LUX-Head & Neck 1): An Open-Label, Randomised Phase 3 Trial. Lancet Oncol. *16*, 583-5945.

147. Burtness B, Haddad R, Dinis J *et al.* (2019) Afatinib Vs Placebo as Adjuvant Therapy After Chemoradiotherapy in Squamous Cell Carcinoma of the Head and Neck: A Randomized Clinical Trial. JAMA Oncol. .

148. Freudlsperger C, Burnett JR, Friedman JA *et al.* (2011) EGFR-PI3K-AKT-mTOR Signaling in Head and Neck Squamous Cell Carcinomas: Attractive Targets for Molecular-Oriented Therapy. Expert Opin Ther Targets. *15*, 63-741.

149. Cantley LC. (2002) The Phosphoinositide 3-Kinase Pathway. Science. *296*, 1655-16575573.

150. Lui VWY, Hedberg ML, Li H *et al.* (2013) Frequent Mutation of the PI3K Pathway in Head and Neck Cancer Defines Predictive Biomarkers. Cancer discovery. *3*, 761-7697.

151. Laplante M; Sabatini DM. (2012) mTOR Signaling in Growth Control and Disease. Cell. *149*, 274-2932.

152. Dutcher JP. (2004) Mammalian Target of Rapamycin Inhibition. Clin Cancer Res. *10*, 6382S-7S18 Pt 2.

153. Rini BI. (2008) Temsirolimus, an Inhibitor of Mammalian Target of Rapamycin. Clin Cancer Res. *14*, 1286-12905.

154. Nguyen SA, Walker D, Gillespie MB *et al.* (2012) mTOR Inhibitors and its Role in the Treatment of Head and Neck Squamous Cell Carcinoma. Curr Treat Options Oncol. *13*, 71-811.

155. Hasskarl J. (2018) Everolimus. Recent Results Cancer Res. *211*, 101-123.

156. Dancey JE; Monzon J. (2011) Ridaforolimus: A Promising Drug in the Treatment of Soft-Tissue Sarcoma and Other Malignancies. Future Oncol. *7*, 827-8397.

157. Pongas G; Fojo T. (2016) BEZ235: When Promising Science Meets Clinical Reality. The oncologist (Dayton, Ohio). *21*, 1033-10349.

158. Dolly SO, Wagner AJ, Bendell JC *et al.* (2016) Phase I Study of Apitolisib (GDC-0980), Dual Phosphatidylinositol-3-Kinase and Mammalian Target of Rapamycin Kinase Inhibitor, in Patients with Advanced Solid Tumors. Clin Cancer Res. *22*, 2874-288412.

159. Zhao Y; Adjei AA. (2014) The Clinical Development of MEK Inhibitors. Nat Rev Clin Oncol. *11*, 385-4007.

160. Ngan H, Liu Y, Fong AY *et al.* (2020) MAPK Pathway Mutations in Head and Neck Cancer Affect Immune Microenvironments and ErbB3 Signaling. Life science alliance. *3*, e2019005456.

161. Li L, Zhao G, Shi Z *et al.* (2016) The Ras/Raf/MEK/ERK Signaling Pathway and its Role in the Occurrence and Development of HCC. Oncol Lett. *12*, 3045-30505.

162. *Trametinib Dimethyl Sulfoxide - National Cancer Institute.* Available at: https://www.cancer.gov/about-cancer/treatment/drugs/trametinib. Accessed Sep 27, 2021.

163. Shirley M. (2018) Encorafenib and Binimetinib: First Global Approvals. Drugs. *78*, 1277-128412.

164. Gross AM, Wolters PL, Dombi E *et al.* (2020) Selumetinib in Children with Inoperable Plexiform Neurofibromas. N Engl J Med. *382*, 1430-144215.

165. Delord J, Italiano A, Awada A *et al.* (2021) Selective Oral MEK1/2 Inhibitor Pimasertib: A Phase I Trial in Patients with Advanced Solid Tumors. Target Oncol. *16*, 37-461.

166. Weekes CD, Von Hoff DD, Adjei AA *et al.* (2013) Multicenter Phase I Trial of the Mitogen-Activated Protein Kinase 1/2 Inhibitor BAY 86-9766 in Patients with Advanced Cancer. Clin Cancer Res. *19*, 1232-12435.

167. Adjei A, Adjei A, LoRusso P *et al.* (2017) A Phase I Dose-Escalation Study of TAK-733, an Investigational Oral MEK Inhibitor, in Patients with Advanced Solid Tumors. Invest New Drugs. *35*, 47-581.

168. Elmore S. (2007) Apoptosis: A Review of Programmed Cell Death. Toxicol Pathol. *35*, 495-5164.

169. Hanahan D; Weinberg RA. (2011) Hallmarks of Cancer: The Next Generation. Cell. *144*, 646-6745.

170. Adams JM; Cory S. (2007) The Bcl-2 Apoptotic Switch in Cancer Development and Therapy. Oncogene. *26*, 1324-13379.

171. Sia J, Szmyd R, Hau E *et al.* (2020) Molecular Mechanisms of Radiation-Induced Cancer Cell Death: A Primer. Front Cell Dev Biol. *8*, 41.

172. Maier P, Hartmann L, Wenz F *et al.* (2016) Cellular Pathways in Response to Ionizing Radiation and their Targetability for Tumor Radiosensitization. Int J Mol Sci. *17*1.

173. Gudkov AV; Komarova EA. (2003) The Role of p53 in Determining Sensitivity to Radiotherapy. Nat Rev Cancer. *3*, 117-1292.

174. Kale J, Osterlund EJ; Andrews DW. (2018) BCL-2 Family Proteins: Changing Partners in the Dance Towards Death. Cell Death Differ. *25*, 65-801.

175. Hemann MT; Lowe SW. (2006) The p53-Bcl-2 Connection. Cell Death Differ. *13*, 1256-12598.

176. Cerami E, Gao J, Dogrusoz U *et al.* (2012) The cBio Cancer Genomics Portal: An Open Platform for Exploring Multidimensional Cancer Genomics Data. Cancer Discov. *2*, 401-4045.

177. Raudenská M, Balvan J; Masařík M. (2021) Cell Death in Head and Neck Cancer Pathogenesis and Treatment. Cell Death Dis. *12*, 1922.

178. Perini GF, Ribeiro GN, Pinto Neto JV *et al.* (2018) BCL-2 as Therapeutic Target for Hematological Malignancies. J Hematol Oncol. *11*, 651.

179. Guerra VA, DiNardo C; Konopleva M. (2019) Venetoclax-Based Therapies for Acute Myeloid Leukemia. Best Pract Res Clin Haematol. *32*, 145-1532.

180. Zerp SF, Stoter R, Kuipers G *et al.* (2009) AT-101, a Small Molecule Inhibitor of Anti-Apoptotic Bcl-2 Family Members, Activates the SAPK/JNK Pathway and Enhances Radiation-Induced Apoptosis. Radiat Oncol. *4*, 47.

181. Stein MN, Goodin S, Gounder M *et al.* (2020) A Phase I Study of AT-101, a BH3 Mimetic, in Combination with Paclitaxel and Carboplatin in Solid Tumors. Invest New Drugs. *38*, 855-8653.

182. Swiecicki PL, Bellile E, Sacco AG *et al.* (2016) A Phase II Trial of the BCL-2 Homolog Domain 3 Mimetic AT-101 in Combination with Docetaxel for Recurrent, Locally Advanced, Or Metastatic Head and Neck Cancer. Invest New Drugs. *34*, 481-4894.

183. Baggstrom MQ, Qi Y, Koczywas M *et al.* (2011) A Phase II Study of AT-101 (Gossypol) in Chemotherapy-Sensitive Recurrent Extensive-Stage Small Cell Lung Cancer. J Thorac Oncol. *6*, 1757-176010.

184. Ow TJ, Thomas C, Fulcher CD *et al.* (2020) Apoptosis Signaling Molecules as Treatment Targets in Head and Neck Squamous Cell Carcinoma. Laryngoscope. *130*, 2643-264911.

185. Britt EL, Raman S, Leek K *et al.* (2019) Combination of Fenretinide and ABT-263 Induces Apoptosis through NOXA for Head and Neck Squamous Cell Carcinoma Treatment. PLoS One. *14*, e02193987.

186. Ow TJ, Fulcher CD, Thomas C *et al.* (2019) Optimal Targeting of BCL-Family Proteins in Head and Neck Squamous Cell Carcinoma Requires Inhibition of both BCL-xL and MCL-1. Oncotarget. *10*, 494-5104.

187. Yang B, Liu T, Qu Y *et al.* (2018) Progresses and Perspectives of Anti-PD-1/PD-L1 Antibody Therapy in Head and Neck Cancers. Front Oncol. *8*, 563.

188. Prendergast GC, Malachowski WP, DuHadaway JB *et al.* (2017) Discovery of IDO1 Inhibitors: From Bench to Bedside. Cancer Res. *77*, 6795-681124.

189. Moon YW, Hajjar J, Hwu P *et al.* (2015) Targeting the Indoleamine 2,3-Dioxygenase Pathway in Cancer. J Immunother Cancer. *3*, 51.

190. Laimer K, Troester B, Kloss F *et al.* (2011) Expression and Prognostic Impact of Indoleamine 2,3-Dioxygenase in Oral Squamous Cell Carcinomas. Oral Oncol. *47*, 352-3575.

191. Schneider S, Kadletz L, Wiebringhaus R *et al.* (2018) PD-1 and PD-L1 Expression in HNSCC Primary Cancer and Related Lymph Node Metastasis - Impact on Clinical Outcome. Histopathology. *73*, 573-5844.

192. Zou W, Wolchok JD; Chen L. (2016) PD-L1 (B7-H1) and PD-1 Pathway Blockade for Cancer Therapy: Mechanisms, Response Biomarkers, and Combinations. Sci Transl Med. *8*, 328rv4328.

193. Elbers JBW, Al-Mamgani A, Tesseslaar MET *et al.* (2020) Immuno-Radiotherapy with Cetuximab and Avelumab for Advanced Stage Head and Neck Squamous Cell Carcinoma: Results from a Phase-I Trial. Radiother Oncol. *142*, 79-84.

194. Seidel JA, Otsuka A; Kabashima K. (2018) Anti-PD-1 and Anti-CTLA-4 Therapies in Cancer: Mechanisms of Action, Efficacy, and Limitations. Frontiers in oncology. *8*, 86.

195. *Ipilimumab - National Cancer Institute.* Available at: https://www.cancer.gov/about-cancer/treatment/drugs/ipilimumab. Accessed Sep 27, 2021.

196. Castellanos JR, Purvis IJ, Labak CM *et al.* (2017) B7-H3 Role in the Immune Landscape of Cancer. Am J Clin Exp Immunol. *6*, 66-754.

197. Yang S, Wei W; Zhao Q. (2020) B7-H3, a Checkpoint Molecule, as a Target for Cancer Immunotherapy. International journal of biological sciences. *16*, 1767-177311.

198. Picarda E, Ohaegbulam KC; Zang X. (2016) Molecular Pathways: Targeting B7-H3 (CD276) for Human Cancer Immunotherapy. Clin Cancer Res. *22*, 3425-343114.

199. Chen J, Chen C, Ku K *et al.* (2015) Glycoprotein B7-H3 Overexpression and Aberrant Glycosylation in Oral Cancer and Immune Response. Proc Natl Acad Sci U S A. *112*, 13057-1306242.

200. Sieviläinen M, Wirsing AM, Hyytiäinen A *et al.* (2021) Evaluation Challenges in the Validation of B7-H3 as Oral Tongue Cancer Prognosticator. Head Neck Pathol. *15*, 469-4782.

201. Grénman R, Pekkola-Heino K, Joensuu H *et al.* (1992) UT-MUC-1, a New Mucoepidermoid Carcinoma Cell Line, and its Radiosensitivity. Arch Otolaryngol Head Neck Surg. *118*, 542-5475.

202. Lepikhova T, Karhemo P, Louhimo R *et al.* (2018) Drug-Sensitivity Screening and Genomic Characterization of 45 HPV-Negative Head and Neck Carcinoma Cell Lines for Novel Biomarkers of Drug Efficacy. Mol Cancer Ther. *17*, 2060-20719.

203. Pemovska T, Kontro M, Yadav B *et al.* (2013) Individualized Systems Medicine Strategy to Tailor Treatments for Patients with Chemorefractory Acute Myeloid Leukemia. Cancer Discov. *3*, 1416-142912.

204. Potdar S, Ianevski A, Mpindi J *et al.* (2020) Breeze: An Integrated Quality Control and Data Analysis Application for High-Throughput Drug Screening. Bioinformatics. *36*, 3602-360411.

205. Yadav B, Pemovska T, Szwajda A *et al.* (2014) Quantitative Scoring of Differential Drug Sensitivity for Individually Optimized Anticancer Therapies. Sci Rep. *4*, 5193.

206. Zhang J, Chung TDY; Oldenburg KR. (1999) A Simple Statistical Parameter for use in Evaluation and Validation of High Throughput Screening Assays. J Biomol Screen. *4*, 67-732.

207. Ianevski A, Giri AK; Aittokallio T. (2020) SynergyFinder 2.0: Visual Analytics of Multi-Drug Combination Synergies. Nucleic Acids Res. *48*, W488-W493W1.

208. He L, Kulesskiy E, Saarela J *et al.* (2018) Methods for High-Throughput Drug Combination Screening and Synergy Scoring. Methods Mol Biol. *1711*, 351-398.

209. Carey TE, Kimmel KA, Schwartz DR *et al.* (1983) Antibodies to Human Squamous Cell Carcinoma. Otolaryngol Head Neck Surg. *91*, 482-4915.

210. Schindelin J, Arganda-Carreras I, Frise E *et al.* (2012) Fiji: An Open-Source Platform for Biological-Image Analysis. Nat Methods. *9*, 676-6827.

211. Businaro L, De Ninno A, Schiavoni G *et al.* (2013) Cross Talk between Cancer and Immune Cells: Exploring Complex Dynamics in a Microfluidic Environment. Lab Chip. *13*, 229-2392.

212. Penttinen A, Suleymanova I, Albert K *et al.* (2016) Characterization of a New Low-Dose 6-Hydroxydopamine Model of Parkinson's Disease in Rat. J Neurosci Res. *94*, 318-3284.

213. Dunn OJ. (1964) Multiple Comparisons using Rank Sums. Technometrics. *6*, 241-2523.

214. Grünwald V, Keilholz U, Boehm A *et al.* (2015) TEMHEAD: A Single-Arm Multicentre Phase II Study of Temsirolimus in Platin- and Cetuximab Refractory Recurrent and/Or Metastatic Squamous Cell Carcinoma of the Head and Neck (SCCHN) of the German SCCHN Group (AIO). Ann. Oncol. *26*, 561-5673.

215. Day TA, Shirai K, O'Brien PE *et al.* (2019) Inhibition of mTOR Signaling and Clinical Activity of Rapamycin in Head and Neck Cancer in a Window of Opportunity Trial. Clin. Cancer Res. *25*, 1156-11644.

216. Edmondson R, Broglie JJ, Adcock AF *et al.* (2014) Three-Dimensional Cell Culture Systems and their Applications in Drug Discovery and Cell-Based Biosensors. Assay Drug Dev Technol. *12*, 207-2184.

217. Puente XS, Sánchez LM, Overall CM *et al.* (2003) Human and Mouse Proteases: A Comparative Genomic Approach. Nat Rev Genet. *4*, 544-5587.

218. Ribeiro Franco PI, Rodrigues AP, de Menezes LB *et al.* (2020) Tumor Microenvironment Components: Allies of Cancer Progression. Pathol Res Pract. *216*, 1527291.

219. Wang Z, Valera J, Zhao X *et al.* (2017) mTOR Co-Targeting Strategies for Head and Neck Cancer Therapy. Cancer Metastasis Rev. *36*, 491-5023.

220. Boni JP, Hug B, Leister C *et al.* (2009) Intravenous Temsirolimus in Cancer Patients: Clinical Pharmacology and Dosing Considerations. Semin Oncol. *36 Suppl 3*, 18.

221. Bossi P, Resteghini C, Paielli N *et al.* (2016) Prognostic and Predictive Value of EGFR in Head and Neck Squamous Cell Carcinoma. Oncotarget. *7*, 74362-7437945.

222. Khaznadar SS, Khan M, Schmid E *et al.* (2018) EGFR Overexpression is Not Common in Patients with Head and Neck Cancer. Cell Lines are Not Representative for the Clinical Situation in this Indication. Oncotarget. *9*, 28965-2897548.

223. Wu M; Zhang P. (2020) EGFR-Mediated Autophagy in Tumourigenesis and Therapeutic Resistance. Cancer Lett. *469*, 207-216.

224. Kwon Y, Kim M, Jung HS *et al.* (2019) Targeting Autophagy for Overcoming Resistance to Anti-EGFR Treatments. Cancers (Basel). *11*9.

225. Arnold L, Enders J; Thomas SM. (2017) Activated HGF-C-Met Axis in Head and Neck Cancer. Cancers (Basel). *9*12.

226. Rossi L; Corvò R. (2002) Retinoic Acid Modulates the Radiosensitivity of Head-and-Neck Squamous Carcinoma Cells Grown in Collagen Gel. Int J Radiat Oncol Biol Phys. *53*, 1319-13275.

227. Laird JH, Lok BH, Ma J *et al.* (2018) Talazoparib is a Potent Radiosensitizer in Small Cell Lung Cancer Cell Lines and Xenografts. Clin Cancer Res. *24*, 5143-515220.

228. Lund-Andersen C, Patzke S, Nähse-Kumpf V *et al.* (2014) PLK1-Inhibition can Cause Radiosensitization Or Radioresistance Dependent on the Treatment Schedule. Radiother Oncol. *110*, 355-3612.

229. Wouters A, Pauwels B, Lardon F *et al.* (2010) In Vitro Study on the Schedule-Dependency of the Interaction between Pemetrexed, Gemcitabine and Irradiation in Non-Small Cell Lung Cancer and Head and Neck Cancer Cells. BMC Cancer. *10*, 441.

230. Argiris A, Pennella E, Koustenis A *et al.* (2013) Pemetrexed in Head and Neck Cancer: A Systematic Review. Oral Oncology. *49*, 492-5016.

231. Tse C, Shoemaker AR, Adickes J *et al.* (2008) ABT-263: A Potent and Orally Bioavailable Bcl-2 Family Inhibitor. Cancer Res. *68*, 3421-34289.

232. Al-Samadi A, Awad SA, Tuomainen K *et al.* (2017) Crosstalk between Tongue Carcinoma Cells, Extracellular Vesicles, and Immune Cells in in Vitro and in Vivo Models. Oncotarget. *8*, 60123-6013436.

233. Liu M, Wang X, Wang L *et al.* (2018) Targeting the IDO1 Pathway in Cancer: From Bench to Bedside. J Hematol Oncol. *11*, 1001.

234. Lin DJ, Ng JCK, Huang L *et al.* (2021) The Immunotherapeutic Role of Indoleamine 2,3-Dioxygenase in Head and Neck Squamous Cell Carcinoma: A Systematic Review. Clin Otolaryngol. *46*, 919-9345.

235. Stasikowska-Kanicka O, Wągrowska-Danilewicz M; Danilewicz M. (2018) Immunohistochemical Analysis of Foxp3+, CD4+, CD8+ Cell Infiltrates and PD-L1 in Oral Squamous Cell Carcinoma. Pathol Oncol Res. *24*, 497-5053.